

---

# **Inaugural-Dissertation**

**zur  
Erlangung der Doktorwürde  
der  
Naturwissenschaftlich-Mathematischen Gesamtfakultät  
der  
Ruprecht-Karls-Universität  
Heidelberg**

**vorgelegt von  
Diplom-Biologin Anja Meier  
aus Münster**

Tag der mündlichen Prüfung:.....

---

# **Visualization and Characterization of HBV-Receptor Interactions**

**Anja Meier  
2010**

Referees: Prof. Dr. Stephan Urban  
Prof. Dr. Martin Löchelt

---

## Summary

The human hepatitis B virus (HBV) is characterized by a pronounced liver tropism and a restricted host range. While the viral determinants essential for the host cell entry are well characterized, little is known about cellular factors involved in early steps of HBV infection. Proteoglycans have been described as primary attachment factors, but neither a receptor molecule nor the exact entry pathway is elucidated yet.

Peptides comprising the first 47 amino acids (HBVpreS/2-48<sup>myr</sup>) of the preS1-domain of the HBV surface protein L have been shown to inhibit an infection *in vitro* and *in vivo* with high specificity. The full inhibitory potential of HBVpreS/2-48<sup>myr</sup> relies on the integrity of an essential region (amino acids 9 - 15) and the presence of an acylation. This correlates with viral requirements for infectivity: mutations in the essential region (amino acids 11, 12 and 13) or the removal of the myristoylation render HBV particles non-infectious. It therefore is assumed that HBVpreS/2-48<sup>myr</sup> and the virus address a common factor on the hepatocyte. This work aimed to visualize and characterize the interaction with this factor.

Fluorescence microscopy and flow cytometry showed that fluorescently labeled peptides (HBVpreS/2-48<sup>myr</sup>-K-FITC) bind to the plasma membrane of differentiated hepatocytes in a sequence- and myristoylation-dependent manner. The binding was not restricted to HBV-susceptible cells like primary hepatocytes (PH) from human or tupaia, and HepaRG cells, but was also detected on PH from non-permissive species (mouse, rat, dog and woodchuck). This demonstrated that a binding-competent preS1-receptor is present also in non-susceptible species. The refractoriness of these cells towards HBV infection therefore must be independent from the receptor interaction.

HBV infects only differentiated hepatocytes. Correlating to that, de-differentiation of PH was accompanied by a loss of the ability to bind HBVpreS/2-48<sup>myr</sup>-K-FITC. Vice versa, HepaRG cells gained binding competence during differentiation, demonstrating that the expression of a functional preS1-receptor depends on the differentiation status of a cell. Sustaining this assumption, hepatoma cell lines like HepG2 and HuH7 did neither bind HBVpreS/2-48<sup>myr</sup>-K-FITC. Their non-permissiveness therefore can *inter alia* be explained by a lack of a functional receptor.

To determine the affinity of the peptide-receptor interaction, binding curves for HBVpreS/2-48<sup>myr</sup>-K-FITC-binding to the cell surface of PH were calculated with data from flow cytometry and mass spectrometry. This revealed a bimodal mechanism, consisting of (i) a sequence- and myristoylation-dependent binding to a receptor with a high affinity ( $K_D \sim 60$  nM), and (ii) a non-specific, low-affinity-interaction ( $K_D > 2000$  nM), that depended only on the myristoylation. Analysis of the binding kinetics on PH showed that equilibrium of the high-affinity interaction was established after 10 minutes. Thereby, the peptide-receptor complexes exhibited an extraordinary high stability over time ( $t_{1/2} \sim 11$  hours), which indicated a low metabolic turn-over rate. These complexes were tightly associated with the actin cytoskeleton, as they did not show lateral movement within the membrane after photobleaching and co-localized with actin.

In order to extend these findings and to investigate the interaction of HBV particles with cells, fluorescently labeled HBV-Alexa488 was produced and characterized on a single-particle level. Chemical labeling of cell-culture derived virus yielded infectious particles of a high purity and bright fluorescence. Detection of HBV-Alexa488 on HepaRG cells showed a binding behavior similar to that of unlabeled HBV. Binding could be enhanced with PEG and inhibited by heparin. The labeled virus produced here can be applied for future single-virus tracing experiments.

---

## Zusammenfassung

Das humane Hepatitis B Virus (HBV) zeichnet sich durch einen ausgeprägten Leber- und Wirtstropismus aus. Während die Bedingungen für die Infektiosität eines HBV Partikels gut untersucht sind, ist aufseiten der Wirtszelle nur wenig über die frühen Schritte der Infektion bekannt. Außer Proteoglykanen, die als primäre Bindungsfaktoren dienen, sind bisher keine zellulären Rezeptormoleküle identifiziert worden.

Peptide, die aus den N-terminalen 47 Aminosäuren (AS) der präS1-Region des HBV-Oberflächenproteins L bestehen (HBVpräS/2-48<sup>myr</sup>), können eine Infektion *in vitro* und *in vivo* spezifisch inhibieren. Dabei sind eine Sequenz in der sog. essentiellen Region (AS 9 - 15), sowie eine Acylierung am N-Terminus Voraussetzung für die inhibitorische Aktivität dieses Peptids. Parallel hängt auch die Infektiosität eines HBV Partikels von diesen Faktoren ab: Rekombinante Viren, die Mutationen in der essentiellen Region tragen oder denen die Myristoylierung des L-Proteins fehlt, sind nicht infektiös. Aufgrund dieser Korrelation wird angenommen, dass HBVpräS/2-48<sup>myr</sup> und das Virus einen gemeinsamen Faktor auf der Hepatozyte adressieren. Ziel dieser Arbeit war es, diesen Faktor zu visualisieren und dessen Bindung zu charakterisieren.

Mittels Fluoreszenzmikroskopie und Durchflusszytometrie (FACS) konnte gezeigt werden, dass fluoreszenz-markierte Peptide (HBVpräS/2-48<sup>myr</sup>-K-FITC) an die Plasmamembran von differenzierten Hepatozyten binden. Diese Bindung war von der Peptidsequenz und der Myristoylierung abhängig, aber nicht von der Suszeptibilität der Zielzelle. So wurde neben HBV-infizierbaren primären Hepatozyten von Mensch/ Tupaia und HepaRG Zellen auch eine Bindung an Hepatozyten von nicht-infizierbaren Spezies (Maus, Ratte, Hund und Waldmurmeltier) gezeigt. Die Beständigkeit dieser Zellen gegenüber einer HBV Infektion kann also nicht durch das Fehlen eines präS1-Rezeptors erklärt werden.

Da HBV ausschließlich differenzierte Hepatozyten infizieren kann wurde untersucht, ob es einen Zusammenhang zwischen dem Differenzierungsgrad und der präS1-Rezeptor Expression einer Zelle gibt. Es wurde gezeigt, dass Hepatozyten im Laufe der Dedifferenzierung ihre Bindefähigkeit für HBVpräS/2-48<sup>myr</sup>-K-FITC verlieren. Im umgekehrten Fall erlangen HepaRG Zellen diese Fähigkeit erst mit Erreichen eines differenzierten Zustandes. Auch Hepatoma Zelllinien, wie z.B. HepG2 oder HuH7 Zellen, zeigten keine Bindung von HBVpräS/2-48<sup>myr</sup>-K-FITC. Die Expression eines funktionalen Rezeptors hängt also vom Differenzierungszustand einer Zelle ab.

Um die Affinität der Rezeptorbindung zu bestimmen, wurden mittels FACS und Massenspektrometrie Bindungskurven für die Interaktion von HBVpräS/2-48<sup>myr</sup>-K-FITC mit der Plasmamembran von PH erstellt. Diese zeigten einen bimodalen Bindemechanismus, bestehend aus (i) einer Sequenz- und Myristoylierungs-abhängigen Interaktion mit einem hoch-affinen Rezeptor ( $K_D \sim 60$  nM), und (ii) einer unspezifischen, nur Myristoylierungs-abhängigen Bindung von geringerer Affinität ( $K_D > 2000$  nM). Untersuchungen zur Bindungskinetik zeigten, dass ein Reaktionsgleichgewicht bereits nach 10 Minuten erreicht ist, und dass die Peptid-Rezeptor Komplexe mit einer langen Halbwertszeit von  $t_{1/2} \sim 11$  Stunden relativ lange auf der Zelloberfläche verbleiben. Dies spricht für eine langsame Metabolisierung. Wie Analysen zur lateralen Mobilität und Co-Lokalisations-Experimente ergaben, zeigten die Peptid-Rezeptor-Komplexe dabei eine Interaktion mit dem Aktin- Zytoskelett.

Um auch das Bindeverhalten von HBV-Partikeln untersuchen zu können, wurden durch chemische Kopplung von Alexa-Fluor488 Fluoreszenz-markierte, infektiöse HBV-Partikel hergestellt (HBV-Alexa488). Diese zeigten ein Bindeverhalten auf HepaRG Zellen, ähnlich dem von nicht-markiertem HBV, und eignen sich für eine zukünftige Verwendung zur Untersuchung der Virusbindung und Virusaufnahme in Echtzeit.

---

## Table of Contents

1.	Introduction.....	1
1.1	Hepatitis B .....	1
1.2	Molecular Virology of the Hepatitis B Virus .....	2
1.2.1.	Classification of the Hepadnaviridae and their host range .....	2
1.2.2.	Animal models for HBV .....	3
1.2.3.	The Structure of HBV particles .....	4
1.2.3.1.	HBV envelope proteins and preS1-derived lipopeptides .....	5
1.2.3.2.	The liver tropism of HBVpreS/2-48 <sup>myr</sup> .....	7
1.2.4.	The HBV replication cycle .....	8
1.2.4.1.	HBV entry and cell culture systems .....	8
1.2.4.2.	Post-entry steps of an HBV infection .....	9
1.3	Epidemiology and pathogenesis.....	10
1.4	Therapy.....	11
1.4.1.	Immune system modulators .....	11
1.4.2.	Antiviral drugs .....	11
1.4.3.	HBV preS-derived lipopeptides as entry inhibitors .....	12
2.	Materials and Methods .....	13
2.1	Materials.....	13
2.1.1.	Eukaryotic cells .....	13
2.1.1.1.	Cell lines.....	13
2.1.1.2.	Primary cells .....	13
2.1.2.	Cell culture media.....	14
2.1.3.	Chemicals and reagents.....	16
2.1.4.	Consumables .....	18
2.1.5.	Technical equipment and instruments.....	19
2.1.6.	Special software .....	20
2.2	Methods .....	21
2.2.1.	Cell culture.....	21
2.2.1.1.	Cultivation of cell lines .....	21
2.2.1.2.	Preparation and cultivation of freshly isolated primary hepatocytes.....	21
2.2.1.3.	Thawing and handling of cryopreserved hepatocytes .....	23
2.2.1.4.	HBV infection of HepaRG cells.....	23
2.2.2.	Peptide binding assays .....	23
2.2.2.1.	Peptide synthesis.....	23

## Table of Contents

2.2.2.2.	Peptide binding to adherent cell culture for microscopy.....	24
2.2.2.3.	Staining of the cells with Phalloidin-Alexa546 or Phalloidin-Alexa565 .....	24
2.2.2.4.	Destruction of the actin cytoskeleton by cytochalasin D .....	24
2.2.2.5.	Peptide binding to cells in solution for flow cytometry .....	24
2.2.2.6.	Competition assays using HBVpreS/2-48 <sup>myr</sup> , heparin or suramin .....	25
2.2.2.7.	Protease digestion of surface proteins.....	25
2.2.2.8.	Quantification of HBVpreS/2-48 <sup>myr</sup> on cells by HPLC-MS/MS .....	26
2.2.3.	Production of fluorescently labeled HBV .....	26
2.2.3.1.	Preparation of HBV-Alexa488.....	26
2.2.3.2.	Biochemical analysis of HBV-Alexa488.....	27
2.2.3.3.	Quantification of HBV-DNA (DNA-dot blot) .....	27
2.2.3.4.	Quantification of fluorescence .....	27
2.2.3.5.	Analytical detection of proteins .....	28
2.2.3.5.1.	Western Blot analysis.....	28
2.2.3.5.2.	Silver gel analysis.....	29
2.2.4.	Microscopy .....	29
2.2.4.1.	Spinning disk confocal microscopy.....	29
2.2.4.2.	Fluorescence recovery after photobleaching.....	30
2.2.4.3.	Total internal reflection fluorescence (TIRF) microscopy .....	30
2.2.4.4.	Measurement of fluorescence on digital images .....	30
3.	Visualization and characterization of the HBV preS1-receptor interaction with fluorescently labeled ligands.....	31
3.1	Fluorescently labeled HBVpreS/2-48 <sup>myr</sup> lipopeptides .....	31
3.1.1.	Production and characterization of fluorescently labeled HBV preS1-lipopeptides.....	32
3.1.2.	Validation of peptide-functionality by infection inhibition experiments.....	33
3.2	Visualization of HBVpreS/2-48 <sup>myr</sup> -K-FITC binding to hepatocytes.....	33
3.2.1.	HBVpreS/2-48 <sup>myr</sup> binds to the plasma membrane of HBV-susceptible hepatocytes in a highly sequence- and myristoylation-specific manner.....	34
3.2.2.	Specific binding of HBVpreS/2-48 <sup>myr</sup> -K-FITC is not restricted to HBV-susceptible cells ....	36
3.3	Characterization of preS1-receptor binding.....	39
3.3.1.	The presence of a preS1-receptor depends on the differentiation state of the cell .....	39
3.3.2.	Glycosaminoglycans do not play a substantial role in receptor-binding of HBVpreS/2-48 <sup>myr</sup> .....	41
3.3.3.	The preS1-receptor is sensitive to protease digestion.....	41
3.4	Characterization of the pharmacodynamic behavior of HBVpreS/2-48 <sup>myr</sup> and the kinetics of receptor binding.....	42

## Table of Contents

3.4.1.	HBVpreS/2-48 <sup>myr</sup> -K-FITC-receptor binding represents a bimodal binding mechanism.....	43
3.4.2.	Determination of the $K_D$ and $B_{max}$ of the peptide-receptor interaction .....	44
3.4.3.	HBVpreS/2-48 <sup>myr</sup> -K-FITC displays fast binding to its receptor .....	47
3.4.4.	The peptide-receptor complexes are retained on the plasma membrane with a half-life of approximately 11 hours .....	47
3.5	High-resolution microscopy and sub-cellular localization of HBVpreS/2-48 <sup>myr</sup> -K-FITC.....	48
3.5.1.	Spinning disk confocal microscopy revealed binding primarily on the cell surface.....	49
3.5.2.	Total internal reflection fluorescence microscopy: analysis of live cells showed the presence of finger-like plasma membrane protrusions that bound HBVpreS/2-48 <sup>myr</sup> -C-Atto565.....	50
3.5.3.	A restricted lateral mobility of peptide-receptor complexes indicated an interaction with the cytoskeleton .....	51
3.5.4.	Clusters of fluorescence showed a partial co-localization with actin .....	53
3.6	Production, characterization and visualization of fluorescently labeled HBV .....	55
3.6.1.	Production of fluorescently labeled HBV particles.....	55
3.6.2.	Biochemical characterization of HBV-Alexa488 .....	55
3.6.3.	Microscopic characterization of HBV-Alexa488 showed the presence of single particles and aggregates .....	57
3.6.4.	HBV-Alexa488 is highly infectious on HepaRG cells .....	58
3.6.5.	HBV-Alexa488 binding to differentiated HepaRG cells can be enhanced by PEG and inhibited by heparin .....	59
4.	Discussion.....	61
4.1	HBVpreS/2-48 <sup>myr</sup> binds to a receptor on the plasma membrane of HBV-susceptible hepatocytes in a highly sequence- and myristoylation-dependent manner .....	61
4.2	The expression of an HBVpreS/2-48 <sup>myr</sup> -receptor is not restricted to HBV-susceptible cells	62
4.3	The presence of a proteinaceous HBVpreS/2-48 <sup>myr</sup> receptor on the plasma membrane depends on the differentiation status of the cell.....	64
4.4	Analysis of the affinity of HBVpreS/2-48 <sup>myr</sup> to its receptor.....	66
4.5	Kinetic analysis of HBVpreS/2-48 <sup>myr</sup> -K-FITC receptor-interaction confirmed a high affinity of binding and demonstrated an unusual high stability of the peptide-receptor complexes...	69
4.6	Sub-cellular localization of receptor-bound HBVpreS/2-48 <sup>myr</sup> revealed an interaction with the (actin) cytoskeleton.....	70
4.7	Visualization of HBV particles.....	72
5.	References.....	75
	Danksagung .....	82

## 1. Introduction

### 1.1 **Hepatitis B**

The term hepatitis describes an inflammation of the liver. The most common cause of hepatitis is a viral infection. There are five main hepatitis viruses, referred to as types A, B, C, D and E.

A disease widely witnessed in young people accompanied by jaundice has already been mentioned by Hippocrates as early as 400 BC, and in 752 AD, Pope Zacharias wrote in a letter about the "jaundice of a contagious nature" (*Hepatology - Principles and Practice*, Kuntz and Kuntz, Springer Verlag 2002). First reports about a parenteral transmissibility of infectious jaundice were drawn up after an epidemic in Bremen (Lürman, 1885) and Merzig (Jehn, 1885). These epidemics developed after the use of a smallpox vaccine that contained a human lymph preparation. Several cases of epidemiological unexplained jaundice occurred within the next decades. All were preceded by a vaccination campaign with a measles convalescent serum, or the infusion of insulin and dextrose with re-used needles.

In 1947, MacCallum discriminated the *icterus epidemica* as type A and the hepatitis developed onto inoculation as type B (MacCallum, 1947). These, at a later date, were to correspond to the hepatitis A virus and the hepatitis B virus. The first step towards the identification of the pathogen of hepatitis B came from studies of genetic polymorphisms of serum proteins by Blumberg, Alter and Bisnich (Blumberg et al. 1965). They detected a novel antigen in the plasma of an Aboriginal patient that reacted with antibodies from a hemophilia patient. This antigen, referred to as Australia antigen, was later brought into context with the development of hepatitis. In parallel, Prince et al. were using a direct approach to search for the viral cause of serum hepatitis. By immunofluorescence microscopy of liver tissue sections they identified a cytoplasmic staining that probably reflected an antibody reaction with the Australia antigen (Prince et al. 1964). They also identified a serum protein in patients with post-transfusion hepatitis, that later was shown to be identical to the Australia antigen (Prince 1968).

In 1970, Dane et al. discovered by electron microscopy small, spherical 42 nm particles in the serum of patients with antigen-associated hepatitis (Dane et al. 1970). These particles turned out to represent infectious hepatitis B virus particles that nowadays still are described as Dane-particles.

## 1.2 Molecular Virology of the Hepatitis B Virus

### 1.2.1 Classification of the Hepadnaviridae and their host range

All members of the family of Hepadnaviridae (hepatitis DNA viruses) share remarkable similarities in the genome organization and the replication strategies. Along with the Spumaviridae (foamy viruses), they are the only known animal DNA viruses that replicate their DNA by reverse transcription of a viral RNA intermediate. Such viruses have otherwise been found only in plants (e.g. cauliflower mosaic virus). Since hepadnaviruses, like the members of the family of Retroviridae, encode a reverse transcriptase, both families are assigned to the group of retroid viruses.

Hepadnaviruses are characterized by an extremely small genome (approximately 3.2 kb), a unique replication strategy, and a very narrow host range and tissue tropism. The family contains two genera, the orthohepadnaviruses, infecting mammals, and the avihepadnaviruses, infecting birds. In addition to host range differences, the division into two genera is based on strong DNA sequence similarities among all orthohepadnaviruses and all avihepadnaviruses, but an almost complete lack of homology between these two groups. Members of the Avihepadnaviridae include the duck hepatitis B virus (DHBV) and the heron hepatitis B virus (HHBV). Based on perceived differences in the host range, the Orthohepadnaviridae have been divided into five distinct species, the human type B (HBV), the woodchuck (WHV), the ground squirrel (GSHV), the arctic ground squirrel (AGSHV) and the woolly monkey (WMHV) hepatitis virus (see Figure 1). Human HBV exists in several genotypes that tend to have distinct geographic distributions. Eight genotypes have been identified, A to H, that show sequence diversities of up to 17 %.

HBV isolates that are closely related in sequence to human HBV have been found also in chronically infected chimpanzees, gorillas, orangutans and gibbon apes (Zuckerman et al. 1978; Verschoor et al. 2001; Thornton et al. 2001), but these primate isolates are rather considered as HBV subtypes than as new species. Interestingly, several studies in wild-born or captive Cercopithecoidea monkeys did not show reactivity against serological markers of HBV (Makuwa et al. 2006; C. Huang et al. 2009), indicating that, if an HBV species exists in these animals, it must be highly divergent. Human isolates have been shown to infect gibbon apes and chimpanzees, but no convincing evidence of an infection of macaques or other members of the Cercopithecoidea family has been described yet. *Macaca sylvanus* is able to replicate HBV *in vivo* post experimental transfection (Gheit et al. 2002) and a recent study demonstrated an HBV replication in primary macaque hepatocytes (Lucifora et al. 2010). However, susceptibility of these animals has not been shown.

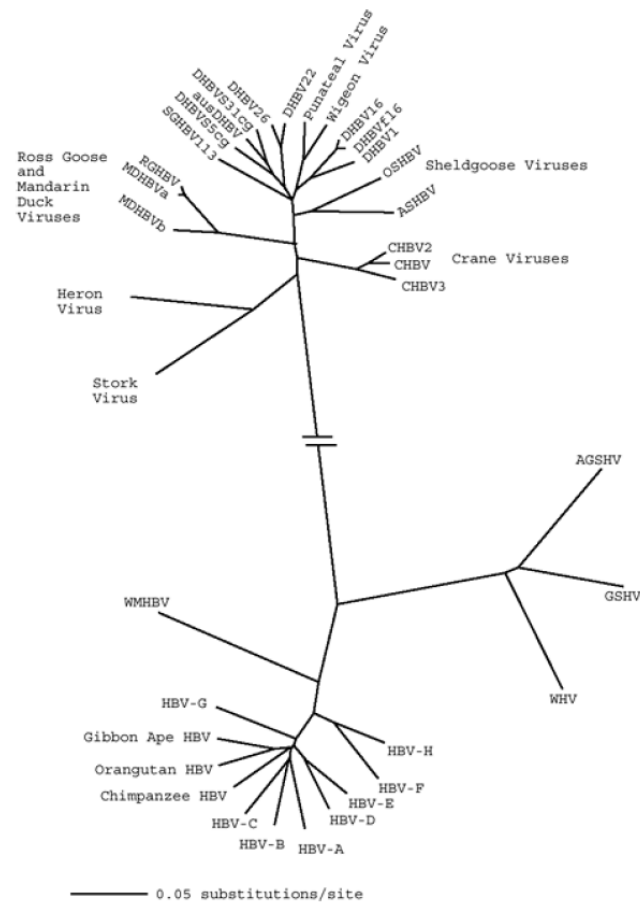


**Figure 1: Phylogenetic tree of the Hepadnaviridae family.** Depicted are the avihepadnaviridae (top) and the orthohepadnaviridae (bottom). The latter encompass the human hepatitis B viruses (HBV) genotypes (A - H), HBV subtypes that naturally occur in apes, and the hepatitis B virus found in woolly monkeys (WMHBV), woodchucks (WHV), ground squirrels (GSHV) and arctic ground squirrels (AGSHV). The dendrogram was constructed using ClustalX. (From: Fields, Virology, 5<sup>th</sup> edition.)

WHV, the woodchuck hepatitis B virus, is another well-studied orthohepadnavirus occurring naturally in marmots. Interestingly, WHV infects woodchucks, but not other rodents like ground squirrels, while the GSHV infects both, woodchucks and ground squirrels (Seeger et al. 1987; Seeger et al. 1991). Although this implies an extremely restricted host range for WHV, HDV with a WHV envelope (wHDV) has been shown to infect chimpanzees (Gerin 2001) and primary human hepatocytes (Gudima et al. 2008). Vice versa, a human enveloped hHDV could enter and (transiently) infect woodchuck hepatocytes *in vivo* without the need for a helper virus (Netter et al. 1994). An infection of woodchucks or primary woodchuck hepatocytes with HBV has not been described.

### 1.2.2. Animal models for HBV

Chimpanzees are the only animals fully permissive for an HBV infection. Their susceptibility has been described firstly after induction of an acute infection by injection of serum from human HBV carriers (Barker et al. 1975). Although chimpanzees do not develop a chronic disease, they have seen use in studying the pathogenesis of an acute infection (Will et al. 1982) and played an important role in the

development of safe vaccines (e.g. (Berthelot et al. 1984). However, due to the strong ethical constraints and the high costs, the experimental use of chimpanzees has been limited.

In 1996, tree shrews (*Tupaia belangeri*) have been described as the first non-primate species to be susceptible to human HBV infection (Yan et al. 1996; Walter et al. 1996). Although Tupaia are phylogenetically relative closely related to humans, they form their own order (*Scandentia*) within the mammals. Because of the accentuated host restriction of hepadnaviruses, it was surprising to find that Tupaia are susceptible to the human HBV. However, experimental infection of tree shrews is not highly efficient and causes only a mild, transient infection with low viral titers. Primary hepatocytes isolated from the liver of Tupaia are well susceptible to HBV infection and therefore provide a valuable source of HBV-permissive cells for *in vitro* experiments. Moreover, primary Tupaia hepatocytes were also used for the construction of chimeric mouse livers that could be infected with HBV (Dandri et al. 2005).

Even though HBV does not infect mice, several transgenic mouse models have been developed to study the mechanisms of HBV replication (Araki et al. 1991) and oncogenicity of viral genes *in vivo* (Kim et al. 1991). The first transgenic mouse system that produced high levels of complete viral particles without any evidence of cytopathology was developed by (Guidotti et al. 1995)). Nowadays, several mouse models are available that are based on transduction (adenoviral gene transfer), transfection (hydrodynamic injection) or transplantation of HBV-susceptible cells into mice (Trimeramouse, implantation of permissive hepatocytes in SCID mice or uPa-transgenic mice). For an overview see (Dandri et al. 2006).

### 1.2.3. The Structure of HBV particles

One characteristic trait of hepadnaviruses is the presence of three different particle forms in the plasma of infected patients (Figure 2). Besides genome-containing, infectious Dane particles, there exist subviral spheres and filaments with a diameter of approximately 20 nm and different lengths. These non-infectious, subviral particles are released constitutively from infected cells and can reach titers  $10^3$  to  $10^5$  times higher than that of infectious virions (up to  $10^{10}$  GE/ ml blood). Their exact role in the HBV life cycle is unknown, but it is assumed that they facilitate virus spread and maintenance in the host by adsorbing virus-neutralizing antibodies.

The infectious Dane particle has a size of 42 - 47 nm and consists of an enveloped icosahedral nucleocapsid containing the viral genome. The nucleocapsid has a diameter of approximately 28 nm. Two types of capsids can be found after expression in *E. coli* (Crowther et al. 1994). The major part of capsids corresponds to shells of 120 core protein dimers, with a triangulation number of  $T = 4$ . A smaller population of capsids consists of 90 copies and corresponds to a  $T = 3$  shell. Both particle

forms can be found also in patients, but infectious particles possess a T = 4 shell only (Roseman et al. 2005; Dryden et al. 2006).

The nucleocapsids contain a single copy of a partially double-stranded DNA genome. The viral polymerase is covalently coupled to its 5'-end via the terminal protein (TP). The polymerase provides an endogenous DNA polymerase activity with two functional domains, the reverse transcriptase (RT) and the RNase H.

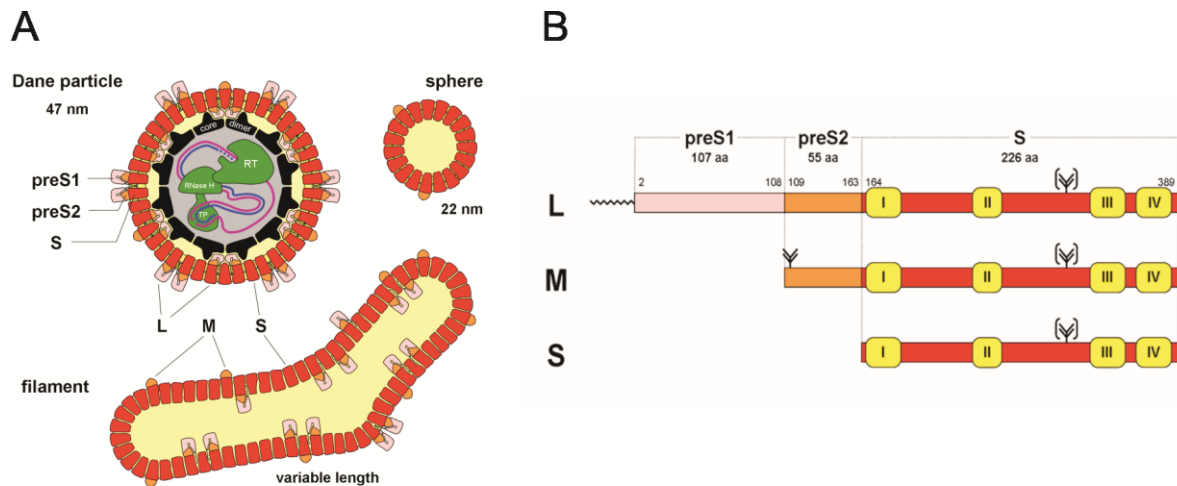


**Figure 2: Structure of the HBV particle forms and the envelope proteins.** (A) The serum of infected patients contains infectious Dane particles and empty subviral spheres and filaments. Dane particles enclose the viral capsid, consisting of core protein (black) and protecting the partially double-stranded DNA genome (purple and blue). Covalently bound to the genome is the viral polymerase (green), with a reverse transcriptase domain (RT), an RNase H activity and the terminal protein (TP). The capsid is enveloped by a lipid bilayer (red) that incorporates the envelope proteins L, M and S. Subviral particles do not contain capsids. (B) The HBV envelope proteins share the C-terminal S domain (red) with the transmembrane domains I - IV (yellow). The M protein possesses an additional preS2 sequence (orange), and the L protein is further elongated with the preS1 domain (pink). The L protein is modified by an N-terminal myristoylation. (Potential) glycosylation sites are indicated with (Y). Schematics from: Stefan Seitz.

### 1.2.3.1. HBV envelope proteins and preS1-derived lipopeptides

The viral envelope includes three forms of transmembrane proteins, the large (L), middle (M) and small (S) protein, which are incorporated together with host lipids during virus budding into the endoplasmic reticulum (ER). The L, M and S proteins are present on Dane particles in a ratio of about 1:1:4 (Heermann et al. 1984). Spheres contain M and S proteins at a ratio of about 1:2 and only trace amounts of L, whereas filaments contain approximately equal amounts of M and L. All three envelope proteins are derived from one single open reading frame (ORF) and therefore share their C-terminal S-domain (see Figure 2).

The M protein comprises an N-terminal extension (preS2) of 55 amino acids, and the L protein is further elongated by additional 108 to 119 amino acids, depending on the genotype. The latter domain is referred to as preS1 region.

The S domain bears a potential N-glycosylation site at position N-146 which is used only partially. A second potential N-glycosylation site is located at position N-4 in the preS2 domain. Because of the cytosolic orientation of the preS2 domain during protein synthesis, this site is modified only in the M protein but not in the L protein. Threonine located at position 37 in the preS2 domain is O-glycosylated in both, the L and M protein.

Another important modification that is common for probably all hepadnaviral L proteins is the N-terminal myristoylation (Persing et al. 1987). Cytoplasmic N-myristoyl transferases recognize a sequence within the 9 N-terminal amino acids and co-translationally attach myristate, a 14-carbon saturated fatty acid, to glycine at position 2.

The role of the S protein in HBV entry is only partially understood. It is known that antibodies directed against the antigenic loop of the S protein can block an infection *in vivo* and *in vitro*, indicating that this part is involved in viral entry (Iwarson et al. 1985; Shearer et al. 1998). However, proteolytic removal of the preS1 regions from HBV particles results in a loss of infectivity. The S protein therefore is needed, but not sufficient for HBV entry.

In contrast to the M protein, the L protein is absolutely essential for the viral infectivity. Particularly important are the first 77 amino acids (Le Seyec et al. 1999) and the N-terminal myristoylation (Gripon et al. 1995). The L-protein can exist in a dual topology that either exposes its preS1-part to the inner or the outer phase of an HBV particle.

Interestingly, it has been shown that synthetic peptides comprising an N-terminal part of the preS1 region can specifically inhibit HBV infection *in vitro* and *in vivo* (Gripon et al. 2002; Joerg Petersen et al. 2008). Comprehensive studies using recombinantly or synthetically produced peptides showed that the first 8 amino acids (19 amino acids in genotype A) and the residues 19 to 28 are dispensable for infection inhibition. Residues 29 to 48 enhance the inhibitory activity, and the sequence between amino acids 9 and 15 is absolutely essential (Gripon et al. 2005; Schulze et al. 2010). Even minor changes, like the substitution of L- amino acids with their respective enantiomeric D- forms, lead to a complete loss of activity. Correlating to that, recombinant HBV particles carrying mutations in the positions 11 to 13 are noninfectious (Engelke et al. 2006). This and its high conservation among all HBV genotypes indicate an important role of the essential region 9-NPLGFFP-15 in receptor binding.

Also the N-terminal myristoylation is required for both, inhibitory activity of the peptide and infectivity of the virion. While removal of the acylation enhances the  $IC_{50}$  of synthetic peptides by a factor of  $\sim 1000$ , elongation of the fatty acid chains led to a reduction of the  $IC_{50}$ . A detailed

mutational analysis of the sequence requirements of preS1-mediated receptor binding has recently published by (Schulze et al. 2010).

### 1.2.3.2. The liver tropism of HBVpreS/2-48<sup>myr</sup>

Pharmacokinetic studies of uPA/RAG-2 mice that were transplanted with susceptible primary hepatocytes from *Tupaia belangeri* showed that HBVpreS-derived lipopeptides (HBVpreS/2-48<sup>myr</sup> and HBVpreS/2-48<sup>stea</sup>) accumulate in the liver of those animals. Surprisingly, no preferential accumulation of HBVpreS/2-48<sup>myr</sup> in regions enriched in susceptible hepatocytes was detected (Petersen et al. 2008).

A comprehensive pharmacokinetic study of a set of mutant preS1 peptides revealed a tropism for the liver of normal mice and rats that completely correlated with the inhibitory activity on HBV infection (Alexa Schieck, diploma thesis) (see Figure 3). While the wild type peptide accumulated in the liver with a high efficacy, the same mutations that resulted in a loss of activity also led to a loss of liver specificity. Biodistribution experiments revealed that a peptide in which an amino acid in the essential region was mutated (G12E) was distributed over all organs. A non-myristoylated peptide (HBVpreS/1-48) was excreted from the body within 4 hours.

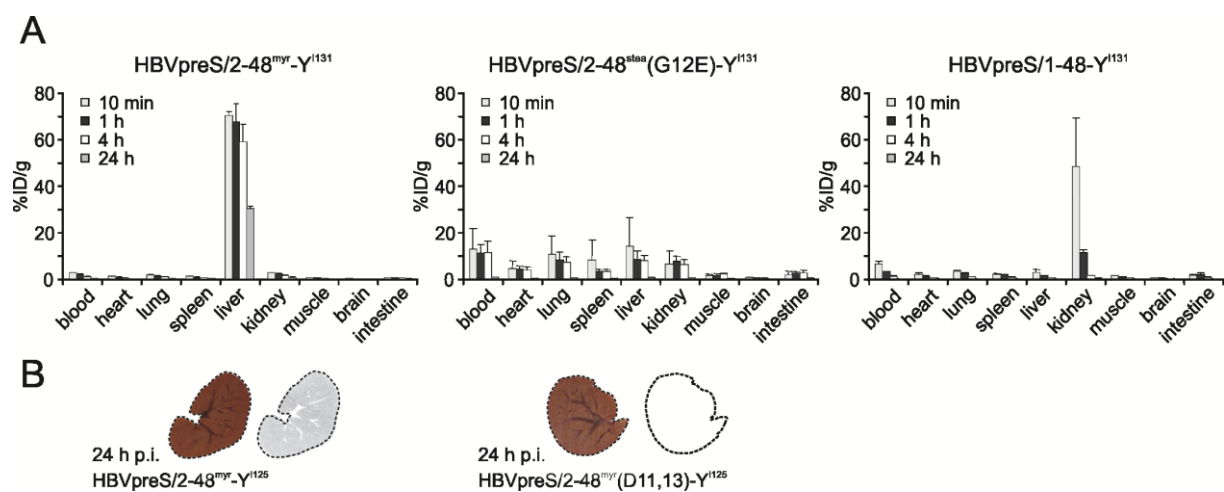


**Figure 3: The biodistribution of HBVpreS/2-48<sup>myr</sup> and inhibitory inactive mutants in mice.** (A) NMRI mice were injected i.v. with a radioactively labeled (-Y<sup>131</sup>) HBV-inhibitory peptide HBVpreS/2-48<sup>myr</sup> (left), an inactive mutant HBVpreS/2-48(G12E)<sup>stea</sup> (middle) and a non-myristoylated peptide HBVpreS/1-48 with a 1000-fold higher IC<sub>50</sub> (right). Organs were harvested from 3 animals per time point and radioactivity was measured in a  $\gamma$ -counter. (B) Autoradiography of liver sections was performed 24 h p.i. of iodinated HBVpreS/2-48<sup>myr</sup> (left) or the inactive derivative HBVpreS/2-48<sup>myr</sup>(D11,13) (right). Data: Alexa Schieck.

These findings showed that HBVpreS/2-48<sup>myr</sup> is specifically retained in the liver of even non-susceptible animals. The complete correlation of the requirements for an inhibitory activity on HBV infection with that for a liver tropism of the peptide indicated that HBVpreS/2-48<sup>myr</sup> binds to a specific factor that is expressed in the liver and plays an essential role in HBV entry. It is clear that primary human and *Tupaia* hepatocytes, as well as HepaRG cells express such a factor, since infection

of these cells can be inhibited with HBVpreS/2-48<sup>myr</sup>. However, these data do not allow us to exclude the presence of this factor also on non-parenchymal cells.

These findings furthermore suggested a role of the preS1 part for the liver tropism of HBV virions. The impact of respective mutations on the liver tropism of virus particles remains to be tested.

#### 1.2.4. The HBV replication cycle

##### 1.2.4.1. HBV entry and cell culture systems

The early steps of HBV infection are not well understood. Investigations towards HBV entry have been hampered by the lack of suitable cell culture systems. Studies were limited to the use of primary hepatocyte cultures from human or *Tupaia belangeri*.

In 2002, Gripon et al. described the first human hepatoma cell line HepaRG susceptible to HBV infection as a result of an *in vitro* differentiation process. The HepaRG cell culture system is based on a differentiation process that is induced by DMSO and, additionally, hormones. This cell line is derived from a liver tumor of a chronically infected HCV patient. In contrast to other hepatoma cell lines (e.g. HepG2, Huh7), HepaRG cells exhibit only a few major chromosomal rearrangements, are pseudodiploid and therefore much less likely altered (Gripon et al. 2002b).

HepG2 cells have been described as permissive after treatment with DMSO (Bchini et al. 1990; Paran et al. 2001), but these data could not be affirmed by others. However, transfection of different HepG2- or HuH7-derived hepatoma cell lines with an overlength HBV genome led to the production of infectious virions (Sells et al. 1987; Sureau et al. 1986; Tsurimoto et al. 1987; Shih et al. 1989), indicating that the refractoriness of these cells has to be attributed to an earlier step of infection. In HepG2 cells for example, a restricted nuclear import of HBV capsids has been supposed (Qiao et al. 1994), or an overexpression of serine protease inhibitor Kazal (SPIK) (Lu & Block 2004).

A major drawback of the use of primary hepatocyte cultures is that they lose their susceptibility within the first days after isolation (Gripon et al. 1988). This probably is due to a process referred to as dedifferentiation. It has been observed that a number of liver-specific functions are progressively lost with time when hepatocytes are isolated and cultivated (review Elaut et al. 2006). These phenotypic changes are primarily the result of fundamental changes in gene expression concomitant with a diminished transcription. Discussed inducers for a dedifferentiation are e.g. the stress during perfusion and isolation, the disruption of the normal tissue architecture and the adaptation to the conditions *in vitro*. This process can be slowed down by the presence of DMSO, a widely used differentiating agent that has been shown to induce a hepatocyte arrest in the cell cycle phase G1 (Cable & Isom 1997).

HBV binding components have been isolated from plasma membranes of primary hepatocytes or hepatic cell lines (e.g. HepG2), but none of these potential binding factors has convincingly been

shown to be essential for HBV infection. An overview about molecules discussed as potential HBV receptors is given in a review by (Glebe & Urban 2007). Until now, the only reliable study towards HBV binding factors has been described by (Schulze et al. 2007), demonstrating that glycosaminoglycans serve as primary attachment factors for HBV.

Also the entry pathway of HBV is poorly understood. A recent study suggested a caveolae-dependent entry of HBV in HepaRG cells stably expressing dominant-negative forms of caveolin-1 and dynamin-2 (Macovei et al. 2010). However, direct evidence for a role of these molecules for virus uptake was not presented. The use of chemical compounds to inhibit cellular functions such as functional endocytosis, acidification of endosomes or integrity of the cytoskeleton has been described widely to investigate viral entry mechanisms. These experiments, however, strongly manipulate natural cellular processes, so that secondary effects cannot be excluded and results have to be interpreted with caution.

#### 1.2.4.2. Post-entry steps of an HBV infection

After fusion of the viral and a cellular membrane, the nucleocapsid is released into the cytoplasm. It then is transported to the nucleus, where a nuclear localization signal in the N-terminal region of the core protein facilitates nuclear import (Kann et al. 1999). Within the nuclear pore capsids dissociate and the viral genome (rcDNA) is released into the nucleoplasm (Rabe et al. 2003). After repair of the partially double stranded rcDNA genome, covalently closed circular DNA (cccDNA) is formed and transcribed by the cellular RNA polymerase II. Posttranscriptional regulation does not involve splicing, but regulation of the transport of viral transcripts from the nucleus into the cytoplasm by a posttranscriptional regulatory element (PRE), where translation of the viral mRNAs takes place.

Packaging of the pre-genomic RNA (pgRNA) is induced by binding of the viral polymerase to the packaging signal  $\epsilon$  located at the 5'-end of the pgRNA. This interaction leads to the recruitment of core proteins and assembly of the nucleocapsid. Within the nucleocapsid, maturation of the pgRNA is achieved by reverse transcription to obtain rcDNA. Mature nucleocapsids can either be re-imported to the nucleus, enhancing the cccDNA pool, or bud to a post-ER/ pre-Golgi compartment to be secreted.

In contrast to HDV budding, that involves an association of a C-terminal proline/ glycine-rich domain of the large delta antigen with a tryptophan-rich region in the cytosolic loop of HBV S-protein (Komla-Soukha & Camille Sureau 2006), the budding of HBV is poorly understood. It is assumed that the HBV nucleocapsid interacts with an L-protein isoform that exposes the N-terminal part at the cytosolic side of the membrane (Bruss 2004).

In the ER membrane, HBV surface proteins tend to accumulate posttranslationally in microdomains. If a critical density is reached, budding of particles can take place even in absence of nucleocapsids. This results in the constitutive secretion of subviral spheres and filaments.

### 1.3 Epidemiology and pathogenesis

HBV is transmitted by a parenteral infection. The main routes of infection are perinatal transmission, blood and percutaneous transmission, and sexual transmission.

Although safe vaccines are available, more than 1/3 of the current world population shows serological markers of an HBV infection and about 350 million people live with a chronic infection (WHO, revised August 2008). Hepatitis B is endemic in China, other parts of Asia and in Africa. In these regions, most infections occur perinatally or during the early childhood. The prevalence of HBV infection is shown in Figure 4.

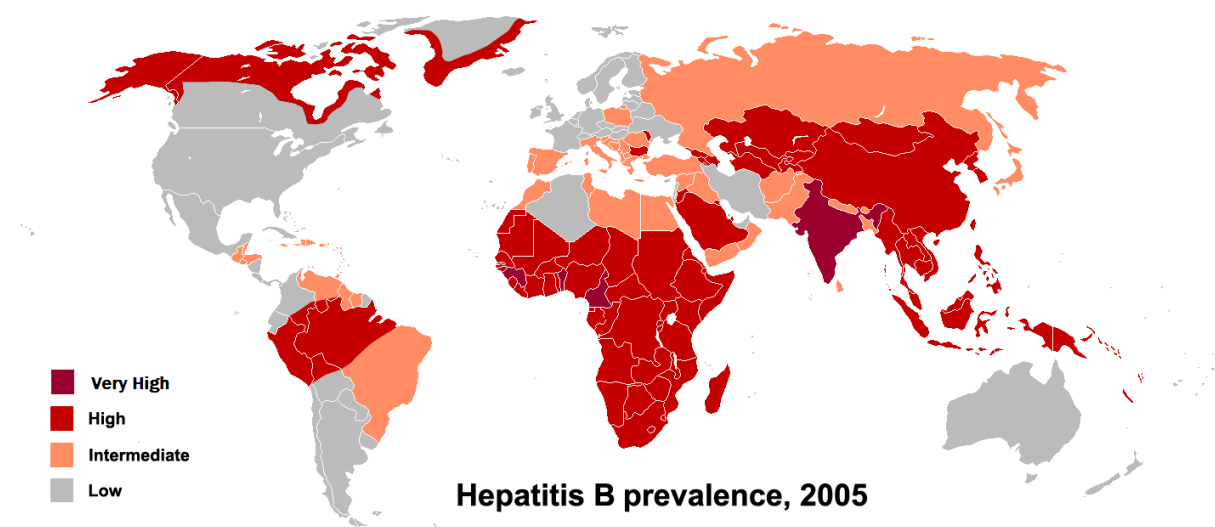


**Figure 4: Geographic distribution of HBsAg prevalence.** (From: CDC Traveler's Health, Yellow Book 2007).

Each year over 1 million people die from HBV-related chronic liver disease, including cirrhosis and hepatocellular carcinoma (HCC). HCC is one of the most common types of cancers worldwide, and HBV is responsible for at least 75 % of all cases.

The severity of an HBV infection depends on different factors like e.g., the age at the time point of infection, the presence of co-infections with HCV, HIV or HDV, and alcohol consumption. 65 % of infected healthy middle-aged people do not show symptoms after HBV infection, whereas about 35 % develop acute hepatitis that in most cases (90 - 95 %) cures. The most typical symptom of an acute hepatitis is jaundice. However, 5 - 10 % of hepatitis B patients develop a chronic infection that in up to 1/3 of all cases can lead to a chronic liver inflammation. Chronic hepatitis B often results in HCC.

The likelihood that an HBV infection will become chronic rises with younger ages. About 90 % of infants infected during the first year of life develop a chronic infection.

HBV replicates almost exclusively in hepatocytes and is noncytopathic. The pathogenesis of a chronic infection is credit to a reaction of the immune system that is based on the recruitment of cytotoxic T-

cells due to antigen presentation. T-cells in turn can recruit macrophages and neutrophils that induce an inflammation in the liver.

## 1.4 Therapy

For an acute hepatitis B there is no specific treatment. Symptoms can be relieved but a curative antiviral therapy generally is not applied. Chronic hepatitis B, in contrast, needs treatment aiming to stop progression of the disease and to improve the functions of a potentially damaged liver. Several effective drugs are available, but a complete clearance of an HBV infection is rare.

### 1.4.1. Immune system modulators

A widely known modulator of the immune system is interferon- $\alpha$  (IFN- $\alpha$ ). Treatment for several months can achieve an HBeAg seroconversion in 30 - 40 % of the patients. Response to IFN- $\alpha$  differs between HBV genotypes (Erhardt et al. 2005). Whereas genotypes A and B show good response (in 40 - 45 % of the cases) genotypes C and D show a seroconversion rate of only 15 - 25 %. In immunotolerant hepatitis B patients, the response is very poor (9 %).

The use of IFN- $\alpha$ , that in some cases requires daily injections, has lately been supplanted by a new derivate. By covalent attachment of polyethylenglycol (PEG), the serum half life time of IFN- $\alpha$  could be enhanced up to 10-fold. PEGylated IFN- $\alpha$  (PEG-IFN- $\alpha$ ) therefore needs only one administration a week. Both drugs have been shown to achieve comparable results, but due to the more comfortable application the use of PEG-IFN- $\alpha$  is preferred.

A major drawback of the treatment with interferon is the severity of side effects. Besides a dose-dependent incidence of flu-like symptoms, adverse effects include e.g. bone marrow suppression and psychiatric complications.

### 1.4.2. Antiviral drugs

Nucleoside or nucleotide analogues compete with naturally occurring purines and pyrimidines for binding to the HBV DNA polymerase. Nucleotide analogues consist of a base, a sugar moiety and a phosphate residue, whereas nucleoside analogues lack the phosphate residue. These drugs block replication by terminating the polymerase reaction.

Unlike interferon, nucleos(t)ide analogues are well tolerated by patients with hepatitis B and significant improvement of hepatic synthetic function has been documented. The most frequently used drugs are lamivudine, adefovir, entecavir, telbivudine and tenofovir. Among those the three latter are most potent in HBV DNA suppression.

Nucleos(t)ide analogues can be applied also in long-term therapy. Unfortunately, the effectiveness and durability of response is compromised by the emergence of mutations in the HBV DNA polymerase. This leads to selective drug resistances. The risk of an emergence of drug-resistant mutants increases primarily with the duration of the therapy. Lamivudine is associated with the highest rate of resistance, reaching approximately 70 % by year four of treatment (Lok et al. 2001).

Combination therapies using lamivudine and PEGylated interferon- $\alpha$ , or a combination of nucleoside and nucleotide analogues have been described, but there is only limited data on the efficacy of these therapies.

In the last years, a new class of non-nucleos(t)ide inhibitors has been described. Heteroaryldihydropyrimidine and other derivatives act as allosteric effectors that deregulate capsid assembly (Deres et al. 2003). *In vitro*, it leads to the formation of aberrant capsid particles and to the dissociation of metastable HBV capsids (Stray et al. 2005). *In vivo*, this mechanism is assumed to deplete the pool of core protein available for virion assembly. Alkylated imino sugars, like n-(n-Nonyl)-deoxygalactonojirimycin, have been shown to possess an antiviral activity on HBV (Mehta et al. 2001) by destabilization of HBV capsids or prevention of their maturation (Lu et al. 2003).

#### 1.4.3. HBV preS-derived lipopeptides as entry inhibitors

Based on the study of the preS1-requirement for HBV infection, a region encompassing the N-terminal amino acids 2 to 77 of the L protein has been found to be essential (Le Seyec et al. 1999). Another study described an N-terminally myristoylated peptide comprising this region (HBVpreS/2-78<sup>myr</sup>), that blocked HBV infection on PHH and HepaRG cells (Gripon et al. 2002). Interestingly, this sequence includes epitopes for monoclonal antibodies (e.g., MA18/7 or 5a19) that block the binding of HBV particles to PHH (Maeng et al. 2000) and HepG2 (Neurath et al. 1986), and neutralize HBV infection on PTH (Glebe et al. 2003). These findings led to the investigation of the ability of preS1 sequences to inhibit HBV infection.

HBVpreS/2-48<sup>myr</sup> has been described as the prototype of inhibitory peptides that block HBV infection *in vitro* and *in vivo* with high specificity and efficacy (Gripon et al. 2005; Petersen et al. 2008). A study towards the pharmacokinetic behavior of this peptide has been described above. As a first-in-class HBV entry inhibitor HBVpreS/2-48<sup>myr</sup> ("Myrcludex B") is currently being developed for clinical use. The thesis presented here will give some insights into pharmacodynamic features of Myrcludex B - derivatives.

## 2. Materials and Methods

### 2.1 Materials

#### 2.1.1. Eukaryotic cells

##### 2.1.1.1. Cell lines

Cell line	Description	Reference
HEK 293-T	human embryonic kidney cells, transformed with the SV40 large T-antigen	DuBridgE et al., 1987
HepAD38	stably transfected derivative of HepG2, tetracyclin-inducible virus producer cell line	Ladner et al., 1997
HepaRG	human hepatoma cell line that can be differentiated	Gripon et al., 2002
HepG2	human hepatoma cell line	ATCC# HB-8065
HuH7	human hepatoma cell line	JCRB# 0403

##### 2.1.1.2. Primary cells

#### Cryopreserved hepatocytes

Species	Description	Batch	Ordering number	Company/Origin
Cynomolgus monkey hepatocytes	Male Cynomolgus Monkey	LOT C8	454930	BD Gentest
	Male Cynomolgus Monkey	LOT C10	454930	BD Gentest
	Male Cynomolgus Monkey	LOT JNM	M00305	Celsis
Dog hepatocytes	Male Beagle Dog	LOT OES	M00205	Celsis
	Male Beagle Dog	LOT DXB	M00205	Celsis
Human hepatocytes	no information	#349	-	HepaCULT
	no information	#431	-	HepaCULT
	no information	#357	-	HepaCULT

	no information	#636	-	HepaCULT
Pig hepatocytes	Male Gottingen Minipig	LOT XNG	M00615	Celsis
Rabbit hepatocytes	Male New Zealand White Rabbit	LOT ()MC	F00405	Celsis
	Female New Zealand White Rabbit	LOT TAH	M00405	Celsis
Rat hepatocytes	Male Rat (Sprague Dawley)	LOT 06830	454701	BD Gentest
	Male Rat (Sprague Dawley)	LOT 11316	454701	BD Gentest
Rhesus monkey hepatocytes	Male Rhesus Monkey	LOT YUL	M00315	Celsis
Tupaia hepatocytes	Female Tupaia Belangerii	PD Dr. J. Petersen, University Hospital Hamburg-Eppendorf		

### Freshly isolated hepatocytes

Species	Description	Age	Company/ Origin
Mouse hepatocytes	Female NMRI	52 - 77 days	Charles River
Rat hepatocytes	Female Sprague Dawley	8 - 12 weeks	Charles River
Woodchuck hepatocytes	no information	no information	Prof. Dr. M. Roggendorf, University Hospital Essen

#### 2.1.2. Cell culture media

Description	Use	Basic medium	Supplements
PMH I	Attachment medium for PMH	Williams E	10 % FCS 50 U/ ml penicillin 50 µg/ ml streptomycin 2 mM L-glutamine
PMH II	Cultivation medium for PMH	Williams E	As PMH I, without 10 % FCS
PHH I	Attachment medium for PHH	Williams E	10 % FCS 50 U/ ml penicillin 50 µg/ ml streptomycin 50 µM hydrocortisone-

			hemisuccinate 5 µg/ml insuline 2 mM L-glutamine
PHH II	Cultivation medium for PHH	Williams E	As PHH I, without 10 % FCS
PHH II + DMSO	Cultivation medium for PHH	Williams E	As PHH II, additionally 2 % DMSO
HepaRG	Cultivation medium for HepaRG cells	Williams E	50 U/ ml penicillin 50 µg/ ml streptomycin 50 µM hydrocortisone- hemisuccinate 5 µg/ml Insuline
HepaRG diffmed	Differentiating medium for HepaRG cells	Williams E	As HepaRG, additionally 0.5 - 2 % DMSO
HepAD38 (tet on)	Cultivation medium for HepAD38	DMEM/F-12	10 % FCS 50 U/ ml penicillin 50 µg/ ml streptomycin 400 µg/ ml G418 50 µM hydrocortisone- hemisuccinate 0.3 µg/ ml tetracycline
HepAD38 (tet off)	Induction medium for HepAD38 virus production	DMEM/F-12	As HepAD38 tet on, without tetracycline
HepG2	Cultivation medium for HepG2	Williams E	10 % FCS 50 U/ ml penicillin 50 µg/ ml streptomycin 2 mM L-glutamin
Huh7	Cultivation medium for Huh7	DMEM	10 % FCS 50 U/ ml penicillin 50 µg/ ml streptomycin 2 mM L-glutamin
Leibovitz's	CO <sub>2</sub> - independent medium without phenol red for live cell imaging	Leiboviz L-15	50 U/ ml penicillin 50 µg/ ml streptomycin

## 2.1.3. Chemicals and reagents

<b>Compound</b>	<b>Company</b>
Acetic acid	Merck
Acrylamide/ Bisacrylamide (29:1)	Serva
Agarose, UltraPure™	Invitrogen
Alexa Fluor 488, succinimidyl ester	Invitrogen
Ammonium persulfate (APS)	Grüssing
Ampicillin	Sigma
Atto 565, maleimide	ATTO-TEC
Aqua ad iniectabilia	Braun
Bacto™ agar	BD
Bovine serum albumin (BSA), fraction V, ≥ 98 %	Roth
Bromophenol blue	Chroma
CitiFluor CFPVOH, aqueous poly vinyl alcohol	Agar Scientific
CitiFluor AF100, antifadent-PBS solution	Agar Scientific
Collagenase, type IV, 839 units/ mg	Sigma-Aldrich
DAPI (4',6'-Dianidin-2-phenylindol)	Roche
Dimethyl sulfoxide (DMSO), for spectroscopy	Merck
Disodium hydrogen phosphate dihydrate (Na <sub>2</sub> PO <sub>4</sub> 2H <sub>2</sub> O)	J.T.Baker
Dithiothreitol (DTT), molecular biology grade	Fermentas
Dulbecco's modified eagles medium (DMEM)	Gibco
Easycoll Separating Solution, 1.124 g/ ml	Biochrom
Ethanol	Riedl-de-Haën
Ethidium bromide	Sigma
Ethylenediaminetetraacetic acid (EDTA)	Roth
FastPlasmid Mini Kit	5Prime
Fetal calf serum (FCS)	PAA, Biowest
Glutamine, L-	Invitrogen
Glu-c (V8 protease)	Merck
Glycerine	Roth
Glycin	Applichem
Hydrogen chloride (HCl)	Merck
Hydrocortison-hemisuccinate	Sigma

---

Incidin Special Spray	Ecolab
Insulin	Sigma
Isopropyl alcohol	AppliChem
Leibovitz's medium, L-15 (without phenol red)	Gibco
Loading dye, 6x	MBI
Methanol	J.T.Baker
Megaprime™ DNA labeling system	GE Healthcare
Milk powder	Roth
Orange G	Sigma
Paraformaldehyde (PFA)	Sigma
P <sup>32</sup> dCTPs	Perkin Elmer
Phosphate buffered saline (PBS 10x), pH 7.2	Gibco
Penicillin (5000U/ml), Streptomycin (5000µg/ml)	Gibco
PerfectPrep Endofree Plasmid Maxi Kit	5Prime
Polyethylenglycol 8000 (PEG)	Merck
Polyethylenimine (PEI)	Sigma
Polyvinylpyrrolidone	Merck
Potassium chloride (KCl)	J.T.Baker
Potassium dihydrogen phosphate (KH <sub>2</sub> PO <sub>4</sub> )	Gerbu
Qiagen Midi Plasmid Kit	Qiagen
Qiaquick Gel Extraction Kit	Qiagen
Silver nitrate (AgNO <sub>3</sub> ), 99 %	Acros Organics
Sodium azide (NaN <sub>3</sub> )	Riedel-de-Haën
Sodium chloride (NaCl)	Grüssing
Sodium citrate	Sigma
Sodium dodecyl sulfate (SDS)	Serva
Sodium hydroxide (NaOH)	J.T. Baker
Standard culture-medium	Merck
Sucrose	Roth
Tetramethylethylenediamine (TEMED)	Roth
T4 Ligase buffer (10 x)	New England Biolabs
Tris(hydroxymethyl)aminomethane (Tris)	Roth
Triton® X-100	Merck
Trypsin, with or without phenol red	Gibco
Tween® 20	Roth

Vectashield® Mounting Medium with DAPI	Linaris
William's medium E	Gibco

#### 2.1.4. Consumables

Name	Company
96-well plate, flexible, Polyvinylchlorid	BD Falcon
Centrifuge Tubes (Ultra- clear, 11x 60 mm)	Laborgeräte Beranek
Cell culture flask (T 75cm <sup>2</sup> )	Corning
Cell culture plate (12- well)	Corning
Column (Microspin™ G-25)	GE Healthcare
Cover slips	Marienfeld GmbH
Lab-Tek chambered coverglass (8 well)	nunc
Microassay plate (black, clear bottom)	Greiner
μ-dishes (35 mm, high)	ibidi
Nitrocellulose Membrane	Schleicher & Schuell
Nylon-Membrane (positively charged)	Roche
Objective slides	Corning, Thermo Scientific
Pasteur pipettes	WU Mainz
Parafilm	Pechiney Plastic Packaging
Petri dishes	Greiner Bio-one
Pipette tips	Star Lab
Pipette tips filtered	Star Lab
Reaction tubes (1,5 ml, 2 ml)	Sarstedt
Reaction tubes (for AxSYM, 2 ml)	Sarstedt
Reaction tubes (0,2 ml)	Biozym
Serological pipettes (5 ml, 10 ml, 25 ml)	Corning
Tubes (15 ml, 50 ml)	Greiner
Whatman paper	Whatman

## 2.1.5. Technical equipment and instruments

<b>Apparatus</b>	<b>Manufacturer</b>
Camera CyberShot DSC S75	Sony
Centrifuge, Multifuge® 3-SR	Heraeus
Centrifuge, Fresco 21 and Biofuge pico (table top centrifuges)	Heraeus, Thermo Scientific
Centrifuge (J2-21 M/E)	Beckman
Electrophoreses Power Supply (EPS 500/400, EPS 3500)	Pharmacia Monacor
Electron multiplying charge coupled devices (EM-CCD cameras)	Hamamatsu
- C9100-50	Hamamatsu
- ORCA-AG	
Flow cytometers	
- FACS Calibur	BD
- FACS Canto II	BD
Fraction recovery system	Beckman
Freezer (-80°C)	NAPCO
Fridge/ Freezer (4°C, -20°C)	Liebherr
Gel chambers for SDS -PAGE	Amersham Pharmacia
Glassware	Schott
Heat block (Ori-Block OB-3)	Techne
Hybridization oven (BFED 23)	Binder GmbH
Ice machine (MF-30 AS)	Scotsman
Incubator (37°C, CO <sub>2</sub> )	Heraeus, Thermo scientific
Incubator shaker	Gallenkamp
Licor Odyssee	Licor
Magnet stirrer	IKA
Microwave	Daewoo
Microscopes	
- Spinning Disk confocal ERS-FRET on TE2000 inverted	Perkin Elmer, Nikon
- Total Internal Reflection Fluorescence on Ti inverted	Perkin Elmer, Nikon
- Axiovert 25	Zeiss
Laminar airflow cabinet	Napco, The Baker Company

Minifold Dot blot system (96-well)	Whatman
Multichannel Pipette (P200)	Eppendorf
Neubauer Counting Chamber (Improved 0.1 mm, 0.0025 mm <sup>2</sup> )	Assistent Germany
pH-meter (632)	Metrohm
Phosphor-Imager, FX	Bio-Rad
Pipettes (P20, P200, P1000)	Gilson
Pipette (P2)	Eppendorf
Pipettors	Brand
Plates for SDS-PAGE (glass and alumina plates)	Amersham Pharmacia
Printer (P91, for agarose gel pictures)	Mitsubishi
Pump	Vaccuubrand
Scale	Kern
Spectrophotometer (Nanodrop 1000 UV-VIS)	Thermo scientific
Thermomixer comfort	Eppendorf
Transfer chamber (SD Transfer Cell)	Bio-Rad
Ultracentrifuge (Discovery 90SE)	Sorvall
Ultracentrifuge rotors (SW-60, TH641)	Sorvall
UV-table and lamp	M&S Laborgeräte
Vortexer	Neolab
Water bath	Medingen, B. Braun

#### 2.1.6. Special software

<b>Name</b>	<b>Company</b>
CellQuest Pro	BD
CorelDraw Graphics Suite	Corel
FACSDiva	BD
GraphPrism	GraphPad
ImageJ	(open source program)
NIS elements	Nikon
Odyssey	Licor
Photoshop	Adobe
SigmaPlot	Systat Software

---

Virtual Dub	Open source
Volocity	Perkin Elmer
Volocity Demo	Perkin Elmer
Quantity One	BioRad

---

## 2.2 Methods

### 2.2.1. Cell culture

All cell culture works were performed sterile under a laminar flow.

#### 2.2.1.1. Cultivation of cell lines

All cell lines were cultivated at 37°C, with a humidity of 95 % and 5 % CO<sub>2</sub>.

Experiments utilizing the hepatoma cell lines HepG2 and HuH7, and the cell line 293T were performed after passaging these cells in culture no more than 30 times. For passaging, cells were detached from the substrate by trypsin treatment, and diluted 10- to 20-fold in new cell culture flasks.

Undifferentiated HepaRG cells were passaged by 5-fold dilution every 2 weeks. To induce differentiation, HepaRG cells were seeded at a density of  $1.25 \times 10^6$  cells/ well (12-well) and differentiation was performed as described in Gripon et al. (2002).

#### 2.2.1.2. Preparation and cultivation of freshly isolated primary hepatocytes

##### Primary hepatocytes from mice or rats

Primary mice or rat hepatocytes were prepared from 52 - 77 days old mice or 8 - 12 weeks old rats, respectively. Described here is the isolation of liver cells from mice, numbers or descriptions in brackets indicate the respective volumes or instructions for the isolation of hepatocytes from rats.

NMRI mice (Sprague dawley rats) were killed by cervical dislocation (CO<sub>2</sub>) and the abdomen was opened to expose the liver. A catheter 24G (20G) was carefully inserted into the *Vena cava inferior* and connected to a peristaltic pump. The pump was switched on with a flow rate of 5 - 8 ml/ minute (20 ml/ minute) and immediately after starting the pump, the *Vena portae* was cut to facilitate a retrograde perfusion of the liver. The liver was perfused for at least 5 (10) minutes with EGTA-buffer and afterwards perfused for additional 5 - 10 (at least 10) minutes with collagenase-buffer. Both buffers were pre-warmed in a waterbath to 42°C. After perfusion, the liver was carefully removed and transferred to the remaining collagenase-buffer.

Under a sterile laminar flow, the liver was suspended in collagenase-buffer by cautious pulling apart with sterile tweezers. The liver capsule and, if necessary, the gall bladder were removed and the liver cell suspension was strained through a 100 µm mesh. The cells were collected by centrifugation for 5 (10) minutes at 28 x g and 4 °C. The cell pellet was resuspended in 19 (28) ml Percoll® solution with a density of 1.063 g/ ml, and centrifuged for 10 (20) minutes at 50 x g at 4°C without brake. This step allowed the separation of parenchymal from non-parenchymal cells. Due to the bigger size of the parenchymal cells, the hepatocytes sedimented more quickly compared to other liver cells. Percoll® strengthened this effect. After centrifugation, the supernatant was removed and the resulting pellet, containing purified hepatocytes, was washed with cold William's E medium to get rid of remaining Percoll®. Cells were re-collected by centrifugation for 5 (10) minutes at 28 x g and 4 °C.

If the cells were destined for peptide binding studies in solution, the pellet was resuspended in the respective peptide binding solution, i.e. PMH II, PHH II or HepaRG Diffmed. The final cell suspension was checked for viability and the cell number by trypan blue exclusion.

If the cells were destined for microscopical analysis, the hepatocytes were seeded on cover slips that had been coated with 0.1 mg/ ml rat tail collagen over night. Seeding was performed in the respective attachment-medium, i.e. PMH I or PHH I, using the respective densities listed in table below.

---

### Buffers

---

EGTA perfusion buffer	2 mM L-Glutamine, 0.5 % Glucose, 25 mM HEPES, 2 mM EGTA, pH7.4 → diluted in PBS, sterile
Collagenase perfusion buffer	2 mM Glutamine, 0.5 % Glucose, 25 mM HEPES, 3 mM CaCl <sub>2</sub> , 3 mg/ ml Collagenase type IV → diluted in plain Williams E, sterile filtered

### Primary human hepatocytes

PHH were obtained by Thomas Weiss, University Hospital Regensburg. The cells were isolated and cultivated in serum-free medium as previously described (Weiss et al. 2003). Tissue samples from liver resections were obtained from patients undergoing partial hepatectomy for metastatic liver tumors of colorectal cancer. Experimental procedures were performed according to the guidelines of the charitable state controlled foundation HTCR (Human Tissue and Cell Research), with the informed patient's consent approved by the local ethical committee of the University of Regensburg.

The PHH were shipped on ice in “cell maintenance medium”. Upon arrival, the cells were diluted with cold PHH I and collected by centrifugation for 3 minutes at 100 x g, 4°C. The cell pellet was resuspended in PHH I (or PHH II for experiments with cells in solution) and cell viability and number was determined by trypan blue exclusion. Cells were seeded on collagen-coated coverslips with the density given in the table below.

Cell type	Seeding density (cells/ cm <sup>2</sup> )	Number of cells/ well (12-well plate)
PMH	0.5 x 10 <sup>5</sup>	0.2 x 10 <sup>6</sup>
PRH	0.5 x 10 <sup>5</sup>	0.2 x 10 <sup>6</sup>
PHH	0.15 x 10 <sup>6</sup>	0.58 x 10 <sup>6</sup>

#### 2.2.1.3. Thawing and handling of cryopreserved hepatocytes

Cryopreserved hepatocytes were delivered frozen in liquid nitrogen or, for PHH and PTH, on dry ice. After arrival, the cells were thawed quickly in a waterbath at 37°C and diluted in 9 ml cold PMH II medium. To recover cells and to remove toxic substances from the freezing medium, cells were centrifuged for 3 minutes at 100 x g and 4°C (or room temperature). The cell pellet was carefully resuspended in PMH II (or a respective medium), and the number and viability of the cells was determined by trypan blue exclusion.

#### 2.2.1.4. HBV infection of HepaRG cells

For an infection with HBV, HepaRG cells were seeded in a 12-well cell culture dish. If not indicated differently, the infection was performed with a multiplicity of genome equivalents (MGE) of 1 x 10<sup>4</sup> GE/ cell. Cells were inoculated with PEG-precipitated stock virus (100-fold concentrated HepAD38 supernatant) in presence of 4 % PEG for approximately 16 hours at 37°C. Subsequently, the virus solution was removed, cells were washed thoroughly, and further incubated with fresh medium. The supernatant was collected from day 4 to 7, and day 7 to 12 after infection, and was analyzed for HBeAg and/ or HBsAg as markers for infection. HBeAg and HBsAg were measured by the commercial enzyme-linked immunoabsorbant assays (ELISA) AxSYM (formerly Architect) and Advia Centaur, according to the manufacturer’s protocol.

### 2.2.2. Peptide binding assays

#### 2.2.2.1. Peptide synthesis

All peptides were synthesized by Alexa Schieck and Thomas Müller (AG Mier, Department of Nuclear Medicine) by solid phase peptide synthesis employing the Fmoc/tBu strategy with HBTU/DIPEA

activation in an Applied Biosystems 433A peptide synthesizer. Fluorescein isothiocyanate was coupled to the  $\epsilon$ -amino group of an artificially introduced lysine at position 49. Alternatively, Atto565-maleimide was linked to an introduced cysteine at position 49. Preparative reversed phase high performance liquid chromatography was carried out using C-18 columns and applying a linear gradient from 100 % water to 100 % acetonitrile in 0.1 % trifluoroacetic acid. Preparations were analyzed using a Merck Chromolith® Performance RP-18e column (100 - 4.6 mm; flow rate of 4 ml/min) and purified by Chromolith® SemiPrep RP-18e column (100 - 10 mm; flow rate of 10 ml/min). The identity of the peptides was controlled by mass spectrometry.

#### 2.2.2.2. Peptide binding to adherent cell culture for microscopy

100  $\mu$ M stock solutions of the respective peptides in 2 % DMSO were diluted to the appropriate final concentration in medium without FCS (if not indicated differently). Cells that were grown on cover slips were incubated with 200 nM of the respective peptide for at least 1 hour at 37°C. After incubation, cells were washed thoroughly with PBS and fixed with 4 % PFA for 30 minutes at room temperature. Before embedding, the PFA was removed by washing the cells twice with PBS. Cover slips were mounted on object slides using mounting medium with DAPI (Vecta Shield Hart Set Mounting Medium with DAPI) or without DAPI (Citifluor AF-100) and stored at 4°C until performance of microscopy.

#### 2.2.2.3. Staining of the cells with Phalloidin-Alexa546 or Phalloidin-Alexa565

In order to visualize the actin cytoskeleton of hepatocytes or HepaRG cells, cells on cover slips were fixed and permeabilized with 0.1 % Triton X-100 in PBS for 20 minutes. Phalloidin-Alexa546/ -Alexa565 was added at 0.05 mg/ml in 0.1 % Triton X-100/ PBS for 15 minutes in the dark, washed with PBS and mounted on object slides as described above.

#### 2.2.2.4. Destruction of the actin cytoskeleton by cytochalasin D

To interfere with actin polymerization, cells grown on cover slips were incubated with 20 or 40  $\mu$ M cytochalasin D diluted in 500  $\mu$ l PMH II for 1 hour at 37°C. Subsequently, the drug was removed, cells were washed carefully with warm PMH II and supplied with 200 nM HBVpreS/2-48<sup>myr</sup>-K-FITC for 1 hour at 37°C. After peptide incubation, cells were washed and fixed as described above.

#### 2.2.2.5. Peptide binding to cells in solution for flow cytometry

For the flow cytometric analysis, freshly isolated or thawed cryopreserved hepatocytes were aliquoted to 0.4 - 0.5  $\times 10^6$  cells in Eppendorf cups or FACS vials. The cells were either pelleted for 3 minutes at 100  $\times$  g and 4°C, and the pellet was resuspended in an appropriate peptide dilution, directly supplied with pre-diluted peptide. Under frequent mixing (to avoid sedimentation), the

hepatocytes were incubated at room temperature for 30 minutes in the dark. The cells were then collected by centrifugation for 3 minutes, 100 x g, and washed 5 times with 1 ml PBS. The washed cells were resuspended in 500  $\mu$ l PBS and fluorescence was immediately measured by flow cytometry.

Flow cytometry of cryopreserved hepatocytes was performed on a FACS Calibur (BD) and the software CellQuest Pro (BD). Freshly isolated hepatocytes were analyzed at a FACS canto II (BD) using the software FACS Diva (BD).

In order to check cell viability, every experiment was controlled by staining the hepatocytes with propidium iodide (PI) in parallel. Therefore, an aliquot of  $0.4 \times 10^6$  cells/ml was incubated with PI, diluted in PMH II medium to a final concentration of 10  $\mu$ M. The cells were incubated for 30 minutes under frequent mixing at room temperature in the dark. Alternatively, a control stain using Hoechst 33342 dye at a concentration of 0.01 mg/ml was performed. The dye, entering live cells and binding to DNA, was added directly to the samples shortly before measurement.

#### 2.2.2.6. Competition assays using HBVpreS/2-48<sup>myr</sup>, heparin or suramin

Competition of binding with unlabeled peptide was performed by co-incubation of HBVpreS/2-48<sup>myr</sup>-K-FITC with a 100-fold excess of HBVpreS/2-48<sup>myr</sup>, or HBVpreS/2-48<sup>myr</sup>(D11,13) as a control. Cells were exposed to a mixture of both, fluorescently labeled and non-fluorescent peptide. (An exception is the experiment with hepatocytes from different species. Here, the competing agents were pre-incubated with the cells for 5 minutes before addition of the fluorescent peptide.) For fluorescence microscopy, 200 nM HBVpreS/2-48<sup>myr</sup>-K-FITC were co-incubated with a 50-fold excess (10  $\mu$ M) of the consensus sequence chHBVpreS/2-48<sup>myr</sup>. All cells were incubated for 0.5 - 1 hour at 37°C.

For competition experiments with heparin and suramin, heparin (600  $\mu$ g/ml) and suramin (200  $\mu$ g/ml) were mixed with 200 nM HBVpreS/2-48<sup>myr</sup>-K-FITC. The mixture was incubated for 30 minutes at 20°C with frequent mixing. Subsequently, the mixture was incubated with cells grown on cover slips for 1 hour at 37°C, washed and fixed.

#### 2.2.2.7. Protease digestion of surface proteins

Protease treatment of freshly isolated PMH was performed in serum-free PMH II. Glu-c was incubated with  $0.5 \times 10^6$  cells for 30 minutes at 37 °C at a final concentration of 40  $\mu$ g/ml and 80  $\mu$ g/ml, respectively. Trypsin was incubated in the same way at 0.005 % or 0.015 %.

After incubation the cells were washed excessively (5 times with 1 ml PBS) and HBVpreS/2-48<sup>myr</sup>-K-FITC was added at a concentration of 200 nM in PMH II.

#### 2.2.2.8. Quantification of HBVpreS/2-48<sup>myr</sup> on cells by HPLC-MS/MS

To determine the fraction HBVpreS/2-48<sup>myr</sup> bound to PRH, PHH and HepaRG cells, the samples were incubated with a dilution series of the peptide in HepaRG Diffmed and subsequently shipped to Prolytic GmbH in order to perform HPLC-MS/MS.

PRH were freshly prepared and PHH were derived from cryopreserved samples. These primary hepatocytes were aliquoted à 0.4 x 10<sup>6</sup> cells/ vial, pelleted by centrifugation for 3 minutes, 100 x g, and the cell pellet was resuspended in serial dilutions containing 0 to 1000 nM HBVpreS/2-48<sup>myr</sup> (Myrcludex B, produced by Bachem) in duplicates. The suspensions were incubated for 30 minutes at 37°C under frequent mixing. Subsequently, the cells were pelleted by centrifugation for 3 minutes, 100 x g, and washed 3 times.

HepaRG cells were bought from Biopredic as differentiated cells in a 24 well plate. After arrival, the cells were treated according to the manufacturer's instructions, applying recovery-medium over night and further cultivate the cells with maintenance-medium. The cells were then incubated with serial dilutions containing 0 to 1000 nM HBVpreS/2-48<sup>myr</sup> (Myrcludex B, produced by Bachem) in duplicates for 30 minutes at 37°C. Afterwards, the cells were washed 3 times with PBS, scraped of the wells, transferred to Eppendorf cups and pelleted.

From all final cell pellets, the supernatant was removed as complete as possible and the cells were weighed, frozen in liquid nitrogen, and shipped on dry ice to Prolytic GmbH.

#### 2.2.3. Production of fluorescently labeled HBV

##### 2.2.3.1. Preparation of HBV-Alexa488

In order to produce fluorescently labeled particles, HBV was purified from HepAD38 cell culture supernatant by heparin affinity chromatography and gel filtration as described by Caroline Gähler, diploma thesis, based on a buffering system with PBS. The purified virus was used for the labeling reaction with Alexa488-succinimidyl ester.

Therefore, a stock solution of Alexa488- succinimidyl ester (5 mg/ ml in DMSO) was diluted at a final concentration of 0.04 mg/ ml with purified virus. The reaction was carried out at room temperature, rotating at 20 rpm, and was stopped after 1 hour by addition of TN buffer (20 mM Tris, 140 mM NaCl). Unbound dye was quenched by the primary amines contained in the TN buffer, and removed by heparin affinity chromatography as described by Caroline Gähler, diploma thesis. The virus peak fractions were further purified and concentrated by sucrose-density gradient ultracentrifugation, applying a gradient from 15 % to 60 % sucrose (w/w in PBS). Ultracentrifugation was performed with 40 000 x g for 20 hours at 20°C. After ultracentrifugation, the gradient was checked by UV light for fluorescent bands, and the gradient was fractionated collecting ~ 0.5 ml fractions.

### 2.2.3.2. Biochemical analysis of HBV-Alexa488

The fractions from the sucrose-density gradient were analyzed by DNA dot blot, measurement of Alexa488- fluorescence, polyacrylamide gel electrophoresis and subsequent western blotting or silver staining.

### 2.2.3.3. Quantification of HBV-DNA (DNA-dot blot)

In order to quantify the DNA content of the sucrose-density fractions, samples (5 - 20  $\mu$ l) of the fractions were spotted directly on PBS- moisturized nylon membrane (positively charged, Roche) using a 96-well Minifold dot blot chamber (Schleicher & Schuell). As a standard, a dilution series of the HBV genome-containing plasmid pCHT-9/3091 ( $5 \times 10^9$ ,  $1 \times 10^9$ ,  $2 \times 10^8$ ,  $4 \times 10^7$ ,  $8 \times 10^6$  and  $1.6 \times 10^6$  molecules per spot) was included. After application, the membrane was washed once with PBS, dried and soaked 2 x 1.5 minutes in soak I buffer in order to denature the DNA. For neutralization, the membrane was soaked 4 x 1 minute using soak II buffer. The DNA was then fixed by incubating the membrane for 30 minutes at 90°C.

To hybridize a HBV-specific, radioactively labeled DNA- probe, the membrane was incubated with hybridization mixture at 68°C, rotating over night. The DNA-probe was made using the Megaprime™ DNA Labeling Systems Kit from GE Healthcare, according to the manufacturer's protocol.

Subsequently, the membrane was washed with DNA dot-blot washing buffer, rotating for 2 x 15 minutes at 68°C and at room temperature. The membrane then was used to expose a BAS-MP (Fuji) film for at least 10 hours. The signal was read and quantified by a Phosphor-Imager FX and the software Quantity One (BioRad).

Buffer/Solution	Composition	
Soak I:	0.5 M NaOH, 1.5 M NaCl	
Soak II:	0.5 M Tris pH 7.4, 3 M NaCl	
Hybridization mix:	6x SSC, 5x Denhardts, 0.5 % SDS, 10 $\mu$ g/ ml calf thymus DNA	
Wash buffer:	1x SSC, 0.5 % SDS	
DNA-probe:	5 $\mu$ l DNA (pCH-9/3091), 5 $\mu$ l random-primer, 16 $\mu$ l H <sub>2</sub> O	→ 5 min, 95 °C
	non-radioactive dATP, dTTP, dGTP, 4 $\mu$ l each,	→ 20 min, 37°C
	5 $\mu$ l 10x reaction buffer, 5 $\mu$ l <sup>32</sup> $\alpha$ P-dCTP, 2 $\mu$ l Klenow polymerase	

### 2.2.3.4. Quantification of fluorescence

To measure fluorescence of the sucrose density fractions, samples (5 - 20  $\mu$ l) of the fractions were diluted with PBS to a final volume of 200  $\mu$ l in black 96-well plates with a transparent, flat bottom.

The fluorescence was analyzed using a Tecan Safire plate fluorometer and the software XLFUOR V4.5, with an excitation wave length of 485 nm and detecting fluorescence emission at 520 nm, both with a bandwidth of 5 nm. The optimal gain was calculated by means of the most fluorescent well.

#### 2.2.3.5. Analytical detection of proteins

Analytical protein electrophoresis was performed under denaturing conditions using SDS-PAGE described in Laemmli et al. (1970).

<b>Buffer</b>	<b>Composition</b>	
1x Running buffer:	0.025 M Tris, 0.086 M Glycin, 0.0035 M SDS	
4x Stacking gel buffer:	0.05 M Tris/HCl pH 8.8, 0.4 % SDS, 0.01 % NaN <sub>3</sub>	
4x Separating gel buffer:	1.5 M Tris/HCl pH 8.8, 0.4 % SDS, 0.01 % NaN <sub>3</sub>	
2x Loading buffer:	200 mM Tris/HCl pH 6.8, 6 % SDS, 20 % Glycerol, 10 % DTT, 0.1 mg/ ml Bromphenolblue, 0.1 mg/ ml Orange-G,	

<b>Solution</b>	<b>4 % Stacking gel</b>	<b>12.5 % Separating gel</b>
H <sub>2</sub> O	11 ml	17.5 ml
4x Stacking gel buffer	5 ml	-
4x Separating gel buffer	-	12.5 ml
Bis-acrylamide	4 ml	20 ml
Temed	10 µl	25 µl
Ammoniumpersulfate	“Spatelspitze”	“Spatelspitze”
	20 ml	50 ml

##### 2.2.3.5.1. Western Blot analysis

For detection by Western Blotting, proteins were transferred on a nitrocellulose transfer membrane (0.45 µm pore size, Whatman) using a semi-dry blotting chamber (BioRad). Subsequently, the membrane was blocked in 10 % milk powder in TBST and antibodies were applied in 2 % milk powder in the respective concentrations. Primary antibodies were incubated on a shaking device over night at 4°C, fluorescently labeled secondary antibodies for 1 hour at room temperature in the dark and in absence of Tween-20. After washing, fluorescence of the secondary antibodies was detected by a

Licor Odyssey and the software Odyssey 2.0, using an excitation wavelength of 700 nm and/ or 800 nm.

<b>Buffer</b>	<b>Composition</b>
1x TBST:	0.14 M NaCl, 0.02 M Tris, 0.05 % Tween-20, pH 8
Schäffer-Nielsen transfer buffer:	0.05 M Tris, 0.02 M Glycin, 0.04 % SDS, 10 % methanol, pH 9 - 9.4

#### 2.2.3.5.2. Silver gel analysis

To detect total protein content, polyacrylamide gels were fixed after electrophoresis with fix I over night, fix II for 30 minutes and fix III for 2 x 15 minutes. Impregnation of the gels was performed for 2 minutes using the impregnation solution, and subsequently proteins were stained by a solution containing AgNO<sub>3</sub>. To visualize the protein-silver precipitates, the gel was incubated with developing solution until proteins were well visible. The reaction was stopped with the stopping solution for approximately 1 minute and the gel was washed, and stored in H<sub>2</sub>O.

<b>Solution</b>	<b>Composition</b>	<b>Protocol</b>
Fix I:	50 % Methanol, 12 % Acetic acid	→ 1 h or o/n
Fix II:	10 % Ethanol, 5 % Acetic acid	→ 30 min
Fix III:	10 % Ethanol	→ 2 x 15 min
Solution A:	0,02 % Sodiumthiosulfate, 0.02 % Formaldehyde	→ 2 min
Solution B:	0.2 % Silvernitate, 0.02 % Formaldehyde	→ 12 min (dark)
Solution C:	3 % Sodium carbonate, 0.02 % Formaldehyde, 0.0003 % Sodiumthiosulfate	→ development
Stopping solution:	3 % Acetic acid	

#### 2.2.4. Microscopy

##### 2.2.4.1. Spinning disk confocal microscopy

Fixed samples were analyzed by spinning disk confocal microscopy, using a Perkin Elmer spinning disk confocal ERS-FRET on Nikon TE2000 inverted microscope, with a Hamamatsu C9100-50 camera and the software Volocity 5.2 (Perkin Elmer). Images were taken with a 100x objective (Planapo NA 1.4,

oil) or 60x objective (Planapo NA 1.2, water immersion). Acquisition times were adjusted to the respective fluorescent signal, but were not changed within an experiment. Most images were taken with a laser power of 100 %.

#### 2.2.4.2. Fluorescence recovery after photobleaching

PMH were grown on collagen-coated LabTek chamber slides (8- chambered) and incubated for 1 hour at 37°C with 200 nM HBVpreS/2-48<sup>myr</sup>-C-Atto565. As a control, PMH were stained with 5 µl/well Dil (Molecular Probes) for 30 minutes at 37°C. After incubation, the cells were washed with PBS and supplied with fresh medium (Leiboviz L-15, without phenol red).

Fluorescence recovery after photobleaching was measured with the hard- and software of the spinning disk confocal microscope described above. Images were taken with a 60x objective (Planapo NA 1.2, water immersion) and bleaching was performed using an UltraVIEW PK Device as bleaching device. Images pre bleaching were captured for 4 seconds at a rate of 2 timepoints per second, recovery images were taken for 30 seconds at the same frame rate. The time lapse was acquired using a 568 nm laser as excitation.

#### 2.2.4.3. Total internal reflection fluorescence (TIRF) microscopy

TIRF was performed on a Nikon Total Internal Reflection Fluorescence (TIRF) on Ti inverted microscope with Nikon Perfect Focus System, using a 100x TIRF objective. Pictures were taken with a Hamamatsu EM-CCD camera.

#### 2.2.4.4. Measurement of fluorescence on digital images

Fluorescence intensities in digital images were measured using the software ImageJ. Therefore, circular regions of the same size were measured with at least 10 measurements per frame in at least 5 different pictures. The mean fluorescence in the selections was used to calculate an average value that directly was used to plot the data.

### 3. Visualization and characterization of the HBV preS1-receptor interaction with fluorescently labeled ligands

#### 3.1 Fluorescently labeled HBVpreS/2-48<sup>myr</sup> lipopeptides

HBVpreS/2-48<sup>myr</sup> has been described to specifically and efficiently inhibit HBV infection *in vivo* and *in vitro*. Infection inhibition is achieved by an interference with viral entry, most probably through the interaction with a specific HBV-receptor. Due to highly similar requirements for their functionality, HBV and HBVpreS/2-48<sup>myr</sup>-peptides are assumed to address a common factor on hepatocytes. The peptides therefore provide a powerful tool to analyze receptor binding.

In order to characterize the interaction of HBVpreS/2-48<sup>myr</sup> with its receptor, a set of fluorescently labeled HBVpreS/2-48<sup>myr</sup> derivatives was synthesized and visualized. Peptide sequences are based on previous findings, that demonstrated a high inhibitory activity of HBVpreS/2-48<sup>myr</sup>, lacking inhibitory activity of HBVpreS/2-48<sup>myr</sup>(D11,13) and an approximately 1000-fold reduced activity of HBVpreS/1-48 (Schulze et al. 2010). An overview about the peptides that have been synthesized is shown in Figure 5.

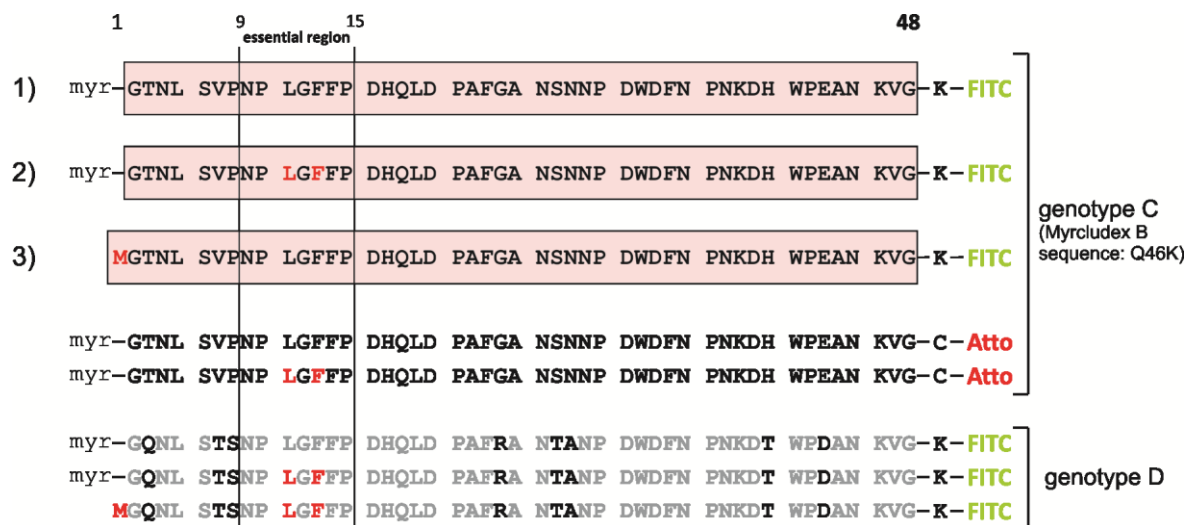


**Figure 5: Fluorescently labeled HBVpreS/2-48<sup>myr</sup> derivatives.** Schematic presentation of the wild type peptide HBVpreS/2-48<sup>myr</sup>-K-FITC (1), comprising amino acids 2 to 48 of the HBV L-protein, the N-terminal myristoylation and a fluorescein isothiocyanate (FITC) moiety. The mutant peptide HBVpreS/2-48<sup>myr</sup>(D11,13)-K-FITC, in which amino acids 11 and 13 are replaced by D-isomers is depicted in (2), and (3) shows the non-myristoylated variant HBVpreS/1-48-K-FITC. Peptides (1) and (2) were additionally labeled with Atto565 (see middle sequences). Experiments that made use of FITC-labeled peptides derived from the genotype D (lower three sequences) are indicated in the following. The essential region is defined by vertical bars and amino acid positions are indicated by numbers.

### 3.1.1. Production and characterization of fluorescently labeled HBV preS1-lipopeptides

#### HBVpreS/2-48<sup>myr</sup>-K-FITC

The selective coupling of fluoresceine isothiocyanine (FITC) to a lysine at position 49 during synthesis ensured an equimolar ratio of one fluorochrome per peptide molecule. This was important in order to conduct comparative binding analysis of a set of peptides.

The purity of every peptide preparation was controlled by analytical HPLC. As shown in the overlay of HPLC profiles from HBVpreS/2-48<sup>myr</sup>-K-FITC, HBVpreS/2-48<sup>myr</sup>(D11,13)-K-FITC and HBVpreS/1-48-K-FITC, peptides appeared as a sharp peak without significant impurities (Figure 6). For further analysis mass spectrometry was performed. All peptides matched the theoretical molecular weight ( $M_r$ , expected) of the respective molecule, with a maximal aberration of 0.5 Da being less than half of the mass of a hydrogen atom ( $^1\text{H}$ ).

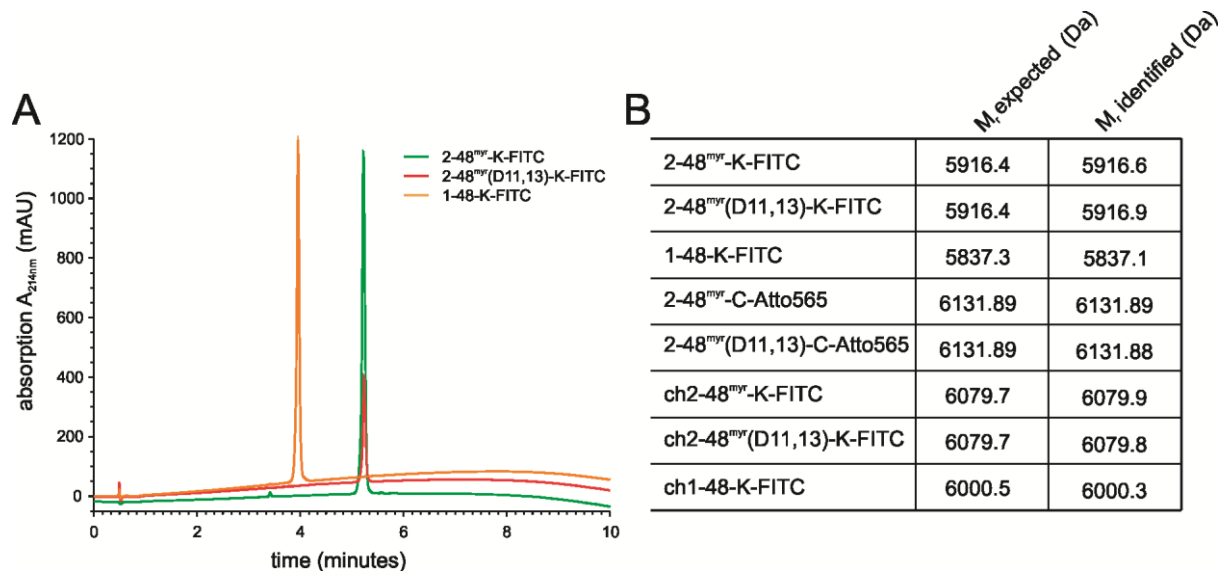


**Figure 6: Purity of the peptide preparations.** (A) The purity of the synthesized peptides was controlled by analytical HPLC. Depicted are exemplary preparations of three different peptides, indicated in green, red and orange. (B) The peptide preparations were checked by mass spectrometry. Expected and identified relative molecular masses ( $M_r$ ) are given as numbers (Da). Peptide names were shortened by deletion of the prefix “HBVpreS/”. ch2-48 = sequence of the genotype D. All other sequences are derived from genotype C.

#### HBVpreS/2-48<sup>myr</sup>-C-Atto565

Since FITC is not suited for live-cell microscopy due to its high photosensitivity, a second batch of peptides was synthesized and labeled with the more bleaching-resistant fluorophore Atto565. It was coupled to an N-terminal cystein (C49) post synthesis. The control of the purity by analytical HPLC (data not shown) and the molecular weight by mass spectrometry (see Figure 6B) indicated the presence of the product HBVpreS/2-48<sup>myr</sup>-C-Atto565.

### 3.1.2. Validation of peptide-functionality by infection inhibition experiments

To test whether the addition of C-terminally coupled fluorophores interferes with the inhibitory characteristics of HBVpreS/2-48<sup>myr</sup>, infection inhibition experiments have been performed on PHH and HepaRG cells.

An exemplary infection inhibition on PHH is shown in Figure 7. Similar to the unlabeled HBVpreS/2-48<sup>myr</sup>, the presence of 250 nM HBVpreS/2-48<sup>myr</sup>-K-FITC during virus inoculation led to a complete inhibition of infection. This demonstrated a functionality of the FITC-labeled peptide. As expected, HBVpreS/2-48<sup>myr</sup>(D11,13)-K-FITC did not inhibit infection, and HBVpreS/1-48-K-FITC exhibited a weak, but negligible inhibitory activity.

Quantitative experiments comparing the effectiveness of HBVpreS/2-48<sup>myr</sup> and its fluorescently labeled derivate have not been performed.

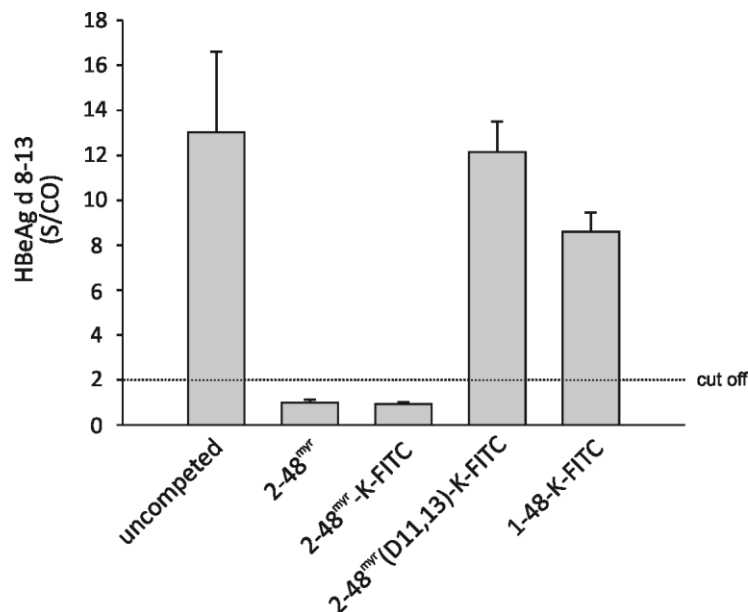


**Figure 7: Inhibitory functionality of HBVpreS/2-48<sup>myr</sup>-K-FITC.** PHH were infected in duplicates with HBV in absence (uncompleted) or presence of 250 nM of the respective peptides. HBeAg as marker for infection was measured in the supernatant collected from day 8 to 13. Peptide names were shortened as indicated in Fig. 6.

### 3.2 Visualization of HBVpreS/2-48<sup>myr</sup>-K-FITC binding to hepatocytes

Despite the detailed knowledge about sequence requirements, the mechanism of action and cellular interaction partners of HBVpreS/2-48<sup>myr</sup> are not known. Since it has been shown that a cellular factor is addressed by the peptide (Gripon et al. 2005), this work aimed to visualize and characterize this interaction. Following the fate of HBVpreS/2-48<sup>myr</sup>-K-FITC after exposure to cells might allow conclusions about the localization of a preS1-receptor, the prerequisites for its expression, and the kinetics and dynamics of the preS1-receptor interaction.

### 3.2.1. HBVpreS/2-48<sup>myr</sup> binds to the plasma membrane of HBV-susceptible hepatocytes in a highly sequence- and myristoylation-specific manner

To test whether a specific interaction of HBVpreS/2-48<sup>myr</sup>-K-FITC with HBV-susceptible cells can be detected, binding studies were performed using the set of peptides described above.

When PHH were incubated with HBVpreS/2-48<sup>myr</sup>-K-FITC, a fluorescent staining of the plasma membrane was observed by spinning disk confocal microscopy (Figure 8). In contrast, the myristoylated mutant peptide HBVpreS/2-48<sup>myr</sup>(D11,13)-K-FITC did not bind to a significant extent at the concentration used here. Neither, binding could be detected using the non-myristoylated HBVpreS/1-48-K-FITC. Both demonstrated the high specificity of binding, since only minor changes of the peptide sequence (amino acids L-11, 13 to D-11, 13) or the removal of the myristoylation resulted in a complete loss of binding. This entirely reflected the respective inhibitory potential of these peptides (Figure 7), and demonstrated that the inactivity of the mutant and non-myristoylated peptide results from their inability to bind a specific receptor on the surface of PHH.

As seen in Figure 8A, the same sequence- and myristoylation-dependent binding phenotype was observed on PTH and HepaRG cells. It is to mention, that HepaRG cells in general showed a relatively weak peptide signal that was difficult to detect. Also, microscopy was hampered by highly fluorescent structures on the cell surface of these cells when incubated with a myristoylated FITC-labeled peptide. These structures probably were a consequence of an unspecific, lipid-mediated binding of acylated peptides, since they were not present after incubation with HBVpreS/1-48-K-FITC. The insular presence of these highly fluorescent spots, and the weakness of the membrane staining after HBVpreS/2-48<sup>myr</sup>-K-FITC incubation, disqualified HepaRG cells as a suitable model for quantitative microscopic binding studies.

The autofluorescence of primary hepatocytes was also relatively bright. But since dot-like autofluorescence was almost exclusively located in the perinuclear region, it did not interfere with the observation of a peptide-mediated plasma membrane staining. Hepatocytes are known for a bright autofluorescence that can be derived from molecules like lipofuscines, flavines or porphyrines. These fluoresce due to their molecular structure, and typically are expressed in metabolizing cells.

To reassess these results by an alternative assay, flow cytometry was performed with primary hepatocytes. Therefore, cryo-preserved PHH were incubated with the set of FITC-labeled peptides in suspension, and fluorescence was measured. Indeed, the same binding phenotype was observed. Only after incubation with HBVpreS/2-48<sup>myr</sup>-K-FITC, PHH showed an approximately 10-fold higher cell-associated fluorescence, compared to the unstained control (see Figure 8C). In contrast, HBVpreS/2-48<sup>myr</sup>(D11,13)-K-FITC showed a slight background binding that was attributed to an unspecific myristoylation-dependent interaction. Incubation with HBVpreS/1-48-K-FITC did not result in a detectable signal.

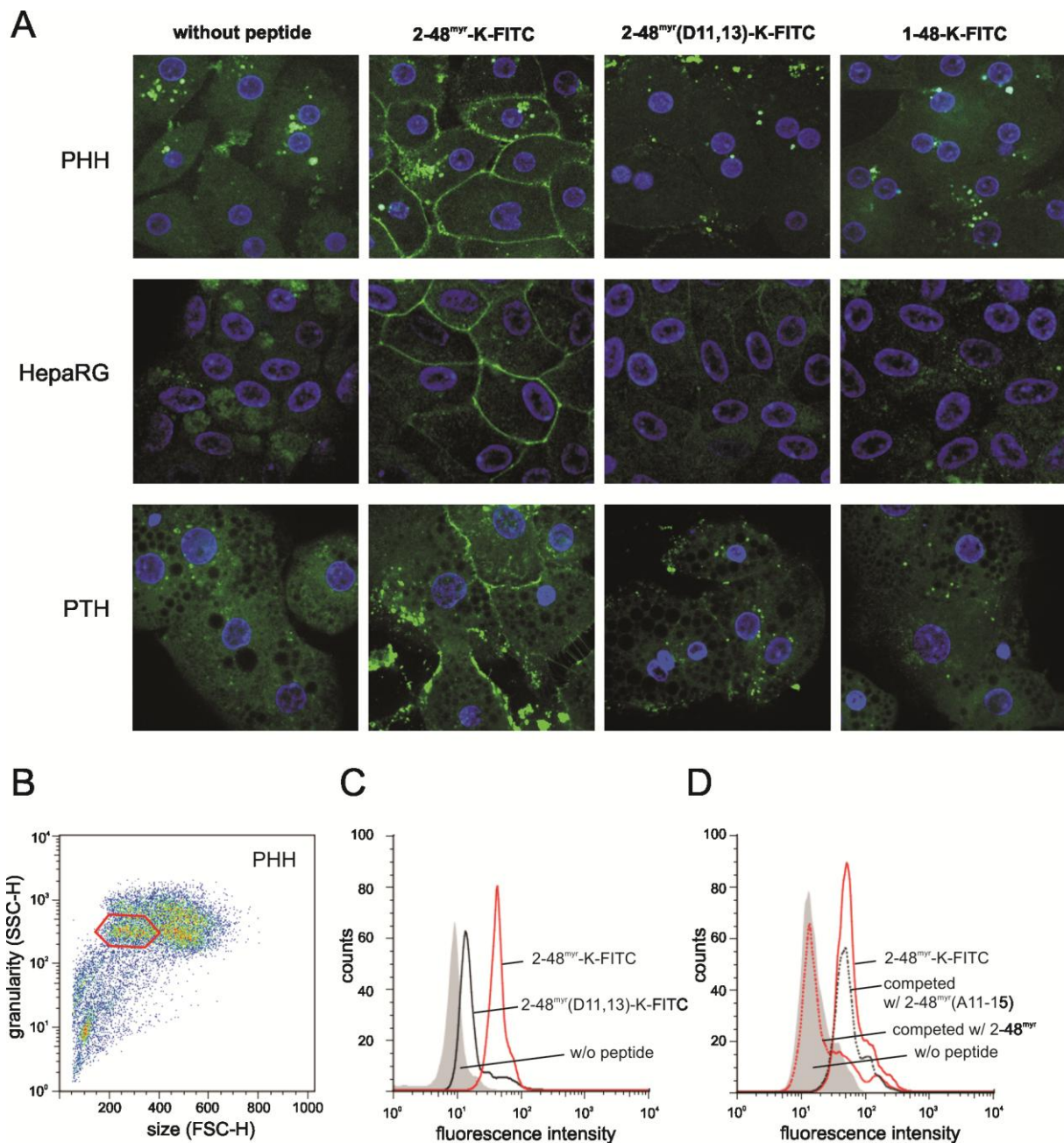


**Figure 8: Specific binding of HBVpreS/2-48<sup>myr</sup>-K-FITC to HBV-susceptible cells.** (A) PHH, HepaRG and PTH were grown on cover slips, incubated with 200 nM of the indicated peptides and fixed. A mock-incubated control showing the autofluorescence of these cells is depicted on the left (without peptide). FITC-fluorescence could be seen on the plasma membrane (green), nuclei were stained with DAPI (blue). Images were obtained by spinning disk confocal microscopy with a 600x magnification. (B) PHH were incubated with the set of peptides at 200 nM in suspension, washed, and cell-associated fluorescence was measured by flow cytometry. The gate shown in red was set on PI-negative cells of homogeneous size and granularity. (C) Binding of HBVpreS/2-48<sup>myr</sup>-K-FITC (red line) was detected by an approximately 10-fold higher fluorescence of the population, compared to the unstained control (filled gray). The mutant peptide (black line) showed slight background binding. (D) Binding of HBVpreS/2-48<sup>myr</sup>-K-FITC could be competed with 20  $\mu$ M HBVpreS/2-48<sup>myr</sup> (red dotted line), but not with HBVpreS/2-48<sup>myr</sup>(D11,13) (black dotted line). Autofluorescence of the cells is shown in gray, filled. Peptide names were shortened as indicated in Fig. 6.

The high specificity of binding could additionally be demonstrated by competition experiments. Using a 100-fold excess of unlabeled HBVpreS/2-48<sup>myr</sup>, binding of HBVpreS/2-48<sup>myr</sup>-K-FITC could be reduced to background levels (Figure 8D). In contrast, an excess of HBVpreS/2-48<sup>myr</sup>(D11,13) had no effect. This demonstrated that HBVpreS/2-48<sup>myr</sup> and its labeled derivate HBVpreS/2-48<sup>myr</sup>-K-FITC address the same factor on the plasma membrane, and that even at a 100-fold excess (20 μM) the mutant peptide HBVpreS/2-48<sup>myr</sup>(D11,13) did not show competitive activity.

### 3.2.2. Specific binding of HBVpreS/2-48<sup>myr</sup>-K-FITC is not restricted to HBV-susceptible cells

Based on in vivo biodistribution studies in mice and rats that showed a sequence- and myristoylation-specific liver accumulation of iodinated HBVpreS/2-48<sup>myr</sup>-Y<sup>131</sup> (see Figure 3, Alexa Schieck, diploma thesis), primary hepatocytes from mice (PMH) and rats (PRH) were tested in vitro for binding of HBVpreS/2-48<sup>myr</sup>-K-FITC.

Despite being non-susceptible to HBV infection, both, PMH and PRH, specifically bound HBVpreS/2-48<sup>myr</sup>-K-FITC as depicted in the confocal images shown in Figure 9A. Consistent with the previous findings on HBV-susceptible cells, no binding was observed after incubation with HBVpreS/2-48<sup>myr</sup>(D11,13)-K-FITC or HBVpreS/1-48-K-FITC. In addition, this correlated also with the sequence- and acylation-dependency of the liver tropism.

These results were confirmed by flow cytometry as seen in Figure 9B-D. The high specificity of binding could again be demonstrated by competition experiments as described above. An excess of unlabeled HBVpreS/2-48<sup>myr</sup> resulted in a reduction of HBVpreS/2-48<sup>myr</sup>-K-FITC binding to background levels, whereas HBVpreS/2-48<sup>myr</sup>(D11,13) had no effect. These observations supported the assumption of the presence of a specific HBVpreS1-receptor on hepatocytes of even non-susceptible mice and rats.

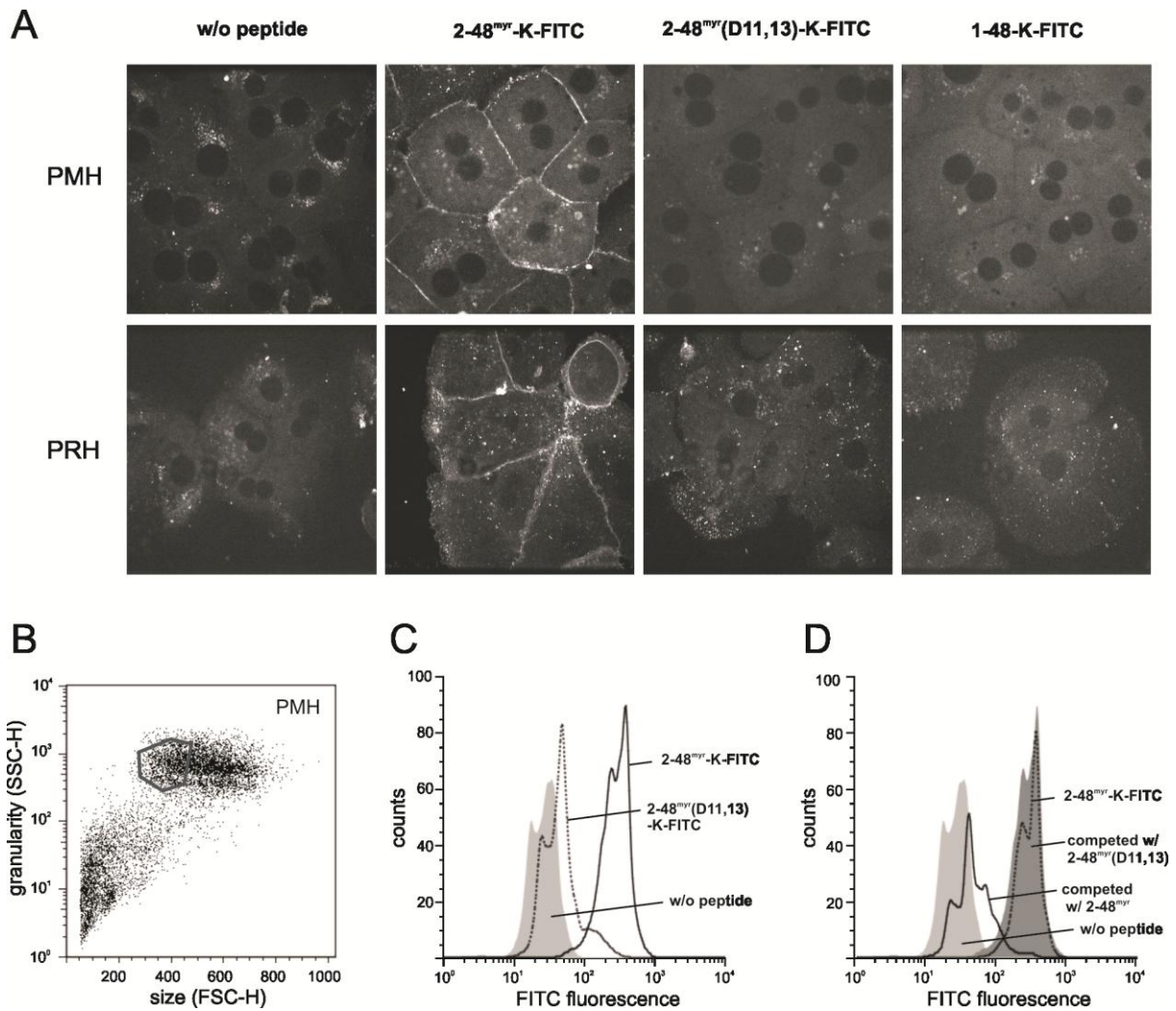


**Figure 9: Specific binding of HBVpreS/2-48<sup>myr</sup> to primary rodent hepatocytes.** (A) Primary hepatocytes from mouse (PMH) and rat (PRH), cultured on cover slips, were incubated with 200 nM HBVpreS/2-48<sup>myr</sup>-K-FITC and the respective derivatives, washed and fixed. Plasma membrane-bound fluorescence was documented by spinning disk confocal microscopy with a 600x magnification. Autofluorescence is shown on the left (without peptide). (B) PMH were incubated with the set of peptides at 200 nM in suspension, washed, and cell-associated fluorescence was measured by flow cytometry. The gate shown in dark grey was set on PI-negative cells of homogeneous size and granularity. (C) Binding of HBVpreS/2-48<sup>myr</sup>-K-FITC (solid line) was detected by an approximately 10-fold higher fluorescence of the population, compared to the unstained control (light gray, filled). The mutant peptide (dotted line) showed slight background binding. (D) Binding of HBVpreS/2-48<sup>myr</sup>-K-FITC (dotted line) could be competed with 20  $\mu$ M HBVpreS/2-48<sup>myr</sup> (solid line), but not with HBVpreS/2-48<sup>myr</sup>(D11,13) (dark grey, filled). Autofluorescence of the cells is shown in light gray, filled. Peptide names were shortened as indicated in Fig. 6.

Based on these findings, a whole set of primary hepatocytes from different species was tested for specific binding of HBVpreS/2-48<sup>myr</sup>-K-FITC. Therefore, flow cytometry was performed with cryopreserved hepatocytes from rats, rabbits, dogs, humans, cynomolgus monkeys, rhesus monkeys and pigs that were incubated with HBVpreS/2-48<sup>myr</sup> and variants thereof. None of these species, except humans, has been shown to be susceptible to HBV infection.

Surprisingly, we found specific binding of HBVpreS/2-48<sup>myr</sup>-K-FITC to some, but not all species. Binding was detected on hepatocytes from rats, rabbits, dogs, and humans, but not on hepatocytes

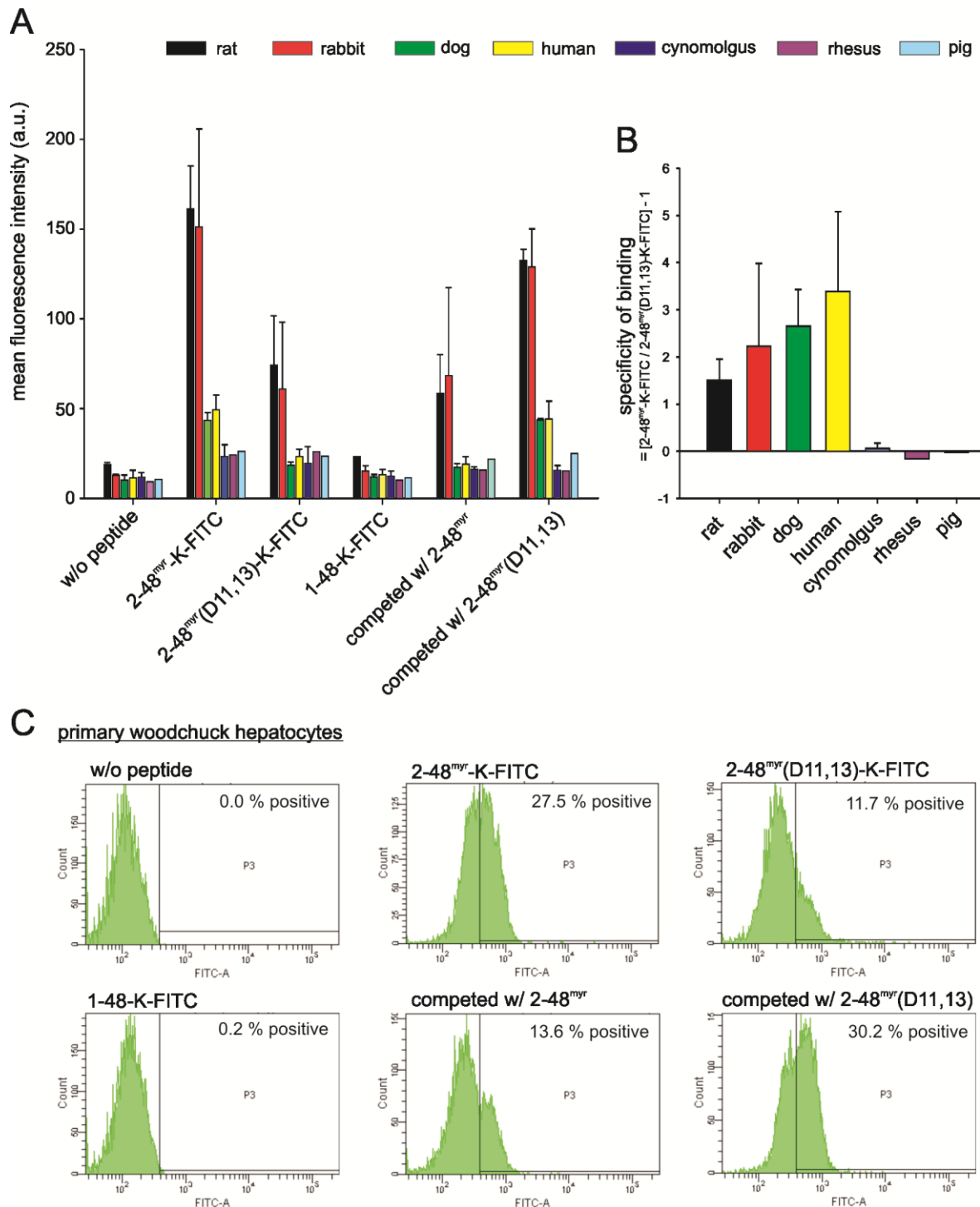


**Figure 10: Species-specific binding of HBVpreS/2-48<sup>myr</sup>-K-FITC to primary hepatocytes.** Cryopreserved primary hepatocytes from rat, rabbit, dog, human, cynomolgus monkey, rhesus monkey and pig were incubated with 200 nM HBVpreS/2-48<sup>myr</sup>-K-FITC and the indicated control peptides. Competition of binding was performed with a 100-fold excess (20  $\mu$ M) of the respective unlabeled wild type or mutant peptide. Cell-associated fluorescence was measured by flow cytometry. Hepatocytes were obtained from  $n = 3$  (human, cynomolgus),  $n = 2$  (rat, rabbit, dog) or  $n = 1$  (rhesus, pig) liver preparations. (A) represents the mean fluorescence intensities of the different samples. (B) shows the normalized values for the specificity of binding. The signal of HBVpreS/2-48<sup>myr</sup>-K-FITC for each species was divided by the respective signal intensity of HBVpreS/2-48<sup>myr</sup>(D11,13)-K-FITC. The resulting factor was subtracted by 1. (C) Freshly isolated primary woodchuck hepatocytes were incubated with 200 nM of the respective peptides as described in A. Depicted are the histograms of the distribution of fluorescence within the gated cell population. Gate P3 indicated the percentage of fluorescence-positive cells, zero was defined using untreated cells (w/o peptide).

from pigs, cynomolgus or rhesus monkeys (Figure 10A). This indicated that a specific preS1-receptor is expressed by hepatocytes from some, but not all non-susceptible species.

Interestingly, the fluorescence intensities after peptide binding differed among the species. Some species like e.g., rats, showed a higher fluorescence after incubation with HBVpreS/2-48<sup>myr</sup>-K-FITC than other species like e.g., humans. However, also the unspecific binding of HBVpreS/2-48<sup>myr</sup>(D11,13)-K-FITC was enhanced. In order to normalize specific binding, the signal intensity of HBVpreS/2-48<sup>myr</sup>-K-FITC was divided by that of HBVpreS/2-48<sup>myr</sup>(D11,13)-K-FITC and subtracted by 1 (if both types of binding contribute equally (factor = 1), no specific binding takes place) (see Figure 10B). Despite relatively high error bars that probably resulted from intra-species variations, the overall tendency showed that hepatocytes from humans, dogs, rabbits and rats specifically bound HBVpreS/2-48<sup>myr</sup>-K-FITC, whereas cynomolgus monkeys, rhesus monkeys or pigs did not.

Flow cytometry with freshly isolated woodchuck hepatocytes showed a specific binding of HBVpreS/2-48<sup>myr</sup>-K-FITC to these cells (C). Although being characterized by a relatively high background binding of HBVpreS/2-48<sup>myr</sup>(D11,13)-K-FITC (~ 12 % positive cells) binding was specific since it could be competed with HBVpreS/2-48<sup>myr</sup> (reduction to background levels, 13.6 % positive). In contrast, competition with HBVpreS/2-48<sup>myr</sup>(D11,13) had no effect (30.2 % positive).

To exclude artifacts, each preparation was checked for cell viability by a control stain with propidium iodide (or Hoechst, respectively). A potential contamination with non-parenchymal cells in the experiment shown in (A) could be excluded since uptake of acetylated low-density lipoprotein, a marker for sinusoidal cells, was not observed (data not shown). The fresh woodchuck hepatocyte preparation contained also non-parenchymal cells, but these could be “gated out” by flow cytometry due to their small size.

### 3.3 Characterization of preS1-receptor binding

#### 3.3.1. The presence of a preS1-receptor depends on the differentiation state of the cell

Hepatocytes isolated from the liver are known to undergo a process in cell culture, referred to as dedifferentiation (review (Elaut et al. 2006b)). For unknown reasons, dedifferentiation can be slowed down by the addition of dimethylsulfoxide (DMSO) to the cell culture medium.

Dedifferentiation of PHH and PTH is accompanied by a loss of the susceptibility to HBV. This has been observed also for DHBV and the infection of primary duck hepatocytes. HepaRG cells, in contrast, gain susceptibility during a DMSO-induced differentiation process (Gripon et al. 2002), substantiating the assumption that permissiveness towards HBV depends on the differentiation state of the cell.

To investigate, whether this restriction might reflect a differentiation-dependent expression of a preS1-receptor, we tested binding of HBVpreS/2-48<sup>myr</sup>-K-FITC to undifferentiated and differentiated

HepaRG cells. Interestingly, peptide binding could be detected only on the differentiated HepaRG cells (Figure 11A, left panel). No signal was detected on undifferentiated cells. This directly demonstrated that the presence of a functional preS1-receptor depends on the differentiation state. For that reason, the lacking susceptibility of the undifferentiated HepaRG cells might be explained by a lack of preS1 receptor expression.

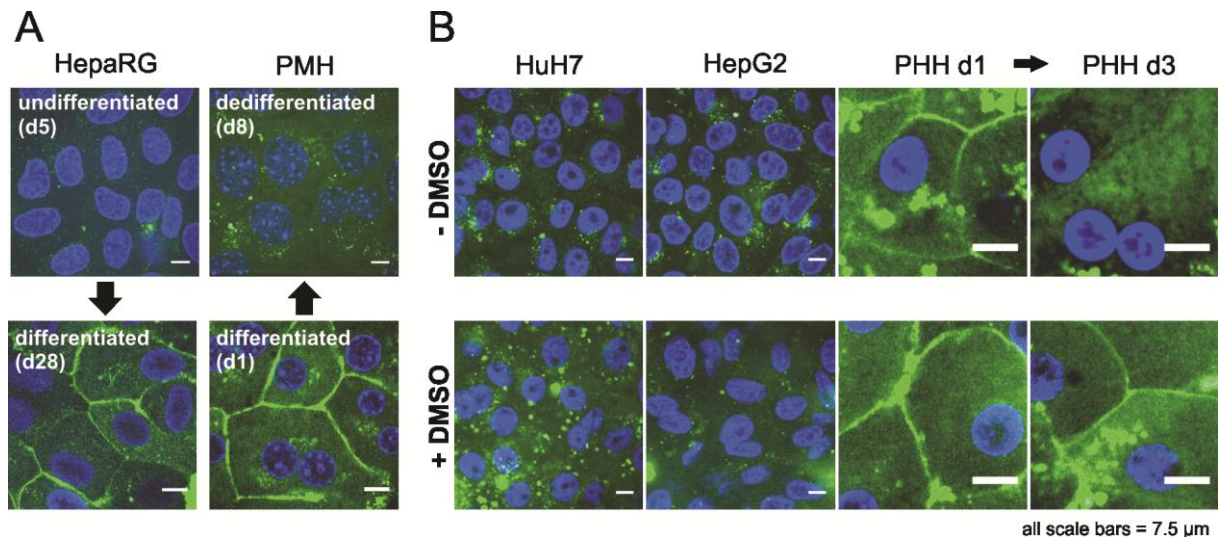


**Figure 11: HBVpreS/2-48<sup>myr</sup>-K-FITC binding depends on the differentiation state of the cell.** (A) HBVpreS/2-48<sup>myr</sup>-K-FITC (200 nM) was incubated with HepaRG cells 5 days (d) (undifferentiated) and 28 d after plating, including a 2-weeks DMSO treatment (differentiated). PMH were incubated on d1 (differentiated) and d8 (dedifferentiated) after isolation and cultivation without DMSO. (B) HuH7 and HepG2 cells were stained with HBVpreS/2-48<sup>myr</sup>-K-FITC in a confluent state (-DMSO) and after a 2-weeks DMSO treatment (+DMSO). PHH cultivated with or without DMSO were stained on d1 and d3 after plating (i.e. d2 and d4, respectively after isolation).

Vice versa, we tested if PMH lose the ability to bind HBVpreS/2-48<sup>myr</sup>-K-FITC during dedifferentiation. For this, peptide binding was performed on day 1 after isolation of PMH and, after a prolonged period of cultivation in absence of DMSO. As shown in Figure 11A (right panel), hepatocytes from the same preparation were able to specifically bind HBVpreS/2-48<sup>myr</sup>-K-FITC on day 1, but lost this ability within 8 days of cultivation. A time-course experiment sustained this observation by measuring the progressive loss of binding ability within 6 days by flow cytometry (unpublished data, Stefan Mehrle). Consistent with the finding that HBV susceptibility of PHH can be maintained over time by the presence of DMSO, also the loss of the peptide binding ability could be delayed (Figure 11B). In contrast to cells that were cultivated without DMSO, PHH cultivated in presence of this differentiating agent were able to bind HBVpreS/2-48<sup>myr</sup>-K-FITC on day 7 after isolation.

To test if hepatoma cell lines, generally regarded as undifferentiated, bind preS1-lipopoptides, we incubated confluent cultures of HepG2 and HuH7 cells with HBVpreS/2-48<sup>myr</sup>-K-FITC. Both hepatoma cell lines display typical functions of the liver but are immortalized and do not achieve cellular differentiation. As shown in Figure 11B HepG2 and HuH7 did not bind HBVpreS/2-48<sup>myr</sup>-K-FITC.

Interestingly, also a treatment with DMSO for 2 weeks did not induce a binding ability of these cells. This indicated that HepG2 and HuH7 lack the ability to express a functional preS1-receptor. It might as well provide an explanation for their non-susceptibility towards HBV infection.

### 3.3.2. Glycosaminoglycans do not play a substantial role in receptor-binding of HBVpreS/2-48<sup>myr</sup>

As for many other viruses, glycosaminoglycans have been found to mediate primary attachment of HBV to the cell (Schulze et al. 2007). The attachment of HBV with negatively charged side chains of heparan sulfate proteoglycans is preS1-dependent and can be inhibited with high concentrations of heparin or suramin.

Although affinity chromatography columns containing heparin sepharose cannot bind HBVpreS/2-48<sup>myr</sup> as a part of the preS1-sequence (Andreas Schulze, PhD thesis), the role of proteoglycans in the interaction of HBVpreS/2-48<sup>myr</sup>-K-FITC with hepatocytes was investigated. Therefore, binding to PMH was competed with heparin and suramin in concentrations that have been shown to inhibit HBV binding to HepaRG cells. As seen in Figure 12 neither heparin, nor suramin showed an effect on HBVpreS/2-48<sup>myr</sup>-K-FITC binding to the plasma membrane. This provided a first indication that glycosaminoglycans do not play a pivotal role in peptide binding. However, the functionality of this assay has not been tested. The validity of the visual read-out was provided by the fact that the effect of binding competition with an excess of unlabeled HBVpreS/2-48<sup>myr</sup> could be detected by a loss of plasma membrane-bound signal (Figure 12, right).

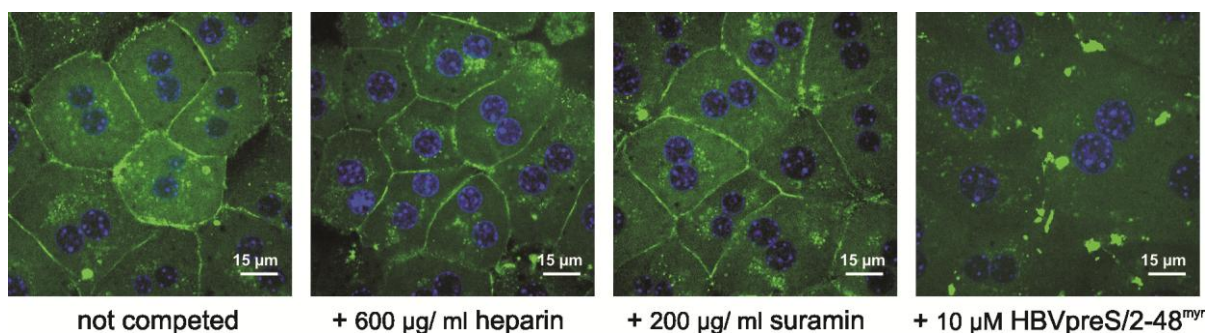


**Figure 12: Binding of HBVpreS/2-48<sup>myr</sup>-K-FITC could not be inhibited by heparin or suramin.** PMH grown on cover slips were incubated with 200 nM of the peptide in presence (+ heparin/ + suramin/ + HBVpreS/2-48<sup>myr</sup>) or absence (not competed) of competitor, and spinning disk confocal microscopy was performed with a 600x magnification on fixed cells. FITC-fluorescence is shown in green, nuclei were stained with DAPI (blue).

### 3.3.3. The preS1-receptor is sensitive to protease digestion

To get first insights into the nature of the preS1-receptor molecule, we investigated if protease digestion of plasma membrane surface proteins by Glu-c and trypsin has an impact on subsequent binding of HBVpreS/2-48<sup>myr</sup>-K-FITC.

As determined by flow cytometry, binding of HBVpreS/2-48<sup>myr</sup>-K-FITC could be reduced to approximately 40 % of the untreated control, when PMH were pre-treated with 40 µg Glu-c (see Figure 13). Pre-treatment with trypsin had a similar effect. The sensitivity of the preS1-receptor to proteolytic digestion clearly suggested a proteinaceous character of this still unknown molecule.

Since both enzymes were removed after pre-incubation by extensive washing of the cells, one could argue that the reduction of binding might result from peptide digestion by residual enzymatic activity. A control experiment in which the reaction was stopped by enzyme saturation (addition of 10 % FCS), excluded this possibility (data not shown).

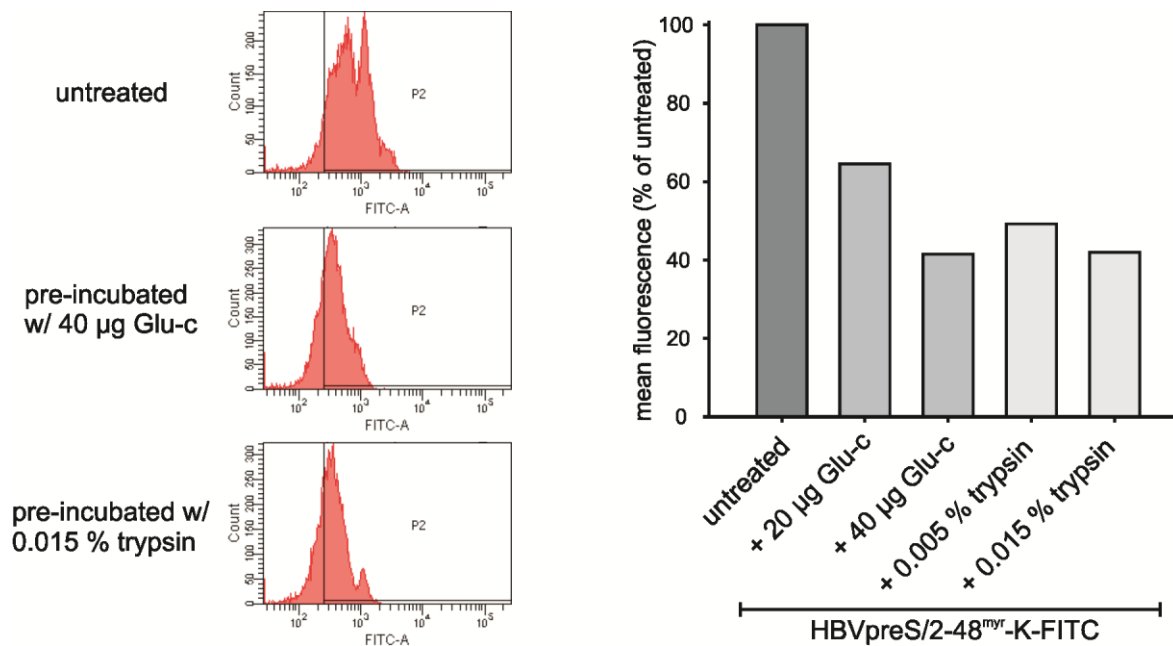


**Figure 13: Proteolytic digestion of surface proteins reduces peptide binding in a concentration-dependent manner.** Freshly isolated PMH were pre-treated with Glu-c (20/ 40 µg) and trypsin (0.005/ 0.015 %). After removal of the enzymes by extensive washing, cells were incubated with 200 nM HBVpreS/2-48<sup>myr</sup>-K-FITC, and cell-associated fluorescence was measured by flow cytometry. Histograms of the fluorescence intensities are depicted on the left; normalized mean fluorescence values (right) are given as percentages of the untreated control.

### 3.4 Characterization of the pharmacodynamic behavior of HBVpreS/2-48<sup>myr</sup> and the kinetics of receptor binding

Despite the very detailed knowledge about sequence requirements of HBVpreS/2-48<sup>myr</sup>-mediated infection inhibition, little is known about its binding mechanism and the mode of action. HBVpreS/2-48<sup>myr</sup> does not prevent virus binding to the cell at concentrations that completely inhibit infection. It presumably interferes with a post-attachment step like endocytosis or fusion. The IC<sub>50</sub> of HBVpreS/2-48<sup>myr</sup> on HepaRG cells is described with 0.14 nM (Schulze et al. 2010).

Application of peptide shortly after virus inoculation has no effect, but when pre-incubated, HBVpreS/2-48<sup>myr</sup>-mediated infection inhibition lasts for several hours ( $t_{1/2} \approx 12$  hours, (Gripon et al. 2005). To get insight into the mechanism of action of HBVpreS/2-48<sup>myr</sup>, the binding and kinetics of HBVpreS/2-48<sup>myr</sup>-K-FITC-receptor interaction were investigated.

#### 3.4.1. HBVpreS/2-48<sup>myr</sup>-K-FITC-receptor binding represents a bimodal binding mechanism

Similar to radio-ligand binding studies, the binding curve of HBVpreS/2-48<sup>myr</sup>-K-FITC was calculated to characterize the peptide-receptor interaction. Therefore, flow cytometry was performed to measure the cell-associated fluorescence intensity of PMH, incubated with a serial dilution of HBVpreS/2-48<sup>myr</sup>-K-FITC. Unspecific binding was determined by incubation with HBVpreS/2-48<sup>myr</sup>(D11,13)-K-FITC and HBVpreS/1-48-K-FITC.

As expected, PMH incubated with the wild type peptide showed increasing fluorescence intensities with increasing concentrations (see Figure 14). However, the curve resulting from these primary data did not show saturation within the concentration range tested (0.05  $\mu\text{M}$  - 3.2  $\mu\text{M}$ ). PMH that were incubated with HBVpreS/2-48<sup>myr</sup>(D11,13)-K-FITC showed a linear, although delayed increase of fluorescence, compared to HBVpreS/2-48<sup>myr</sup>-K-FITC. Concentrations below 0.4  $\mu\text{M}$  did not result in significant binding. Since the non-myristoylated peptide did not show interaction even at the highest concentrations used, it was assumed that the linear increase of HBVpreS/2-48<sup>myr</sup>-K-FITC and HBVpreS/2-48<sup>myr</sup>(D11,13)-K-FITC resulted from an unspecific, myristoylation-dependent binding.

The remarkable difference of the curves at low concentrations, however, indicated different binding mechanisms for the wild type and the mutant peptide. In order to display specific binding only, the fluorescence signals of HBVpreS/2-48<sup>myr</sup>-K-FITC-binding were normalized by subtraction of the signals of HBVpreS/2-48<sup>myr</sup>(D11,13)-K-FITC-binding. The resulting curve showed the characteristics of a typical receptor-ligand interaction, i.e. hyperbolic increase and saturation. This indicated the presence of two modes of binding, being (1), an unspecific, myristoylation-dependent binding at high concentrations, and (2), a highly specific, sequence-dependent binding at low concentrations. Consistent with that bimodal binding mechanisms have been described for other myristoylated proteins also (review (Resh 1999)).

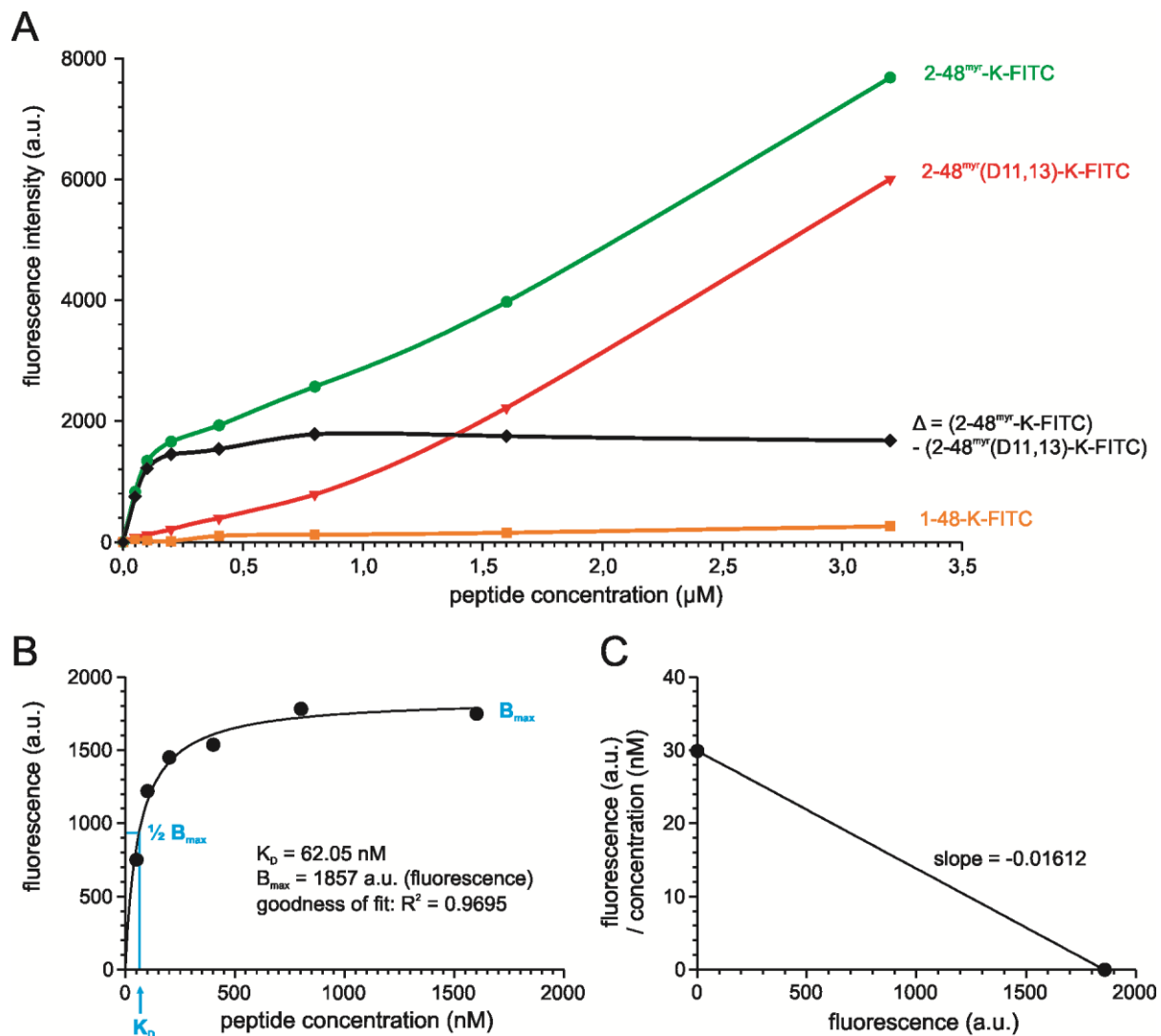


**Figure 14: The bimodal binding mechanism of HBVpreS/2-48<sup>myr</sup>-K-FITC.** (A) PMH were incubated with increasing concentrations (0.05, 0.1, 0.2, 0.4, 0.8, 1.6 and 3.2  $\mu\text{M}$ ) of HBVpreS/2-48<sup>myr</sup>-K-FITC (green), HBVpreS/2-48<sup>myr</sup>(D11,13)-K-FITC (red), and HBVpreS/1-48-K-FITC (orange). Mean fluorescence intensity was measured by flow cytometry and plotted against the respective peptide concentration. Data were normalized by subtracting the autofluorescence. The black line represents specific binding only, normalized as indicated in the graph. (B) Curve fitting of the data normalized for specific binding only (range 0 - 1600 nM) was performed using the function “non-linear regression - specific binding” (GraphPad).  $K_D$  and  $B_{\text{max}}$  were calculated automatically based on the formula described in the text. (C) Linear display of the binding data in a Scatchard plot.

### 3.4.2. Determination of the $K_D$ and $B_{\text{max}}$ of the peptide-receptor interaction

The normalized data obtained by subtraction of the unspecific binding (see Figure 14A) were used to calculate a theoretical binding curve. Based on this it was possible to calculate the dissociation constant  $K_D$  as a measurement of the affinity of the HBVpreS/2-48<sup>myr</sup>-K-FITC-receptor interaction.

$K_D$  describes the affinity of an interaction as the concentration that is needed to achieve a half-maximal binding at equilibrium. By extrapolating ligand-binding to the maximal binding concentration ( $B_{\text{max}}$ ), the half-maximal saturation directly allows the calculation of  $K_D$  using the

function  $[RL] = \frac{B_{\max} \cdot [L]}{K_D + [L]}$ . With  $[RL]$  = receptor ligand complex,  $[L]$  = free ligand, and  $[R]$  = free receptor, this equation can be solved to  $K_D = \frac{[L] \cdot (B_{\max} - [RL])}{[RL]}$ . With  $B_{\max} = [R] + [RL]$  the expression is equal to  $K_D = \frac{[L] \cdot [R]}{[RL]}$ .

$[RL]$  here was the fluorescence intensity (a.u.), and  $[L]$  the peptide concentration (nM). The software GraphPad Prism5 was used for extrapolation and determination of  $B_{\max}$  and  $K_D$ . A correlation coefficient  $R^2$  provided information about how well the theoretical curve fits the real data points.

The theoretical curve resulting from the normalized data is shown in Figure 14B. Linear display of these data is shown in a Scatchard plot (Figure 14C). The slope of the linear regression determines the  $K_D$  by the linear equation  $y = m \cdot x + b$ , with  $m = -1/K_D$ .

Based on these calculations, the  $K_D$  of the interaction between HBVpreS/2-48<sup>myr</sup>-K-FITC and the preS1 receptor was determined to be approximately 60 nM.

It could be argued that the experimental set-up used here did not respect the percentage of unbound peptide, since only cell-associated fluorescence was measured. However, we applied peptide in such an excess that the reduction of unbound ligand in the supernatant could be neglected. Therefore, the number of remaining ligand molecules was defined as equal to the respective input concentration. (Example: assuming a hypothetical number of 300 000 preS1-receptors per cell and a number of  $6 \times 10^7$  peptide molecules applied per cell (= 100 nM), the reduction of ligand would result in a number of  $5.97 \times 10^7$  molecules/cell. This reduction is negligible.) However, this assay was not suited to determine a concentration of  $B_{\max}$ , since this would have required the correlation of fluorescence to a defined fluorophore-peptide concentration. To calculate the total number of receptors on the cell surface of hepatocytes, we performed a similar experiment with PRH, PHH and HepaRG cells, using unlabeled HBVpreS/2-48<sup>myr</sup>. Cell-associated peptide was quantified by HPLC-MS/MS. The cells were incubated with concentrations ranging from 1 to 1000 nM, and cell-associated HBVpreS/2-48<sup>myr</sup> was measured by Prolytic GmbH in ng peptide/ml. Determination of the cell weight enabled us to describe cell-associated peptide as ng peptide/g tissue.

Since unspecific, myristoylation-dependent binding above 400 nM was observed before, the calculations of the theoretical binding curves respected unspecific binding as a linear component ( $[RL] = B_{\max} \cdot [L]/(K_D + [L]) + NS[L]$ ). As depicted in Figure 15, PRH and PHH were characterized by a different  $B_{\max}$  for HBVpreS/2-48<sup>myr</sup>, while the affinity of both receptors for HBVpreS/2-48<sup>myr</sup> was similar. This difference might reflect the previous observation that primary hepatocytes from different species exhibited distinct binding capacities (Figure 10).

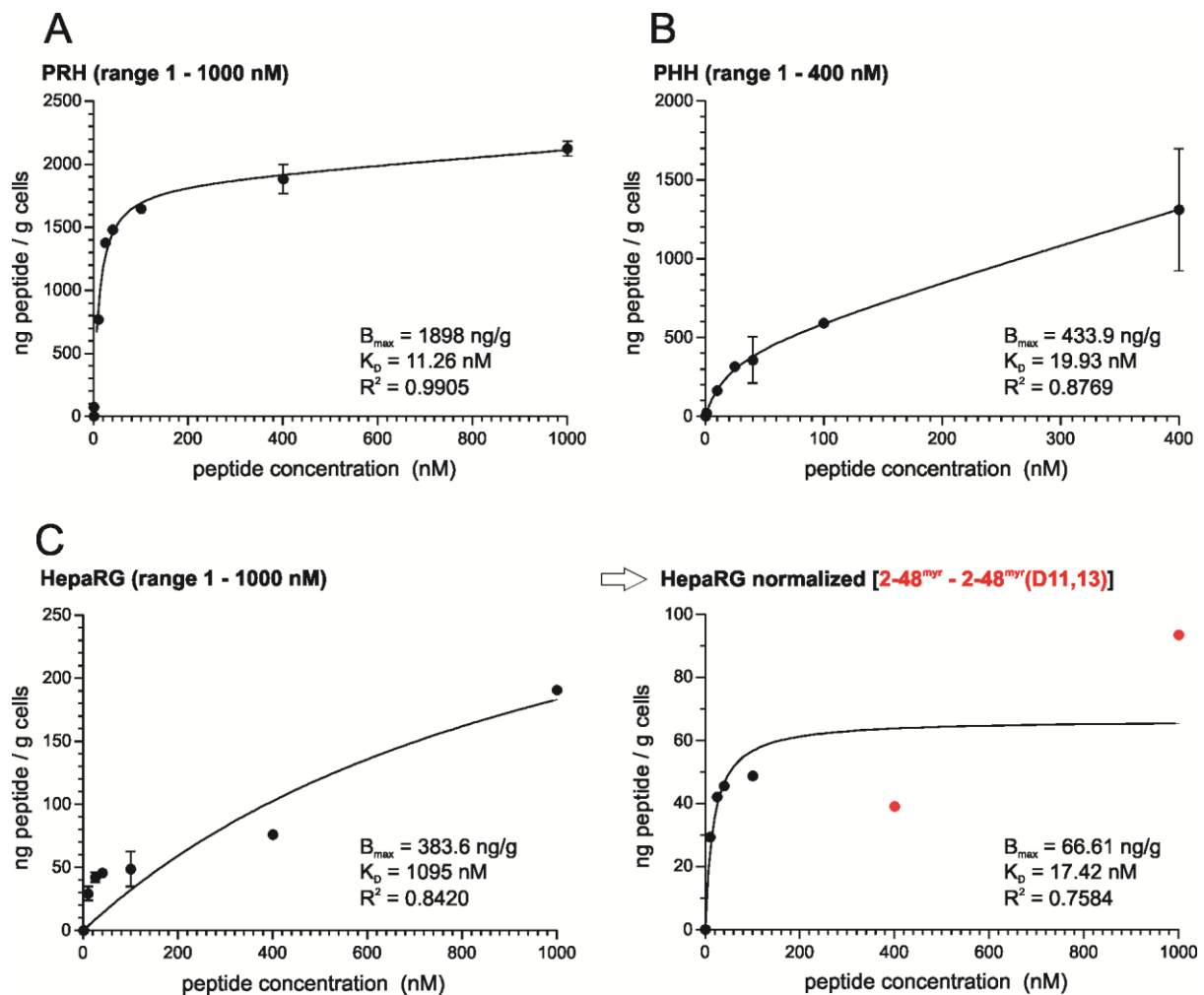


**Figure 15: Binding curves of the interaction of HBVpreS/2-48<sup>myr</sup> with PRH, PHH and HepaRG cells.** Freshly isolated PRH (A), cryopreserved PHH (B), or plated HepaRG cells (C) were incubated with 1, 10, 25, 40, 100, 400 and/ or 1000 nM HBVpreS/2-48<sup>myr</sup>. Cell-associated peptide was quantified by HPLC-MS/MS. Data were processed using the GraphPad Prism5 non-linear regression analysis. (C) Data obtained by incubation of HBVpreS/2-48<sup>myr</sup> on HepaRG cells were plotted before (left), and after (right) normalization by subtraction of unspecific binding. Unspecific binding was determined by measurement of HBVpreS/2-48<sup>myr</sup>(D11,13) (400 and 1000 nM), normalized data points are indicated with red color.  $B_{max}$  = maximal binding concentration (ng peptide/ g cells),  $K_D$  = dissociation constant (nM),  $R^2$  = correlation coefficient.

Surprisingly, HepaRG cells showed a reduced binding capacity, compared to PRH or PHH. As shown in Figure 15C, concentrations up to 100 nM resulted in measurements that were close to the detection limit of the assay. Although these data did not allow calculation of a reliable binding curve, HepaRG cells bound at least 10-fold less peptide (approximately 50 ng/ g cells), compared to PHH (approximately 500 ng/ g cells). This is consistent with infection data that show generally lower values compared with PHH. Additionally, it has been shown that only 10 % of the HepaRG-culture is infected (Andreas Schulze, unpublished data).

An approach to normalize binding was performed by an incubation with 400 and 1000 nM of HBVpreS/2-48<sup>myr</sup>(D11,13). Since the molecular weight of this mutant peptide is equal to that of

HBVpreS/2-48<sup>myr</sup>, it should be detected by HPLC-MS/MS under the same conditions. Indeed, unspecific binding could be measured, resulting in values of 37 ng/ g (at 400 nM) and 97 ng/ g (at 1000 nM).

When the binding curve of HBVpreS/2-48<sup>myr</sup> was normalized by subtraction of the unspecific binding, this led to a theoretical curve, giving a  $B_{\max}$  at very low concentrations (67 ng/ g cells). This implied a saturation of binding sites on HepaRG cells already at low concentrations.

However, the binding curves presented here give only a first indication of the dimensions of  $K_D$  and  $B_{\max}$ . A statistically reliable interpretation would have required much more data points.

#### 3.4.3. HBVpreS/2-48<sup>myr</sup>-K-FITC displays fast binding to its receptor

In order to get insights into the kinetics of HBVpreS/2-48<sup>myr</sup>-K-FITC-receptor binding, a time-course experiment was performed on PHH. Plasma membrane-bound fluorescence intensity in confocal images was determined after incubation with HBVpreS/2-48<sup>myr</sup>-K-FITC for different time periods. As seen in Figure 16A, the fluorescence intensity raised with increasing incubation times. A signal could be detected after only 1 minute of incubation, and equilibrium of binding was reached after approximately 10 minutes. After that, no significant increase of fluorescence could be detected. This is in accordance with observations made by Gripon et al. (2005), who showed that the full inhibitory potential of HBVpreS/2-48<sup>myr</sup> (800 nM) is established on HepaRG cells after 15 minutes of pre-incubation.

#### 3.4.4. The peptide-receptor complexes are retained on the plasma membrane with a half-life of approximately 11 hours

To determine the stability of the peptide-receptor complex, PMH were incubated with HBVpreS/2-48<sup>myr</sup>-K-FITC for a defined time period, washed and further cultivated without the peptide. Fixation at different time points after peptide removal and quantification of the remaining fluorescence enabled the determination of the half-life of HBVpreS/2-48<sup>myr</sup>-K-FITC-receptor complexes on the plasma membrane.

As depicted in Figure 16B, fluorescence at the plasma membrane was still visible after 18 hours. This suggested retention of the peptide on the plasma membrane with a long half-life ( $t_{1/2}$ ), that was calculated to be approximately 11 hours.

This correlated with the  $t_{1/2}$  described by (Gripon et al. 2005), who determined the time needed to regenerate HepaRG-susceptibility after removal of HBVpreS/2-48<sup>myr</sup>. Gripon and colleagues determined  $t_{1/2}$  to approximately 12 hours. *In vivo* biodistribution studies tracking iodinated HBVpreS/2-48<sup>myr</sup>-Y<sup>131</sup> in mice led to a slightly higher  $t_{1/2} \approx 16$  hours (Alexa Schieck, unpublished results).

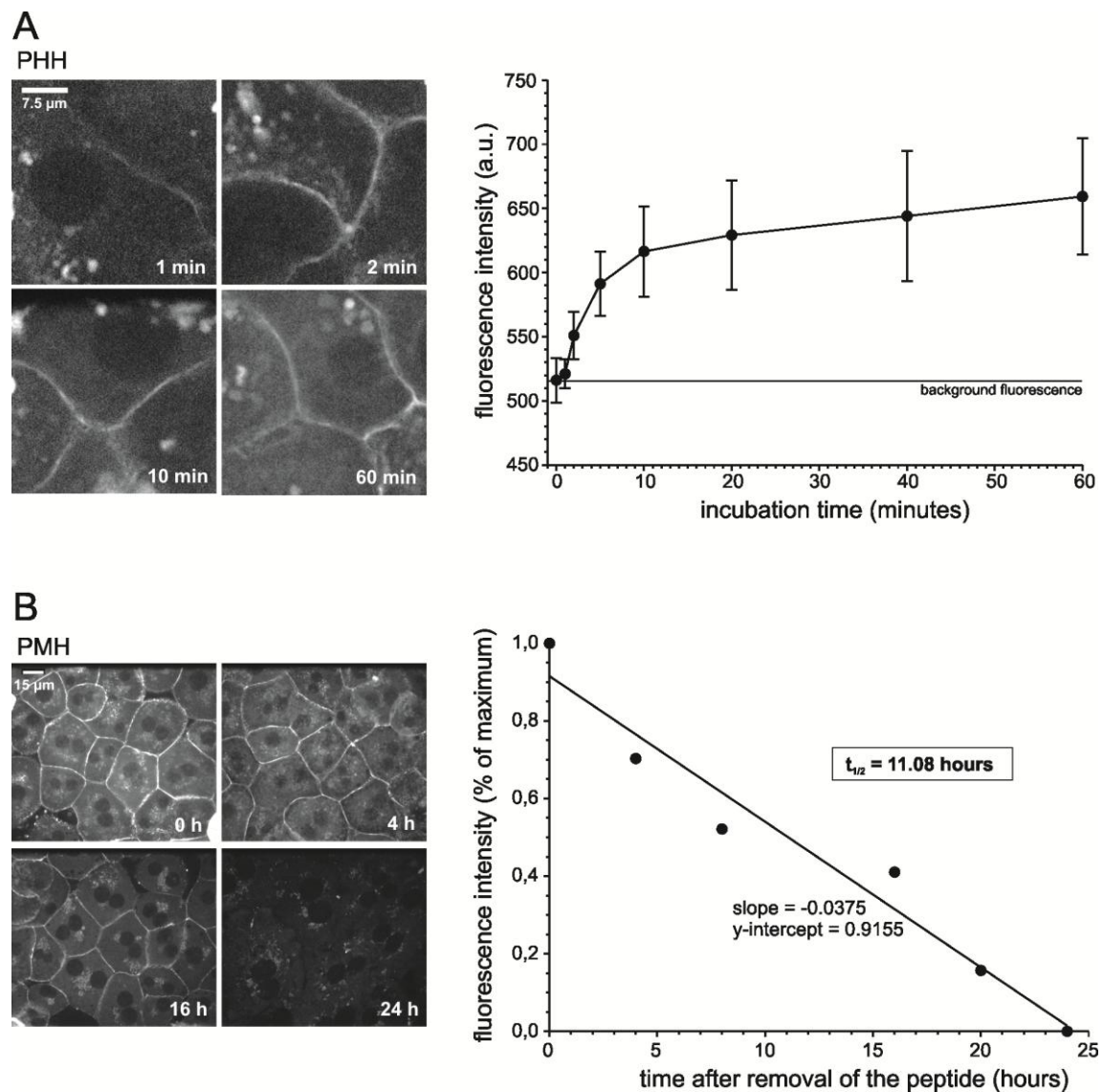


**Figure 16: HBVpreS/2-48<sup>myr</sup>-K-FITC binds to its receptor in a fast and stable manner.** (A) PHH were incubated with 200 nM HBVpreS/2-48<sup>myr</sup>-K-FITC for 1, 2, 5, 10, 20, 40 or 60 minutes. After incubation, cells were washed and immediately fixed. Fluorescence was documented by confocal microscopy (left, blow-ups). Grey values measured in the images reflected the amount of bound peptide and were plotted over time (right). (B) PMH were incubated for 4 hours with 200 nM HBVpreS/2-48<sup>myr</sup>-K-FITC. Peptide was removed and cells were re-incubated for 4, 8, 16, 20 and 24 hours. Fluorescence was documented by confocal microscopy (left), grey values measured in the images were depicted as percentages of the maximum fluorescence observed at  $t = 0$  h (right). The half-life time  $t_{1/2}$  was determined by the linear equation  $y = mx + b$ , with  $m$  (slope) and  $b$  (y-intercept) as indicated and  $y = 0.5$ .

### 3.5 High-resolution microscopy and sub-cellular localization of HBVpreS/2-48<sup>myr</sup>-K-FITC

High-resolution microscopy such as spinning disk confocal or total internal reflection fluorescence (TIRF) microscopy was performed to localize HBVpreS/2-48<sup>myr</sup> binding sites on a sub-cellular level.

### 3.5.1. Spinning disk confocal microscopy revealed binding primarily on the cell surface

Three-dimensional image reconstruction revealed an almost exclusive binding of HBVpreS/2-48<sup>myr</sup>-K-FITC to the plasma membrane of PMH (Figure 17). Therefore, Z-stacks of fixed cells were processed by deconvolution and back-projected to a three-dimensional picture. The ortho-sliced view shows a representative cell from the side.

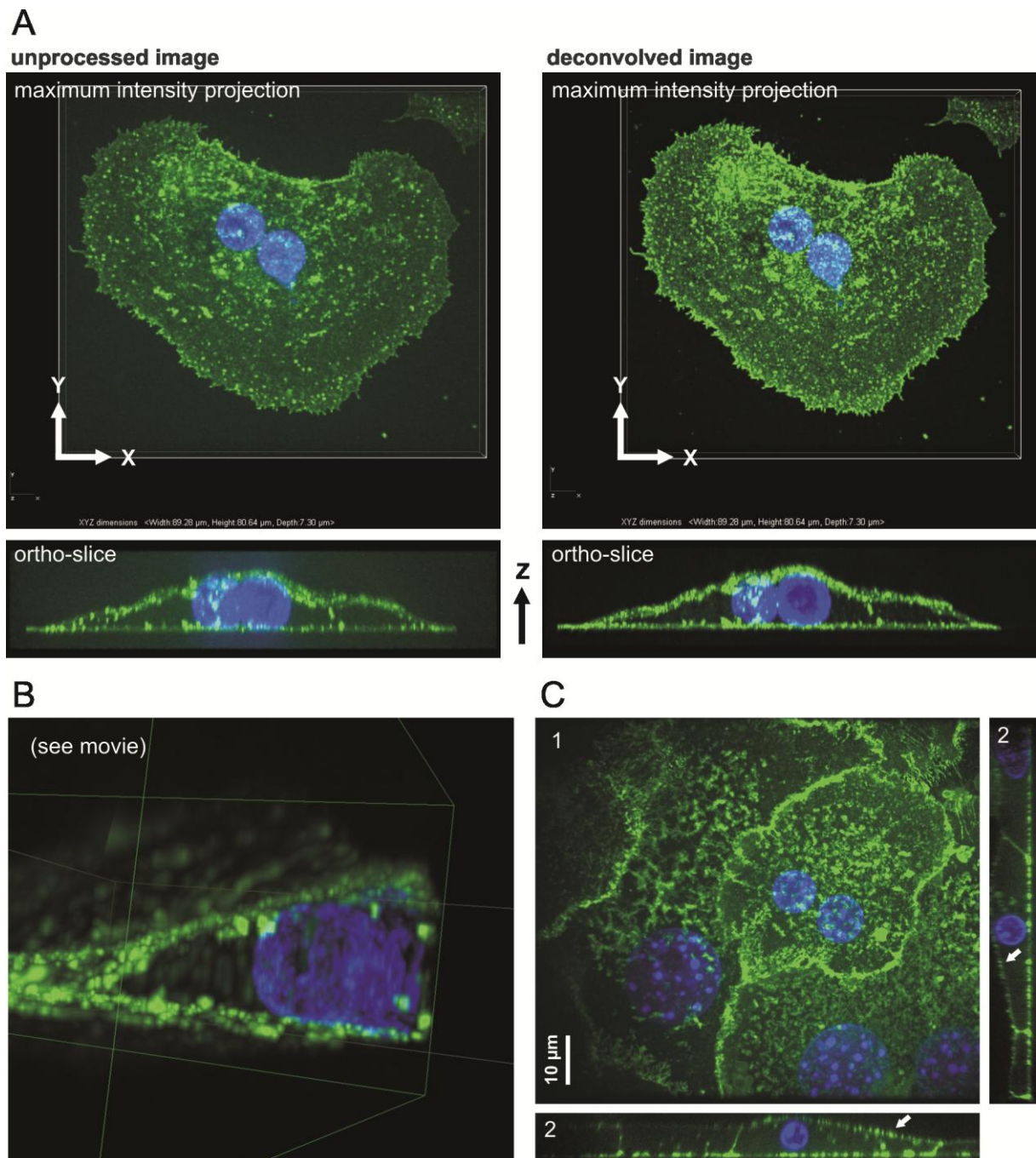


**Figure 17: HBVpreS/2-48<sup>myr</sup>-K-FITC binds to the plasma membrane and is organized in clusters.** (A) Spinning disk confocal microscopy was performed with fixed PRH that were incubated with 200 nM HBVpreS/2-48<sup>myr</sup>-K-FITC for 1 hour. Z-stacks were taken with a 1000x magnification and a Z-spacing of 150 nm. Stacks were reconstructed from non-deconvolved (left) or deconvolved (right) images. Upper panels represent maximum

intensity projections, lower panels the corresponding side views. (B) 3-D animation of a reconstructed, deconvolved Z-stack is provided in the supplementary material. (C) Clusters of fluorescence could be observed on the bottom side (1) and on the top of the cells (2, see arrows). Green: HBVpreS/2-48<sup>myr</sup>-K-FITC, blue: nuclei stained with DAPI.

Since deconvolution of images is prone to create artifacts, an example of a non-deconvolved versus a deconvolved image is presented to demonstrate that the overall appearance of peptide did not change, while the clarity of the image improved.

Although described differently by (Glebe et al. 2005), who showed uptake of HBVpreS/2-48<sup>myr</sup> to PTH and HepG2 cells, we could not confirm an intracellular localization of HBVpreS/2-48<sup>myr</sup>-K-FITC. However, future experiments should include a control of the endocytic activity of the cells.

The plasma membrane-bound fluorescence was found to be organized in clusters. As seen in Figure 17B and C, and the corresponding movie (see supplementary material), these clusters were present on both, the upper, medium-directed cell surface, and the bottom side.

### 3.5.2. Total internal reflection fluorescence microscopy: analysis of live cells showed the presence of finger-like plasma membrane protrusions that bound HBVpreS/2-48<sup>myr</sup>-C-Atto565

Total internal reflection (TIRF) microscopy was performed as an alternative high-resolution microscopy technique. This required the use of a peptide labeled with the more photostable fluorophore Atto565.

Live PMH were therefore incubated with HBVpreS/2-48<sup>myr</sup>-C-Atto565 and HBVpreS/2-48<sup>myr</sup>(D11,13)-C-Atto565, and fluorescence was monitored using the TIRF modus. Shown in Figure 18A is the fluorescence of HBVpreS/2-48<sup>myr</sup>-C-Atto565 bound to a cell. Similar to the clusters observed by spinning disk confocal microscopy, also TIRF microscopy revealed the presence of fluorescence that was organized in clusters that appeared more dotted. The control peptide HBVpreS/2-48<sup>myr</sup>(D11,13)-C-Atto565 did not bind to hepatocytes (data not shown).

Additionally to the clustered binding phenotype, we detected fluorescent finger-like protrusions of the plasma membrane. Time-lapse acquisitions of live cells revealed that these protrusions showed movement (see movie). That these structures were present also on fixed cells can be seen in the confocal image shown in Figure 18A (right).

To get an impression of the kinetics of HBVpreS/2-48<sup>myr</sup>-C-Atto565 binding in real time, hepatocytes were imaged immediately after addition of the peptide. As depicted in Figure 18B, we detected association and dissociation of fluorescent structures throughout the whole time lapse (20 seconds). To display and characterize only a fraction of these fluorescent structures, an axis was defined in x,y and the fluorescence along this axis was displayed by creation of a kymograph. Thereby, mainly two different binding forms were detected: one being characterized by a stability in x,y-position not showing dissociation, the other by changes of the x,y-position and only transient binding. Changes of

the x,y-position reflect a lateral movement. The majority of binding events, however, was represented by a stable interaction without dissociation or lateral mobility.

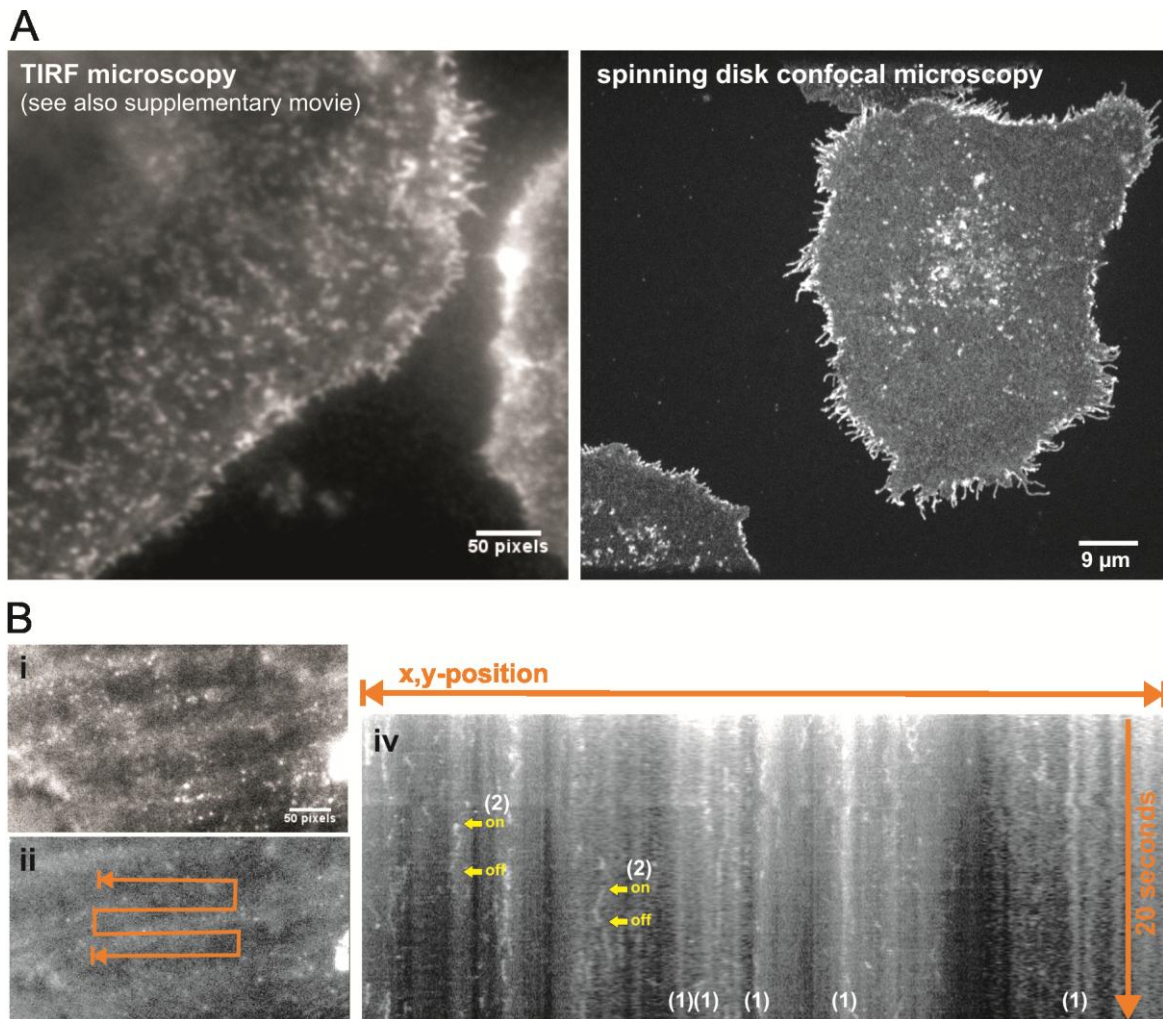


**Figure 18: Binding of HBVpreS/2-48<sup>myr</sup>-C-Atto565 observed by TIRF microscopy in real-time.** (A) PMH were incubated with 200 nM HBVpreS/2-48<sup>myr</sup>-C-Atto565 for 30 minutes, washed and live-cell microscopy was performed in the TIRF modus. Finger-like protrusions seen in the representative frame of a time-lapse acquisition (left) showed movement, as demonstrated in the supplementary movie, and were detectable also on fixed cells by confocal microscopy (right). (B) The interaction of HBVpreS/2-48<sup>myr</sup>-C-Atto565 with the plasma membrane immediately after addition of the peptide was monitored for 20 seconds. A single frame of a representative movie is shown in (i). Fluorescence along a randomly defined line (ii) was displayed as a function of time in a kymograph (iv). Two different binding types were observed, (1) and (2), that differed in their temporal and positional stability.

### 3.5.3. A restricted lateral mobility of peptide-receptor complexes indicated an interaction with the cytoskeleton

The temporal and spatial stability of some peptide-bound structures observed by TIRF microscopy initiated its further investigation by measuring the fluorescence recovery after photo-bleaching (FRAP). Using a high-powered focused laser beam, a small area within the focal plane of the PMH plasma membrane was photo-bleached, and the diffusion of surrounding unbleached molecules was

measured as a function of time. To prevent a possible replenishment with unbleached molecules from the medium, the peptide solution was removed from the cells before starting the acquisition. As a control for fluorescence recovery, PMH were stained with the amphiphilic lipid dye octadecyl indocarbocyanine (DiI), representing the diffusion characteristics of lipids.

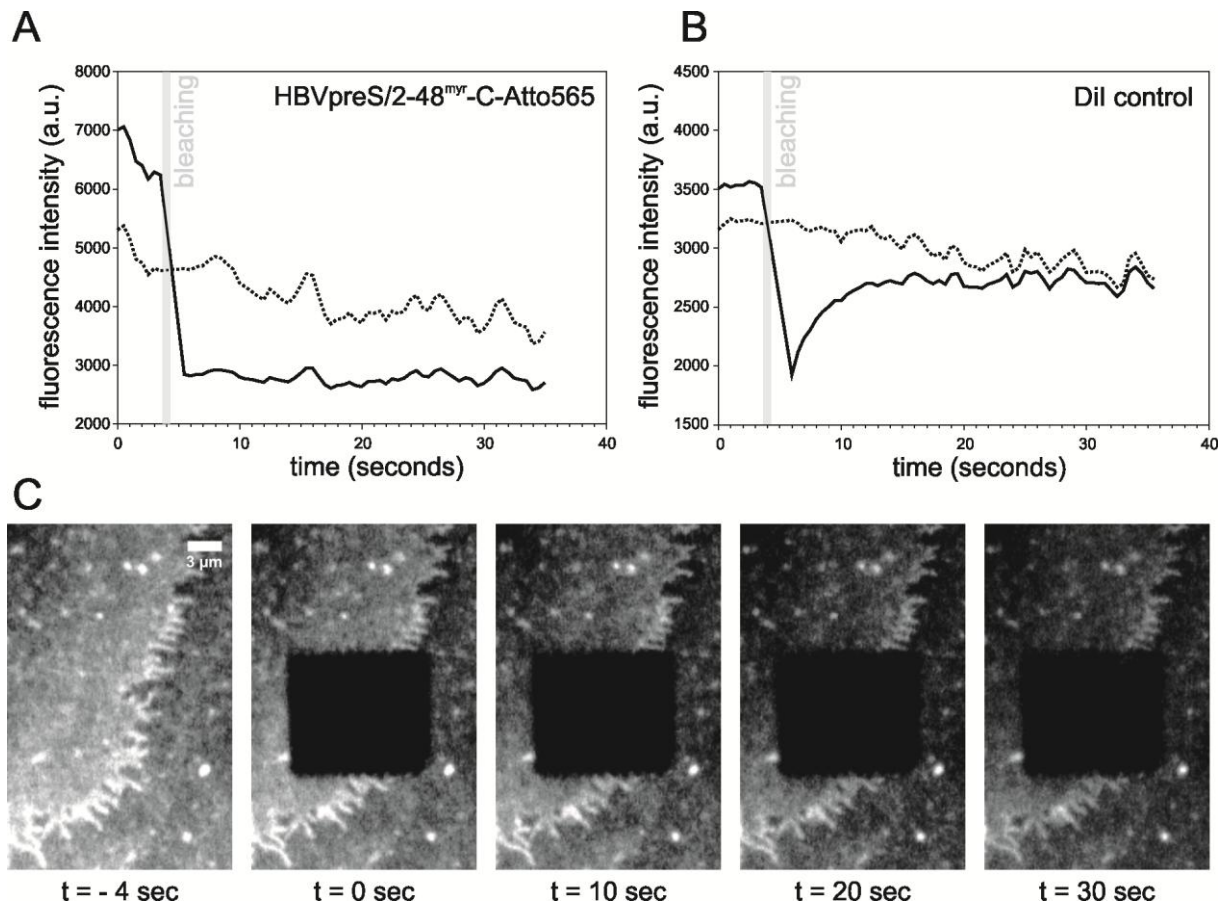


**Figure 19: The peptide-receptor complexes show a restricted lateral mobility.** Live PMH were incubated with (A) HBVpreS/2-48<sup>myr</sup>-C-Atto565 (200 nM) for 1 hour or (B) DiI (5 μl/ ml) for 30 minutes. Cells were washed and time lapses were acquired for 34 seconds. Bleaching was performed after 4 seconds. Fluorescence was quantified in the bleached region (solid lines) and a non-bleached control region (dotted lines). Blow-ups from representative frames of the experiment shown in (A) are depicted in (C).

As seen in Figure 19, bleaching of HBVpreS/2-48<sup>myr</sup>-C-Atto565 led to a loss of fluorescence that was not restored within the measured time period (30 seconds). In contrast, the DiI control stain showed rapid recovery of fluorescence within approximately 6 seconds. The fluorescence intensity of the bleached area and a non-bleached control region was plotted as a function of time to quantify recovery of fluorescence (A and B). Images depicted in (C) represent single frames from a representative time lapse experiment, showing the area of interest on HBVpreS/2-48<sup>myr</sup>-C-Atto565-incubated hepatocytes before and 0, 10, 20 and 30 seconds after the bleaching event.

These data indicated a restricted lateral mobility of the peptide-receptor complexes which was consistent with our previous observation of a temporal and spatial stability in TIRF microscopy. The rapid diffusion of Dil within the plasma membrane demonstrated the functionality of this assay.

#### 3.5.4. Clusters of fluorescence showed a partial co-localization with actin

Restricted lateral mobility is assumed to be mediated by an interaction with the cytoskeleton. To get an impression whether this interaction can be visualized directly, co-localization studies were performed with HBVpreS/2-48<sup>myr</sup>-K-FITC and phalloidin-Alexa565. Phalloidin, a toxin made by the mushroom *Amanita phalloides*, binds F-actin with a high-affinity.

Interestingly, when PMH were incubated with HBVpreS/2-48<sup>myr</sup>-K-FITC, fixed and subsequently stained with phalloidin-Alexa565, we regularly detected an association of peptide and actin in the clustered structures that had been observed previously by confocal microscopy (**Figure 17**). These structures were present on the plasma-directed and the bottom membrane. Striking was the appearance of spots of actin that were surrounded by ring-like structures of bound peptide (B, arrows).

A block of actin polymerization by treatment of the cells with cytochalasin D prior to peptide binding resulted in a rearrangement of the actin cytoskeleton, but in no severe alteration of the peptide binding. We had the impression that the outer membrane borders and finger-like protrusions showed a reduced peptide binding, but the overall distribution was not changed obviously. However, actin foci remained associated with peptide also after cytochalasin D treatment.

Most of the endocytotic pathways that are used by viruses to enter a cell (clathrin- or caveolin-mediated endocytosis, or macropinocytosis) typically involve the presence of actin. The association of actin with the preS1-receptor complexes suggests an involvement of actin during HBV entry.

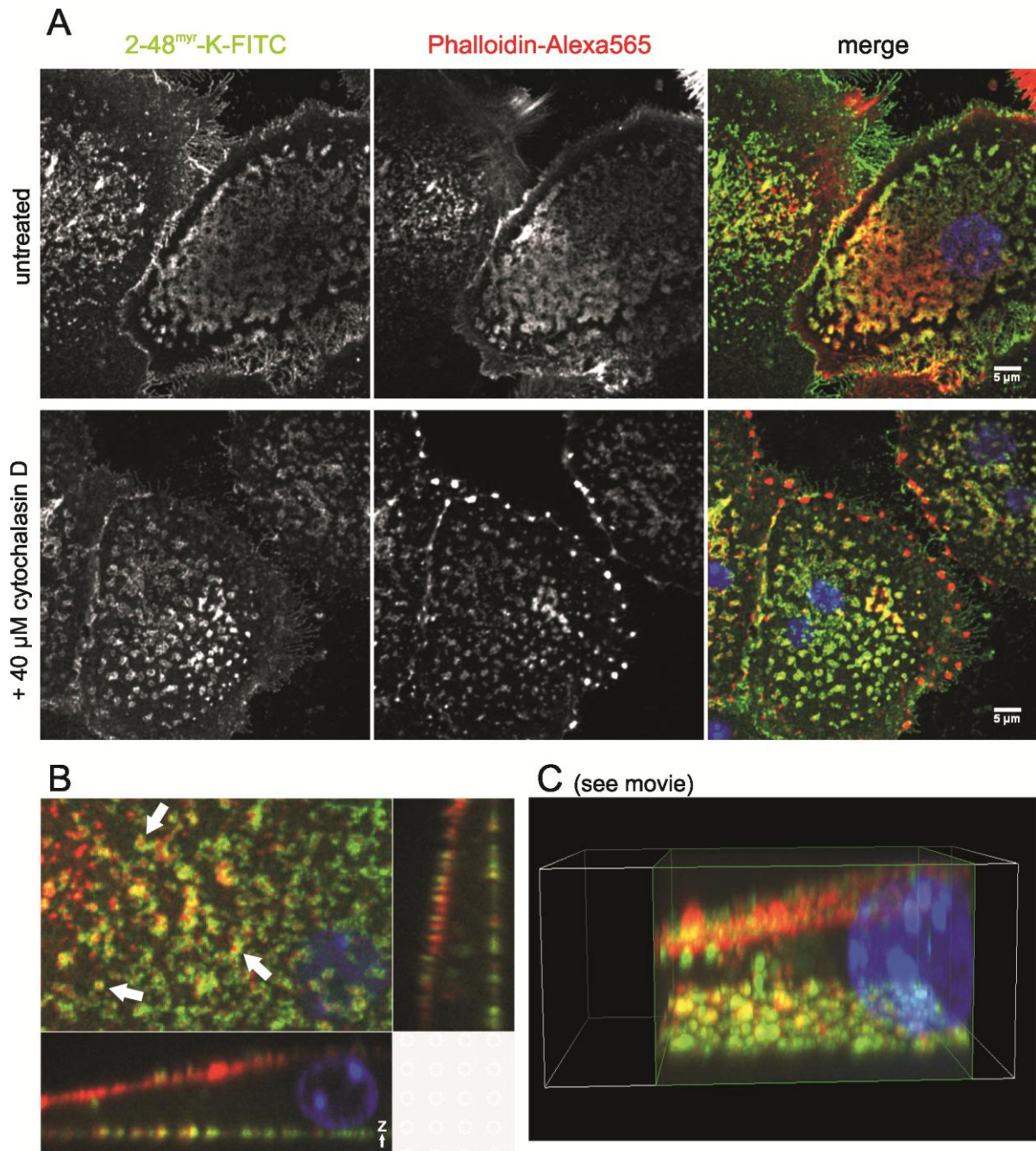


**Figure 20: HBVpreS/2-48<sup>myr</sup>-K-FITC colocalizes with actin.** (A) PMH that were untreated (upper panel) or pre-treated with 40  $\mu$ M cytochalasin D (lower panel) were incubated with 200 nM HBVpreS/2-48<sup>myr</sup>-K-FITC (green). After PFA-fixation, actin was stained with phalloidin-Alexa565 (red) and confocal microscopy was performed with a 1000x magnification. Nuclei were stained with DAPI (blue). (B) Depicted is a blow-up of a reconstructed Z-stack from cells incubated with HBVpreS/2-48<sup>myr</sup>-K-FITC and stained with phalloidin-Alexa565. Co-localization of actin and peptide was observed on the cell bottom (upper left) and the corresponding side-views. Actin spots surrounded by peptide are indicated by arrows. (C) Animated reconstruction of the example shown in B, see movie in the supplementary material.

### 3.6 Production, characterization and visualization of fluorescently labeled HBV

In order to compare the kinetic behavior of HBVpreS/2-48<sup>myr</sup>-K-FITC with that of virions, it would be beneficial to directly track HBV particles in real time. Fluorescent labeling has been described for many viruses (e.g. HIV-1, SV40), but not for HBV. Its small size and the compact genome organization complicate the incorporation of fluorescent proteins or dyes.

#### 3.6.1. Production of fluorescently labeled HBV particles

Several approaches were followed to fluorescently label HBV particles: Besides the incorporation of amphiphilic probes such as octadecyl indocarbocyanines (DiI) or octadecyl oxacarbocyanines (DiO) or lipid analogs like 1,2-dioleoyl-*sn*-glycero-3-phosphoethanolamine-N-carboxyfluorescein (PE-FITC), we applied a chemical labeling strategy based on the reaction of succinimidyl esters (Alexa488 succinimidyl ester) with primary amines on HBV envelope proteins.

The labeling with DiI or DiO resulted in the formation of aggregates during purification and was not further followed. The incorporation of the phospholipid derivative PE-FITC into the HBV envelope membrane resulted in fluorescently labeled HBV particles that could be characterized on a single-particle level. However, infectivity of HBV-PE-FITC particles could not be demonstrated. Moreover, FITC-labeled particles were not suited for live-cell experiments due to the photo-sensitivity of FITC.

Particle labeling with Alexa488 succinimidyl esters yielded fluorescently labeled particles that could be characterized on a single-particle level, that were infectious, and well detectable on HepaRG cells. Therefore, highly purified HBV from HepAD38 cell culture supernatant was labeled with Alexa488 succinimidyl ester. The latter reacts with primary amines as present in lysines in the HBV envelope proteins under formation of stable amide bonds.

After labeling, unbound dye was removed by heparin-affinity chromatography, and the viral peak fractions were further purified and concentrated by sucrose-density gradient centrifugation. As a first control the sucrose gradient was checked after centrifugation for the presence of fluorescent band(s) (not shown).

#### 3.6.2. Biochemical characterization of HBV-Alexa488

Fractions from the sucrose-density gradient centrifugation were analyzed for their HBV DNA content by DNA dot-blot and the presence of Alexa488-fluorescence by fluorometry (Figure 21A). Viral proteins were detected by Western blotting (B) and the purity of the preparation was checked by silver gel analysis (C).

As demonstrated by a representative HBV-Alexa488 preparation, HBV-DNA could be detected in fractions 7 to 10, with a DNA-peak in fraction 9. Excitation with 488-nm light resulted in an emission

of 520-nm fluorescence in the fractions 6 to 12. A possible explanation for the drop of fluorescence in fraction 9 (HBV-DNA peak) could be e.g. quenching of fluorescence. This would implicate an over-labeling of particles. Fluorescence in the fractions 11 and 12 that did not contain HBV-DNA might result from co-purification and labeling of L-containing filaments. The high fluorescence in the earlier fractions 6 and 7 could not be explained but might be derived from protein-contamination.

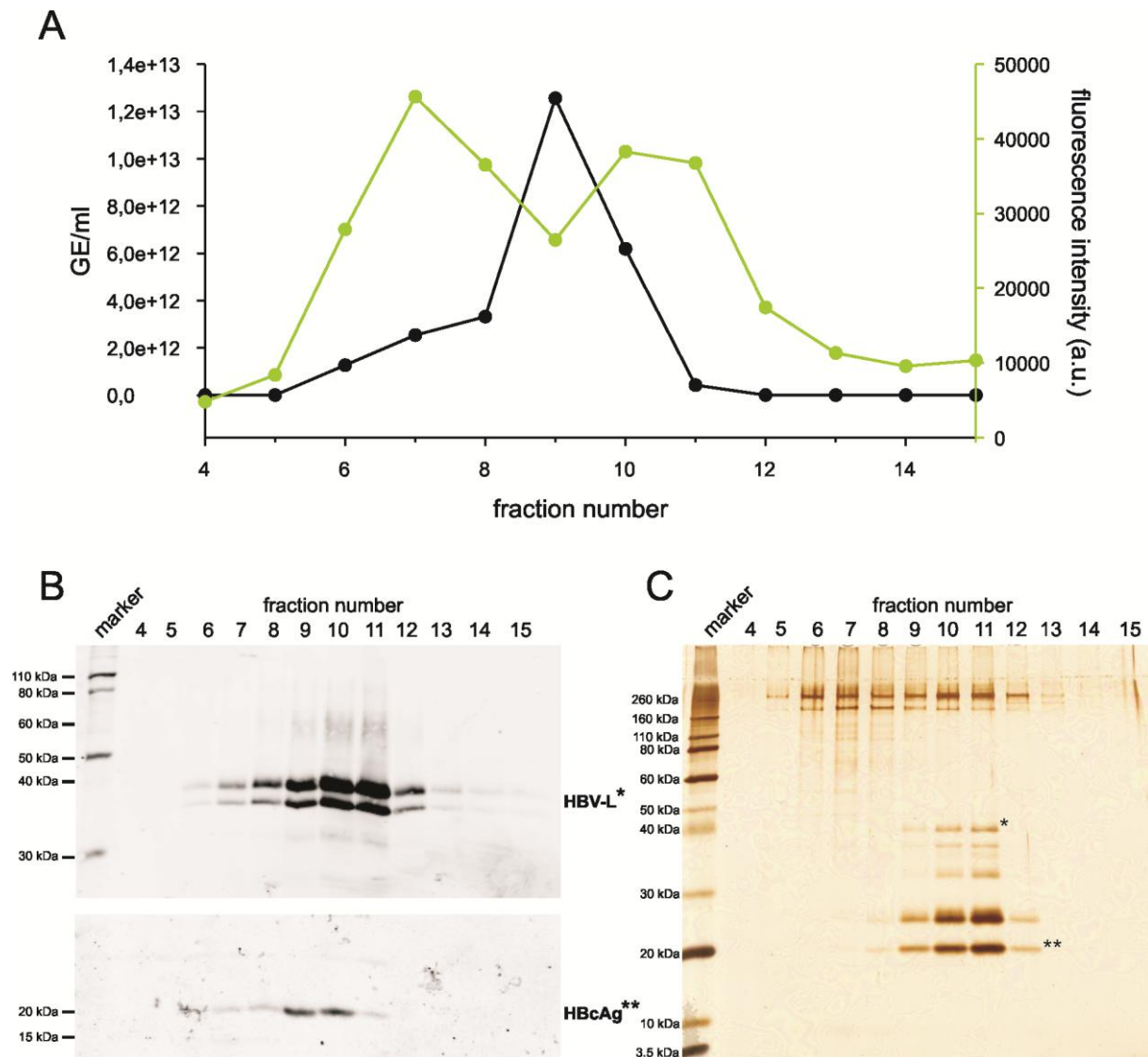


**Figure 21: Biochemical analysis of fractions from a sucrose-density gradient.** (A) HBV-DNA was measured in fractions from a sucrose-density gradient by DNA dot blot (left y-axis, black curve). Alexa488-fluorescence was measured with a fluorometer (right y-axis, green curve). Fractions 4 to 15 were analyzed. (B) SDS-PAGE and subsequent Western blotting detected HBV-L protein (39/42 kDa) by the preS1-specific monoclonal antibody Ma18/7 (upper part of the blot) and core protein (22 kDa) by the polyclonal rabbit serum H363 (lower blot) on the same blot. Sizes of the protein marker are indicated left. (C) Protein content in the fractions was visualized by silver staining of the proteingel after SDS-PAGE. Asterisks indicate L-protein or core-protein, respectively. A size marker is included in the left lane. (A), (B) and (C): each analysis was performed with a 5  $\mu$ l sample of the respective fraction.

A Western blot detected L-protein with the monoclonal antibody Ma18/7 in the fractions 7 to 12, with a peak in fractions 9, 10 and 11. Since fraction 12 did not contain HBV-DNA or core-protein detectable by Western blot with H363, it is likely to contain co-purified HBV filaments. However, a silver gel providing information about the overall protein content showed the presence of a ~ 20 kDa protein in fraction 12, indicating the presence of core protein. This discrepancy could be explained by the co-purification of empty, enveloped cores, but was not further investigated.

For further analysis samples were taken from fraction 8 or 9.

### 3.6.3. Microscopic characterization of HBV-Alexa488 showed the presence of single particles and aggregates

To characterize the sucrose-density gradient peak fraction by fluorescence microscopy, 10- $\mu$ l samples from fraction 8 and fraction 4 were mounted on glass slides and analyzed by spinning disk confocal microscopy. As seen in Figure 22A, the sample derived from a virus peak fraction showed the presence of fluorescent particles, whereas a control sample from fraction 4 did not. HBV-Alexa488 particles could be detected with an exposition time of 300 ms.

To analyze the fluorescence of single particles, fluorescence intensities were measured by an ImageJ function and plotted as a profile. As seen in Figure 22B (upper panel) single particles showed a Gaussian distribution of the fluorescence intensity. Although the size of the fluorescent spot ( $\varnothing \sim 200$  nm) does not directly reflect the size of its origin, it was defined as characteristic for single particles. In contrast to a single particle, aggregates were represented by a broader distribution of the fluorescence (Figure 22B, lower panel). The fluorescence intensity profile of the aggregate shown here as an example, was additionally characterized by two peaks. This could be due to the presence of two (main) sources of fluorescence in close proximity. Therefore, the fluorescence intensity profiles showed overlapping curves that could not be resolved due to the optical limitations.

A statistical analysis of particle sizes within a preparation is shown in (C). Measurement of particle sizes by the ImageJ function *particle analysis* showed, that most particles possessed a small size of one or a few pixel<sup>2</sup> (1 pixel<sup>2</sup>  $\sim 8.1$  nm<sup>2</sup>). However, the preparation contained also a low number of aggregates (up to 87 pixel<sup>2</sup>).

Taken together, these data demonstrated that fluorescently labeled, single HBV-Alexa488 particles could be detected with an exposition time of 300 ms.

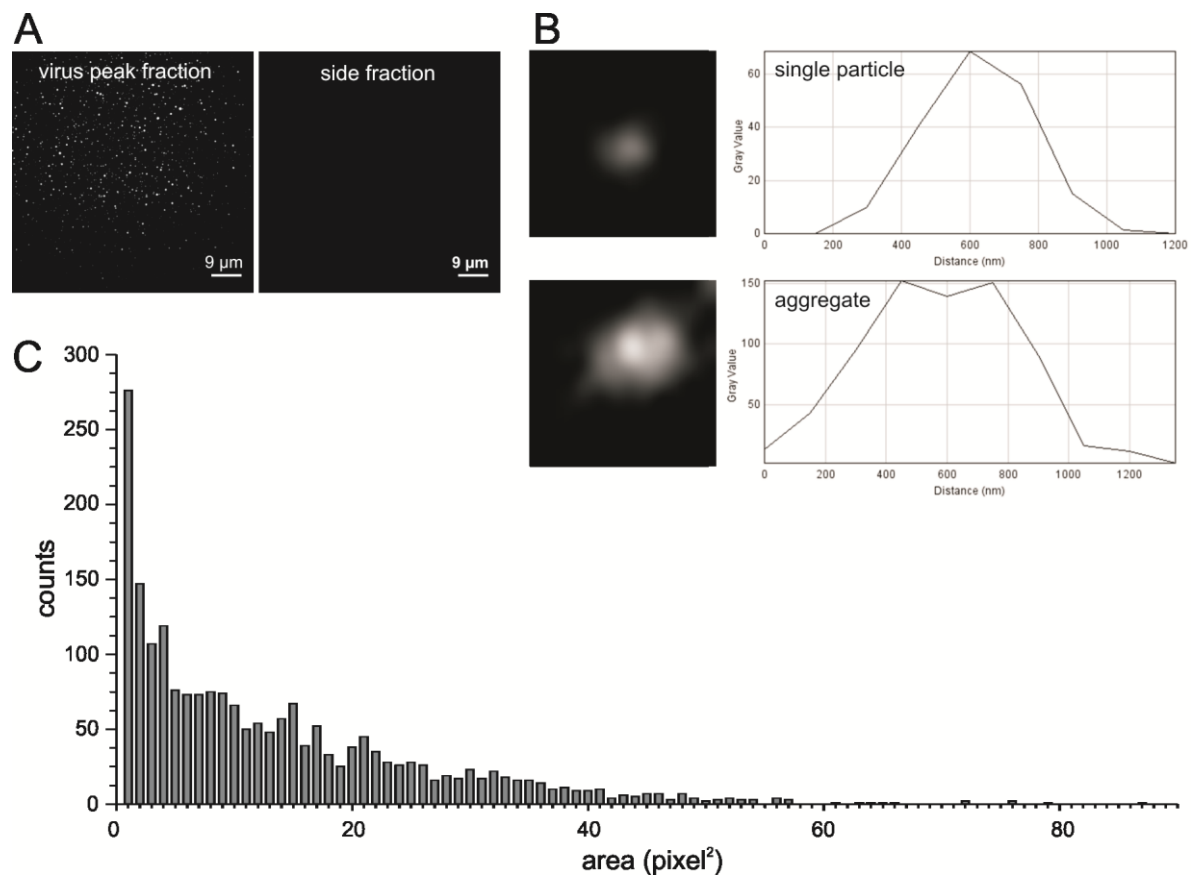


**Figure 22: Microscopic analysis of HBV-Alexa488 particles.** (A) 10- $\mu$ l samples of a peak fraction (fraction 8) and a side fraction (fraction 4) were mounted on glass slides and monitored with the 488-nm laser line by spinning disk confocal microscopy with a 1000x magnification. (B) The profiles of the fluorescence intensities of a representative single particle (upper panel) and an aggregate (lower panel) were measured using the ImageJ plug-in “plot profile”. Fluorescence (grey value) is shown as a.u. and the distance is given in  $\mu$ m. (C) The distribution of particle sizes within 3 representative pictures of the fraction 8 was determined by the ImageJ plug-in “particle analysis”. Particle sizes are given as ( $\text{pixel}^2$ ), numbers of particles (counts) are indicated on the y-axis.

#### 3.6.4. HBV-Alexa488 is highly infectious on HepaRG cells

To test whether HBV-Alexa488 is infectious, HepaRG cells were inoculated with samples from the peak fraction (8) and a side fraction (3) as negative control. HBeAg and HBsAg as markers for infection were measured in the supernatant collected from day 4 to 7, or day 7 to 11 post infection. As demonstrated in Figure 23 an infection was established using Alexa488-labeled HBV. As a positive control we used PEG-precipitated stock virus. The HBsAg-measurement revealed an approximately 6-fold higher HBsAg value for HBV-Alexa488 compared with the PEG-virus. This might be explained by a 6.25-fold higher MGE/ cell in case of HBV-Alexa488. A quantitative measurement of the multiplicity of infection, however, would need the comparison with an equally produced, non-labeled HBV.

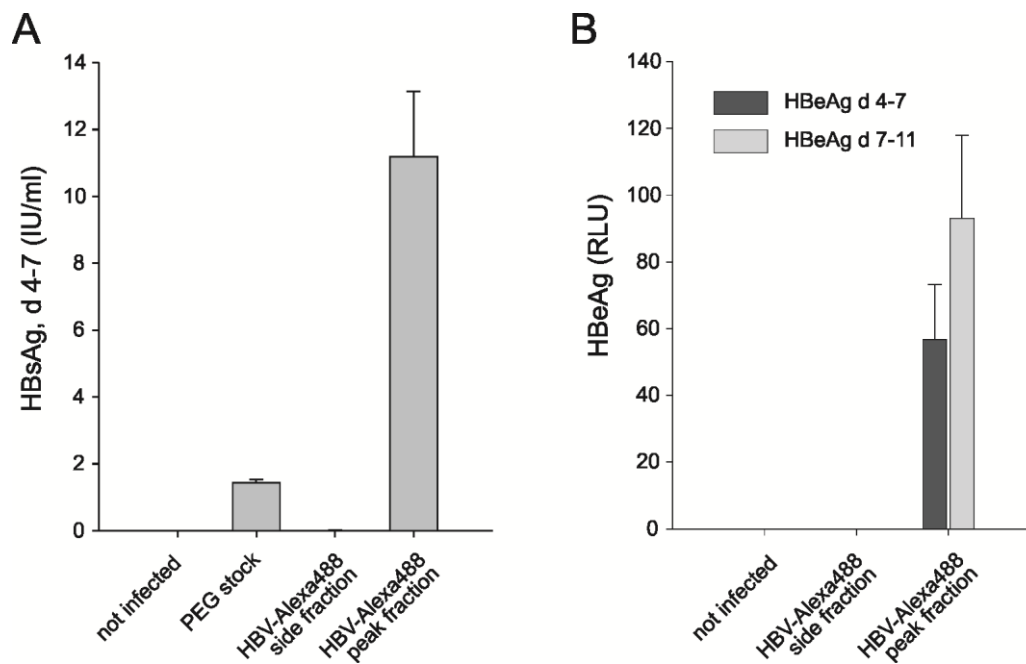


**Figure 23: Infectivity of HBV-Alexa488.** Differentiated HepaRG cells were inoculated o/n without (not infected) or with PEG-precipitated stock virus ( $\sim 1 \times 10^4$  GE/ cell), or HBV-Alexa488 ( $\sim 6.25 \times 10^4$  GE/ cell) from fraction 8 (peak fraction), or a corresponding volume of fraction 3 (side fraction) from the sucrose-density gradient shown in Fig. 21. Markers for infection were measured by ELISA: HBsAg was measured in the supernatant collected from day 4 to 7 (A) and HBeAg was determined from day 4 to 7 and 7 to 11 (B). Cut-off of the assays was HBsAg: 0.05 IU/ ml, HBeAg: 1 RLU.

### 3.6.5. HBV-Alexa488 binding to differentiated HepaRG cells can be enhanced by PEG and inhibited by heparin

In order to check HBV-Alexa488-binding to cells, differentiated HepaRG cells were inoculated with the fluorescently labeled virus for 1.5 hours, washed and the fixed cells were analyzed by spinning disk confocal microscopy. As seen in Figure 24, some HBV-Alexa488 particles could be found on HepaRG cells when incubated in absence of polyethyleneglycol (PEG). Consistent with what has been described for unlabeled HBV (Gripon et al. 1993) the addition of PEG during inoculation enhanced particle binding significantly. A control inoculum (fraction 3) also incubated in presence of PEG did not show particulate fluorescence. Furthermore, binding of HBV-Alexa488 could be inhibited with heparin in concentrations that block HBV binding (Schulze et al. 2007), being an indication for the authenticity of the system. However, the specificity of this binding has to be approved in future experiments, e.g. by the use of neutralizing antibodies.

The maximum intensity projection of HepaRG cells inoculated with HBV-Alexa488 that was derived from a different preparation provides information about the binding distribution. Although not quantified or validated by the use of differentiation-markers, binding appeared to be distributed over all cells and did not show a preference for differentiated hepatocyte-like cells. This has to be further tested in future.

3-dimensional reconstruction of Z-stacks showed a predominant localization of HBV-Alexa488 particles on the medium-directed plasma membrane. Figure 24C and D show an ortho-sliced view and a representative movie included in the supplementary material. Despite the relatively long incubation period of 1.5 hours at 37°C, a significant uptake of these particles was not observed.

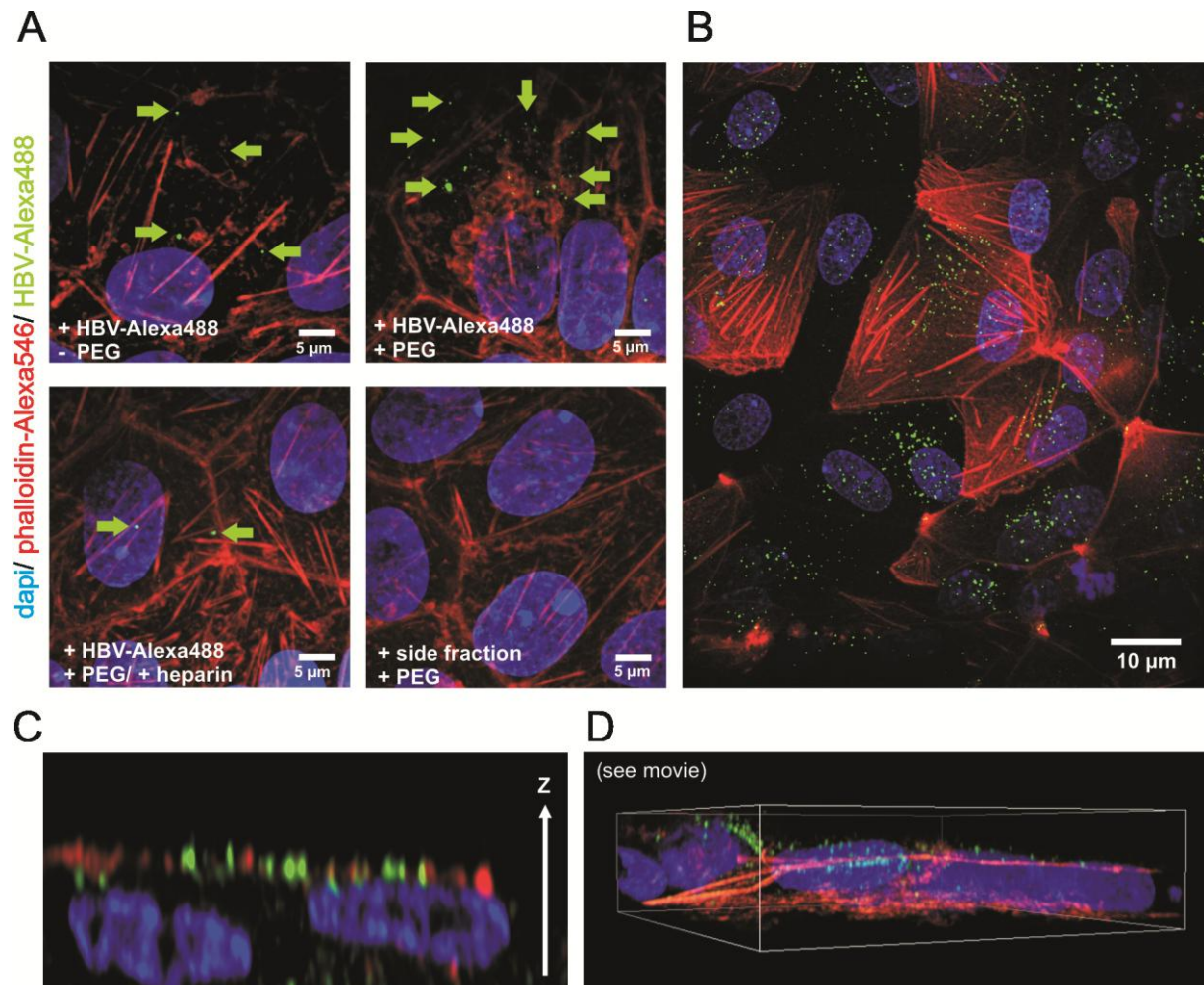


**Figure 24: HBV-Alexa488 binding to differentiated HepaRG cells.** (A) HepaRG cells were incubated with HBV-Alexa488 (fraction 8) in the presence of absence of PEG (4 %) and heparin (600 µg/ ml) for 1.5 hours at 37°C. As a control, cells were incubated with an inoculum from fraction 3 in presence of PEG. Pictures of fixed cells were taken with a 1000x magnification using spinning-disk confocal microscopy. The actin cytoskeleton was stained with phalloidin-Alexa546, nuclei were stained with DAPI. (B) HBV-Alexa488 from a different preparation was incubated with HepaRG cells as described in (A), in presence of 4 % PEG. Pictures shown in (A) and (B) represent maximum projections of Z-stacks. An orthogonal view (C) and an animated 3-D reconstruction (D, see movie in the supplementary material) of a Z-stack from the experiment shown under A, upper right.

#### 4. Discussion

HBVpreS/2-48<sup>myr</sup> inhibits HBV infection *in vitro* and *in vivo* with a remarkably high efficiency and specificity (Gripon et al. 2005; Petersen et al. 2008). Both, the integrity of the preS1-sequence in the essential region (amino acids 9 - 15, genotype D) and the N-terminal myristoylation of HBVpreS/2-48<sup>myr</sup> are essential for the peptide's inhibitory activity. Single amino acids (positions 11, 12 and 13, genotype D) could be identified that are crucial for infection inhibition (Engelke et al. 2006), and the removal of the acylation leads to an extremely reduced inhibitory potential (Gripon et al. 2005).

Both findings tightly correlate with determinants of HBV infectivity: recombinant HBV particles, carrying the same point mutations in context of the L-protein, are non-infectious (Engelke et al. 2006), and the myristoylation of the preS1-domain is absolutely essential for hepadnaviral infectivity (Gripon et al. 1995). This analogy strongly suggests that the virus and the preS1-peptide address a common factor on the hepatocyte at least at one step during infection.

In order to characterize the interaction with this factor, the present work aimed to visualize and characterize receptor binding of fluorescently labeled HBVpreS/2-48<sup>myr</sup> peptides.

##### 4.1 HBVpreS/2-48<sup>myr</sup> binds to a receptor on the plasma membrane of HBV-susceptible hepatocytes in a highly sequence- and myristoylation-dependent manner

As it has been described initially, fluorescently labeled HBVpreS/2-48<sup>myr</sup> interacts with the cell surface of PHH (Gripon et al. 2005). We here provide a detailed analysis of this interaction, using HBVpreS/2-48<sup>myr</sup>-K-FITC and two control peptides, the mutant HBVpreS/2-48<sup>myr</sup>(D11,13)-K-FITC and the non-myristoylated variant HBVpreS/1-48-K-FITC. Both controls do not inhibit the infection with HBV and HDV, respectively.

Fluorescence microscopy and flow cytometry showed that HBVpreS/2-48<sup>myr</sup>-K-FITC specifically bound to the plasma membrane of HBV-susceptible cells like PHH, PTH and HepaRG cells. In contrast, the control peptides did not show binding, demonstrating that the interaction strictly depends on the integrity of the amino acid sequence and the presence of the N-terminal myristoylation. This completely correlated with the inhibitory potential of these peptides and directly showed that the lacking inhibitory activity of the control peptides is a consequence of their inability to bind to a specific preS1-receptor.

The high specificity of binding could be validated by competition experiments. Whereas an excess of unlabeled HBVpreS/2-48<sup>myr</sup> could prevent binding of HBVpreS/2-48<sup>myr</sup>-K-FITC, even a 100-fold excess of the unlabeled mutant peptide had no effect.

#### 4.2 The expression of an HBVpreS/2-48<sup>myr</sup>-receptor is not restricted to HBV-susceptible cells

*In vivo* biodistribution studies have shown that iodinated HBVpreS/2-48<sup>myr</sup>-Y<sup>131</sup> accumulated in the liver of mice, although they are not susceptible to HBV infection (Alexa Schieck, diploma thesis, see Figure 3). In tight correlation with the requirements for the infectivity of an HBV particle, and for the inhibitory activity of preS1-lipopeptides, a mutant and a non-myristoylated peptide did not exhibit a tropism for the liver. Instead, HBVpreS/2-48<sup>myr</sup>(D11,13)-Y<sup>131</sup> was found to be equally distributed over all organs, and HBVpreS/1-48-Y<sup>131</sup> was renally eliminated within one hour. The high specificity with which the wild type peptide was retained in the liver therefore indicated a hepatic presence of a specific preS1-receptor in these non-permissive animals.

This finding is in complete accordance with the *in vitro* data described here. Our observation that hepatocytes from some non-susceptible species, e.g. mice (PMH) and rats (PRH), were able to bind HBVpreS/2-48<sup>myr</sup>-K-FITC in a highly specific manner (see **Figure 9**) strongly suggested an expression of a preS1-receptor on these cells. The restriction of PMH and PRH towards HBV infection therefore is not due to the lack of a preS1-receptor. Since assembly and secretion of infectious virions in PMH and PRH is not hampered after expression of pre- and sub-genomic HBV-RNAs (Yamamura et al. 1990; Araki et al. 1991; Diot et al. 1992), the lacking permissiveness of these cells must be related to another factor. This could be for instance the absence of a co-factor during viral entry and/ or a restricted post-entry step.

Further support that the expression of a functional preS1-receptor is not limited to human primates is provided by the finding that primary hepatocytes from *Tupaia belangerii*, a member of the order *Scandentia*, can be infected with HBV (Yan et al. 1996b), and that the infection can be inhibited by preS1-lipopeptides (Glebe et al. 2005). Our observation that PTH specifically bound HBVpreS/2-48<sup>myr</sup>-K-FITC provided direct evidence for the presence of a functional preS1-receptor on these cells.

Interestingly, we found - additionally to mice, rats and tupaia - a specific interaction of HBVpreS/2-48<sup>myr</sup>-K-FITC also to hepatocytes from rabbits, dogs and woodchucks (**Figure 10**). The fact that these species are phylogenetically only distantly related to humans implies that the preS1-receptor might be an evolutionary conserved molecule.

However, the preS1-receptor is not expressed in all species, since we did not find an interaction of HBVpreS/2-48<sup>myr</sup>-K-FITC with primary hepatocytes from pigs, rhesus and cynomolgus monkeys. These *in vitro* data were affirmed by an *in vivo* analysis of the tropism of HBVpreS/2-48<sup>myr</sup>-Y<sup>131</sup>, which accumulated only in the liver of dogs but not cynomolgus monkeys (Alexa Schieck, unpublished data). This was surprising, since rhesus monkeys (*Macaca mulatta*) and cynomolgus monkeys (*Macaca fascicularis*) are phylogenetically much closer to humans than some of the binding-competent species, like e.g. dogs (order *Carnivora*; see **Figure 25**).

All apes (members of the superfamily *Hominoidea*: gibbons, orang-utan, gorilla, chimpanzees and humans) harbour HBV endemically and some are permissive to an experimental HBV and HDV infection (Barker et al. 1975). Since both, rhesus and cynomolgus monkeys, belong to a different superfamily (*Cercopithecoidea*) within the same parvorder (*Catarrhini*, Old World monkeys), it might be possible that the respective receptor homologue of a common ancestor lost the preS1-binding competence by mutation during the evolution of their lineage. Of course, it must remain speculative, if such a mutation led to the resistance against (and the extinction of) an HBV variant that had been endemic in this superfamily before.

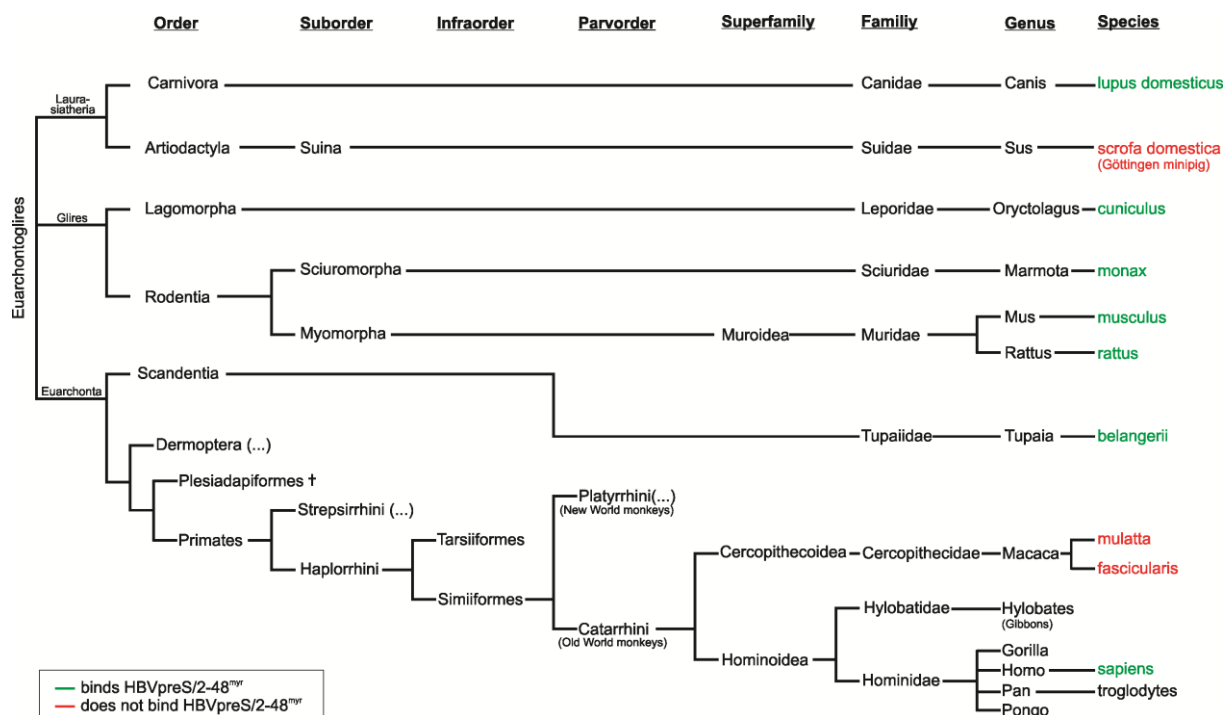


**Figure 25: Phylogenetic tree of HBVpreS/2-48<sup>myr</sup>-K-FITC binding and non-binding species.** The phylogenetic relationship between species that bind (green) or do not bind (red) HBVpreS/2-48<sup>myr</sup>-K-FITC is shown in a dendrogram. Distances do not reflect relative relationship. The data for each lineage were collected from: [www.ncbi.nlm.nih.gov/taxonomy](http://www.ncbi.nlm.nih.gov/taxonomy).

Furthermore, our data showed that primary woodchuck hepatocytes (PWH) specifically bound HBVpreS/2-48<sup>myr</sup>-K-FITC, indicating the presence of a human preS1-receptor homologue on these cells. Although *in vitro* an infection of these cells with HBV failed, it could be shown that HDV, bearing a human (hHDV) or woodchuck (wHDV) envelope, was able to infect PWH (Caroline Gähler, unpublished results). The infection with hHDV was inefficient (compared to that with wHDV), but specific as it could be inhibited by HBVpreS/2-48<sup>myr</sup>. An addition of peptide to the wHDV infection had no effect. Interestingly, primary hepatocytes from rabbits showed a very similar susceptibility upon infection with hHDV, wHDV or HBV. They could be infected with hHDV and wHDV, but not with

HBV, and only hHDV infection was inhibitable with HBVpreS/2-48<sup>myr</sup>. Taken together, this indicated a difference in HDV- and WHV-entry that could be based on the use of different receptor molecules. An alternative explanation would assume that HBVpreS/2-48<sup>myr</sup> acts on the virus, by e.g. inhibiting fusion of viral and cellular membrane as it is described for HIV and the fusion inhibitor T-20. In this model both (HDV and WHV) would utilize the same receptor, but the peptide could act due to sequence-specificities only on the human virus.

Our data furthermore indicated that HBV might bind (or even enter) preS1-binding-competent but non-susceptible hepatocytes, and that further steps in infection are restricted (e.g. membrane fusion, release or transport of nucleocapsids, repair of rcDNA, formation of cccDNA, etc.). HDV in contrast might be well able to establish a first-round, but dead-ended infection in these species. These possibilities have to be systematically tested in the future and may have important implications for the development of a small animal model for HBV and HDV.

#### **4.3 The presence of a proteinaceous HBVpreS/2-48<sup>myr</sup> receptor on the plasma membrane depends on the differentiation status of the cell**

Besides the restricted host range, a second remarkable characteristic of HBV is the limitation to exclusively infect differentiated hepatocytes (Gripon et al. 2002). HepaRG cells, the only permanent cell-culture system known to support the complete viral life cycle, need a differentiation period of two weeks to achieve an HBV-susceptible state. The differentiation is induced by the addition of DMSO, a well-known differentiating agent. Vice versa, PHH lose their susceptibility to infection within several days after isolation, but the permissive state can be maintained by addition of DMSO (Gripon et al. 1988).

The binding experiments with HBVpreS/2-48<sup>myr</sup>-K-FITC demonstrated, that the differentiation status of a cell is directly reflected by the presence of a preS1-receptor. HepaRG cells in the undifferentiated state did not show an interaction with HBVpreS/2-48<sup>myr</sup>-K-FITC, whereas binding could be well detected in a susceptible, differentiated state. On the other hand, PHH lost their ability to bind HBVpreS/2-48<sup>myr</sup>-K-FITC during a de-differentiation process, within one week after plating. The loss of the binding capability could be prevented by the addition of DMSO to the culture medium. The same phenomenon was observed for PMH. These data provide strong evidence that the preS1-receptor expression depends on the differentiation state of the target cells and constitutes the main and maybe only restriction factor for infection in the *human* hepatocytes investigated here, that otherwise support the full replication cycle.

Human hepatoma cell lines isolated and established from hepatocellular carcinoma, are widely used model systems to study liver metabolism and cytotoxicity. However, their use is less popular compared to that of PHH since they are considered to be less differentiated, although some of the

cell lines like HepG2 or Huh7 partially display differentiated liver specific functions (Knowles et al. 1980).

HepG2 cells have been discussed extensively as a potential infection system for HBV and support HBV particle production after transfection of HBV-expression plasmids. Several studies reported specific binding and uptake of HBV in these cells (Bchini et al. 1990; Paran et al. 2001), but credible evidence for a productive infection until now is missing. So far, the refractoriness of HepG2 cells towards HBV infection has been explained e.g. by a block in nuclear transport (Qiao et al. 1994) or the over-expression of a serine protease inhibitor (Lu & Block 2004). Since we neither detected binding of HBVpreS/2-48<sup>myr</sup>-K-FITC to HepG2 cells in an actively dividing state, nor after a two-week treatment with DMSO (**Figure 11**), we suggest that the lack of a functional preS1-receptor is the main reason that limits the successful HBV entry into these cells. A second well-characterized hepatoma cell line, HuH7, that has been described to bind HBV (Qiao et al. 1994) but not to promote infection, as well did show an interaction with HBVpreS/2-48<sup>myr</sup>-K-FITC in neither the untreated, nor the DMSO-treated state. Taken together, these findings further substantiate our hypothesis that the expression of a functional preS1-receptor is dependent on the differentiation status of a cell and represents the major restriction factor for infection. Hepatoma cell lines like HepG2 and HuH7 apparently lost the ability to express a functional preS1-receptor, maybe as a consequence of the cancerous transformation process. A unique feature of the hepatoma cell line HepaRG is that these cells can re-develop a hepatocyte-like phenotype after a prolonged quiescence and maintenance at confluence in combination with DMSO treatment. Since HepaRG cells are less profoundly altered regarding the chromosomal re-arrangement (compared to the other mentioned hepatic cell lines), they have retained an intrinsic ability for a regulated expression of the specific preS1-receptor.

Heparan sulfate proteoglycans have been described to interact with the preS1-region of the HBV L-protein in the viral context (Schulze et al. 2007) and act as primary attachment receptors. HepG2 and Huh7 cells did not bind HBVpreS/2-48<sup>myr</sup> despite the presence of GAGs on their surface. Furthermore, competition experiments with heparin and suramin on PMH did not lead to a significant reduction of peptide binding. Therefore, a major contribution of GAGs to HBVpreS/2-48<sup>myr</sup>-K-FITC binding to the cell surface could be excluded.

In contrast to that, peptide binding could be strongly reduced by proteolytic digestion of cell surface proteins (**Figure 13**). Even if the binding of the preS1-peptide could not be completely abolished after treatment of PMH with trypsin or Glu-c, the decrease of the binding capacity to approximately 40 % provided a direct evidence that at least one essential factor involved in the preS1-receptor interaction is a protein.

#### 4.4 Analysis of the affinity of HBVpreS/2-48<sup>myr</sup> to its receptor

The vast amount of viruses uses proteins on the cell surface as receptors. For HBV, only glycosaminoglycans (GAGs) have been described as primary attachment factors, but this family of macromolecules is ubiquitously distributed in the host organism. The nature of molecule(s) that act(s) as liver-specific receptor(s) is not characterized yet. However, the observation that binding of the preS1-lipopeptide to PMH can be reduced after protease-treatment of the target cells strongly suggested the involvement of a protein-protein interaction during receptor recognition.

In this case, binding of HBVpreS/2-48<sup>myr</sup> to the plasma membrane should exhibit hallmarks of a typical receptor-ligand interaction between two protein partners, i.e. high affinity (low dissociation constant  $K_D$ ) and saturation at low ligand concentrations.

To determine these parameters, we investigated the pharmacodynamics of HBVpreS/2-48<sup>myr</sup>-K-FITC. In a first approach a flow cytometry-based binding assay with PMH was established to plot a binding curve for the interaction with the preS1-receptor.

As seen in **Figure 14**, the wild type and the two control peptides showed binding curves that were very different from each other. At concentrations below 400 nM, binding was detected only for HBVpreS/2-48<sup>myr</sup>-K-FITC. In contrast, concentrations above 400 nM lead to a parallel linear increase of cell-associated fluorescence for both acylated peptides, HBVpreS/2-48<sup>myr</sup>-K-FITC and HBVpreS/2-48<sup>myr</sup>(D11,13)-K-FITC. Since the non-myristoylated peptide did not show significant binding at any concentration tested, it was proposed that the non-saturable binding at concentrations exceeding 400 nM was mediated by the acyl moiety.

In order to display specific binding only, the data of HBVpreS/2-48<sup>myr</sup>-K-FITC binding were normalized by subtracting the unspecific binding represented by the mutant peptide. The resulting curve was characterized by a hyperbolic increase to a plateau. The  $K_D$  could be determined to approximately 60 nM and ~ 90 % saturation was reached at a concentration of ~ 300 nM. Scatchard analysis of these data showed a linear regression, which excluded a cooperative effect during formation of the peptide-receptor complex.

The total binding of HBVpreS/2-48<sup>myr</sup>-K-FITC hence involved two components: (i) a sequence- and myristoylation-dependent binding to a high-affinity receptor conferring liver specificity, and (ii), a non-saturable, low affinity interaction with highly abundant molecules (e.g. phospholipids in the lipid bilayer) that depends exclusively on the presence of the acyl residue.

In an alternative approach we determined the binding dynamics of HBVpreS/2-48<sup>myr</sup> to PRH, PHH and HepaRG cells on the basis of quantitative mass-spectrometry analysis. Therefore, cells were incubated with different concentrations of HBVpreS/2-48<sup>myr</sup>, and the bound fraction was determined by HPLC-MS/MS (performed by Prolytic GmbH). The calculation of binding curves for the respective

cells allowed us to estimate the binding capacity  $B_{\max}$  as a relative measure for the receptor density on the cell surface.

Striking differences were found in the binding capacities of these cell types. PRH exhibited the highest  $B_{\max}$  of approximately 1900 ng peptide/ g cells, and PHH showed a moderate binding capacity of  $\sim 430$  ng peptide/ g cells. Although the limited number of data point restricts the statistical validity of this assay, these findings reflected previous results obtained by the flow cytometric analysis of primary hepatocytes from different species. As depicted in **Figure 15**, PRH showed an about 4-fold difference in the cell-associated fluorescence intensity when compared to PHH that were incubated with an equal concentration of HBVpreS/2-48<sup>myr</sup>-K-FITC. Additionally, the same phenomenon was observed - although not quantified - by fluorescence microscopy. Together, these experiments provided a direct evidence for inter-species variations in the preS1-receptor density between PRH and PHH.

Compared to these two cell types, only a very low amount of bound HBVpreS/2-48<sup>myr</sup>-molecules was found on HepaRG cells. All peptide concentrations applied within the range of specific binding (below 400 nM) resulted in signals that were close to the detection limit of the system. Even higher concentrations did not yield reliable data that could be used to plot a binding curve. It therefore had to be assumed that the  $B_{\max}$  of HepaRG cells is significantly lower than that of the primary hepatocytes. These findings might have important consequences for the determination of an effective dose of HBVpreS/2-48<sup>myr</sup> as entry inhibitor, and suggests the use of the more reliable PHH system in order to estimate the inhibitory concentrations  $IC_{50}$  or  $IC_{90}$ .

In contrast to the cell-type dependent heterogeneity in the  $B_{\max}$  values, there was no significant deviation regarding the affinity of the peptide-receptor interactions. The approximate  $K_D$  values determined by the mass-spectrometric analysis ranged from 11 nM (PRH) to 20 nM (PHH). This is in good agreement with the  $K_D$  of  $\sim 60$  nM as it was defined on PMH by flow cytometry.

A general overview about the range of dissociation constants in protein-protein interactions is given in the table below. The affinity of HBVpreS/2-48<sup>myr</sup>(-K-FITC) to its liver-specific receptor can therefore be regarded as similar to that of DNA-binding proteins or a strong antibody-antigen interaction.

Interaction	$K_D$
Streptavidin-biotin binding	$10^{-14}$ M
Hormone-receptor interaction (human interferon- $\alpha$ )	$10^{-11}$ to $10^{-12}$ M
Antibody-antigen interaction with a good antibody	$10^{-8}$ to $10^{-10}$ M
DNA binding protein with a specific site	$10^{-8}$ to $10^{-10}$ M
Antibody-antigen interaction with a weak antibody	$10^{-6}$ M
Enzyme-substrate interaction	$10^{-4}$ to $10^{-10}$ M
HBVpreS/2-48 <sup>myr</sup> or HBVpreS/2-48 <sup>myr</sup> -K-FITC with an unknown receptor	$\sim 10^{-8}$ M
myristoylated peptide (Gly <sup>myr</sup> , Gly-Ala <sup>myr</sup> , Gly-Ala-Ala <sup>myr</sup> ) with a phospholipid vesicle	$\sim 10^{-4}$ M

modified from *Current Protocols in Protein Science* (1998), p19.1.2

One peculiarity that remains is the high degree of binding of the mutant peptide at high concentrations. It is known that a myristoylation can direct proteins or peptides like e.g. pp60<sup>V-SRC</sup> (Cross et al. 1984; Kamps et al. 1985) or the retroviral Gag-protein (Göttlinger et al. 1989) to plasma membranes, but with a typical  $K_D$  of  $\sim 100$   $\mu$ M the myristoyl residue alone is usually not sufficient to mediate a stable insertion into the phospholipid bilayer (see table; and (Peitzsch & McLaughlin 1993). For example, the  $K_D$  described for the plasma membrane-interaction of a myristoylated peptide MGXsrc, that represents the first 11 amino acids of pp60<sup>V-SRC</sup> of the Rous sarcoma virus, is approximately 75  $\mu$ M (Resh 1989). An efficient anchorage to the plasma membrane usually requires the cooperation of a second motif in form of an additional acylation (e.g. palmitoylation) or sequences that mediate a protein-protein or protein-phospholipid interaction (e.g. short phenylalanine- or lysine-rich stretches).

The  $K_D$  of the myristoyl-dependent interaction of HBVpreS/2-48<sup>myr</sup>(D11,13)-K-FITC clearly lay above 2  $\mu$ M, but for technical reasons the exact affinity could not be determined (data not shown). To test if a second amino acid signal contributed to the membrane targeting, a peptide was synthesized that exhibited a scrambled amino acid sequence. However, HBVpreS/2-48<sup>myr</sup>(scrambled)-K-FITC showed binding dynamics that were very similar to that of HBVpreS/2-48<sup>myr</sup>(D11,13)-K-FITC (data not shown). An artificial cooperative effect of the FITC moiety could be excluded as another possibility to facilitate membrane binding, since the non-labeled mutant peptide (HBVpreS/2-48<sup>myr</sup>(D11,13)) showed the same non-specific binding behavior (HPLC-MS/MS experiments, **Figure 15**).

In summary, these data imply the model of a bimodal binding mechanism: (i) The myristoylation facilitates binding to plasma membrane phospholipids, which can be regarded as highly abundant, but low affinity “non-specific” receptors ( $K_D \gg 2$   $\mu$ M). (ii) The amino acid sequence, in combination with the acyl moiety, mediates binding to the high affinity receptor ( $K_D \sim 60$  nM) which is a liver-specific protein or at least involves a protein component, and which is essential for HBV entry.

Due to the low affinity the non-specific interaction does not interfere with the specific receptor-binding at concentrations below 400 nM. Above 400 nM, it promotes an unspecific binding of additional peptide molecules, but does not compete with the specific preS1-receptor interaction that already is saturated at these concentrations ( $B_{\max}$  of the normalized binding curve).

Mechanistically, one could image two additive effects of the myristoylation-dependent membrane interaction: (i) it might catalyze the preS1-receptor binding by reduction of the peptide diffusion to two dimensions and thereby enhancing the probability to collide with a specific interaction partner. (ii) It might further enhance the rate of successful collisions by inducing a local proximity to the receptor (e.g. in microdomains) and forcing the essential binding motif towards an orientation that is suitable to find a binding pocket on the receptor molecule.

Consequently, the inability of HBVpreS/1-48 to bind at either concentration could be explained by the improbability of successful collisions without catalysis, by a direct participation of the myristoyl residue in the specific receptor interaction or a combination of both factors.

#### **4.5 Kinetic analysis of HBVpreS/2-48<sup>myr</sup>-K-FITC receptor-interaction confirmed a high affinity of binding and demonstrated an unusual high stability of the peptide-receptor complexes**

Analysis of the binding kinetics of HBVpreS/2-48<sup>myr</sup>-K-FITC to the plasma membranes of PHH demonstrated that a binding equilibrium was reached within 10 to 15 minutes after addition of 200 nM peptide. In contrast, the infection process of an HBV particle is assumed to be relatively slow. On HepaRG cells, inoculation periods of 16 to 20 hours at 37°C are needed to achieve a robust infection. The seemingly slow kinetics of the HBV infection compared to the fast on-rate of peptide binding can be easily explained: The instantaneous velocity ( $v$ ) of an association reaction between a ligand (here virus or peptide, respectively) and its receptor can be described in terms of the respective concentrations,  $v = k \cdot [ligand] \cdot [receptor]$ , where  $k$  is the reaction rate constant. The analysis of the peptide binding kinetics was performed at a concentration of 200 nM - that corresponds to  $\sim 6 \times 10^{13}$  molecules in a 500- $\mu$ l incubation volume. The standard infection of HepaRG cells is done in the same volume with a virus stock of approximately  $10^{11}$  GE/ ml in a dilution of 1:20 to 1:25. That corresponds to  $\sim 2.5 \times 10^9$  virus particles per inoculum. The ligand concentrations differ therefore by more than 4 orders of magnitude. Additionally, the receptor concentrations defined as  $B_{\max}$  were shown to be significantly higher in primary hepatocytes than in HepaRG cells. Thus, the differences in the experimental set-up can explain the different observations. In fact, the exposition of PHH to high-titer HBV preparations for only 1 hour resulted in unusually high infection rates (Stefan Seitz, personal communication).

Furthermore, it is problematic on principle to compare the binding kinetics of a 5-kD peptide with the infection kinetics of complete 42-nm virus particles, particularly if the read-out of the infection relies

on late markers like viral proteins secreted by infected cells. The cellular receptor addressed by both might be better accessible to HBVpreS/2-48<sup>myr</sup>, simply due to the smaller size of this ligand. The viral particle in addition possibly has to overcome several obstacles before and after binding to the specific receptor, i.e. for instance retention at its primary attachment factors (heparan sulfate proteoglycans) or an abortive internalization. Taken together, there is no evidence to date that supports the assumption of an inefficient receptor association as limitation for the infection. However, it would be of high interest to investigate the kinetic binding behavior of HBV to PHH, e.g. by the use of fluorescently labeled particles, and to set it into relation to the peptide binding kinetics. Experiments addressing the stability of the peptide-receptor complexes revealed an extraordinary high stability over time. The fluorescent signal of receptor-associated HBVpreS/2-48<sup>myr</sup>-K-FITC could be monitored for more than 18 hours, with a half-life time ( $t_{1/2}$ ) of about 11 hours. Both findings strengthened the assumption of a high-affinity interaction and moreover demonstrated a slow turnover rate of the preS1-receptor-complex. Gripon *et al.* showed that after exposure to HBVpreS/2-48<sup>myr</sup> HepaRG cells regained susceptibility to HBV infection with  $t_{1/2} \sim 12$  hours (Gripon *et al.* 2005). This perfectly correlated with our observations. The extraordinary high stability of HBVpreS/2-48<sup>myr</sup> was additionally confirmed by an *in vivo* study described by Alexa Schieck, who estimated  $t_{1/2}$  of HBVpreS/2-48<sup>myr</sup>-Y<sup>131</sup> to approximately 16 hours (Alexa Schieck, unpublished results).

The mechanisms that lead to the restoration of the concentration of free receptor molecules at the plasma membrane remain to be elucidated. Factors involved in this process could be either a dissociation of the peptide-receptor complex, degradation of the peptide, or substitution of the sequestered target molecule by dynamic turnover (e.g. trafficking).

#### 4.6 Sub-cellular localization of receptor-bound HBVpreS/2-48<sup>myr</sup> revealed an interaction with the (actin) cytoskeleton

High-resolution microscopy and 3-dimensional image reconstruction revealed an almost exclusive localization of HBVpreS/2-48<sup>myr</sup>-K-FITC at the plasma membrane of differentiated hepatocytes (**Figure 17**). This is in discrepancy with a previous study that suggested an uptake and intracellular localization of HBVpreS/2-48<sup>myr</sup> in PTH and occasionally HepG2 cells (Glebe *et al.* 2005). However, Glebe *et al.* used immune cytochemistry to indirectly localize preS1-peptides and moreover did not resolve the third dimension. Here instead, we detected fluorescently labeled peptides in a direct way, providing a much more authentic model system to localize binding.

Single fluorescent spots observed within the cytoplasm were most probably derived from autofluorescence of the cells, since these structures were present also in absence of the peptide, and often represented a Golgi-like morphology. Although our experiments could not completely rule out

an uptake of HBVpreS/2-48<sup>myr</sup>-K-FITC, the long persistence on the plasma membrane ( $t_{1/2} \approx 11$  hours) and the lack of vesicular cytoplasmic structures argued against an efficient endocytosis of receptor-bound HBVpreS/2-48<sup>myr</sup>-K-FITC.

We furthermore could localize the preS1-receptor to the immobile fraction of the plasma membrane (**Figure 19**). By measuring recovery of fluorescence after photobleaching, the peptide-receptor complexes clearly showed a restricted lateral mobility, implicating an interaction with molecules that constrain diffusion within the membrane. The direct comparison of the lateral mobility of a fluorescent lipid-analog (Dil) that proved to be motile, indubitably demonstrated that there was no detectable lateral diffusion of the peptide-receptor complexes. Lateral mobility of membrane proteins in general is limited by interactions with (i) the underlying cytoskeletal network, (ii) with other membrane proteins or lipids, or (iii) with the extracellular matrix. For example, it has been shown that disruption of the cytoskeleton or use of cholesterol-depleting agents increased the lateral mobility of dopamine transporters in the plasma membrane (Adkins et al. 2007). Future experiments addressing these different possibilities with the aim to characterize the specific micro-environment of the preS1-receptor (e.g. by co-localization with raft markers) could contribute to the understanding of the virus entry and the mode of action of the inhibitory preS1-peptides.

To further localize the peptide binding sites on a sub-cellular level, we applied high-resolution light microscopy such as spinning disk confocal or total internal reflection fluorescence (TIRF) microscopy. TIRF microscopy allowed us to visualize HBVpreS/2-48<sup>myr</sup>-C-Atto565 on live PMH with a high resolution down to a single-molecule level. When live PMH were monitored shortly after addition of the peptide, we could observe individual binding events of single molecules (or small aggregates) of HBVpreS/2-48<sup>myr</sup>-C-Atto565. Most of the fluorescent units thereby bound quickly and stably without lateral movement (**Figure 18**).

Visualization of the cell-edges revealed the presence of finger-like membrane protrusions that were abundantly distributed over the whole cell and were associated with fluorescence. A hallmark for differentiated, resting hepatocytes is the formation of microvilli on the cell surface. Although this topic is not well understood to date, it is assumed that the tip compartments of microvilli form pericellular spaces on the cell surface that are separated from the cytoplasm by a tight bundle of actin filaments (Lange 2010). Cellular functions such as glucose transport, transmembrane ion fluxes and Ca<sup>2+</sup> signaling, that are developed during growth arrest and differentiation, are assumed to involve a sequestration of certain transporters and ion channels to the microvilli tips (Lange & Brandt 1990). However, the functional importance of microvilli besides an enlargement of the cell surface remains obscure. In order to interpret the membrane protrusions that resembled microvilli and bound HBVpreS/2-48<sup>myr</sup>-C-Atto565, it is inalienable to clearly identify and classify these structures for

instance by the use of other high-resolution microscopic techniques (e.g. stochastic optical reconstruction microscopy (STORM) or electron microscopy).

Another striking observation was the detection of fluorescent clusters in TIRF and spinning disk confocal microscopy. Although they appeared more distinctive at the bottom side of the hepatocytes that is attached to the cover slip, these clusters were also abundant on the top of the membrane directed towards the cell-culture medium. These clusters were tightly associated with the actin cytoskeleton. As determined by co-localization studies using an F-actin marker, patches of actin were always in close proximity to the peptide-clusters (**Figure 20**). Thereby, actin often appeared to be surrounded by peptide. However, limitations in the optical resolution did not allow a more detailed description.

The treatment of cells with cytochalasin D further substantiated the assumption of an actin-interaction. Cytochalasin D acts by preventing actin polymerization (Goddette & Frieden 1986). It increases the number of actin filament ends and a typical sign is the formation of aggregates or foci that contain actin. Such foci were seen also in our experiment and the the co-localization in these spots seemed to be even enhanced in these spots.

Together, these findings constitute a strong hint at a very tight connection between the actin cytoskeleton and the peptide-receptor complexes. Nearly all endocytic pathways that are described to be utilized by viruses are known to involve the (actin) cytoskeleton (review (Mercer et al. 2010)). Since the peptide-receptor complexes interact with the cytoskeleton either in a direct or indirect way through adaptor proteins, it is likely that actin plays a role in the entry of HBV.

#### 4.7 Visualization of HBV particles

In order to employ the findings made by the visualization of HBVpreS/2-48<sup>mYr</sup> to the analysis of the HBV-cell interaction, and to investigate HBV entry by tracking single particles, we here describe the initial production and characterization of fluorescently labeled particles that can be used in future tracking experiments.

Single virus tracking (SVT) represents an ideal, but technically demanding method to investigate virus entry. The direct observation of fluorescently labeled virus particles in real-time, as described in the past years for many viruses, like e.g. influenza (Lakadamyali et al. 2003), polyoma virus (Ewers et al. 2005) or SV40 (Pelkmans et al. 2001), has helped a lot to understand the viral entry processes and kinetics. In contrast to other microscopic techniques that rely on sample fixation (immunofluorescence, electron microscopy) or to biochemical assays, SVT directly monitors the interactions of particles and cells on live cells. It therefore reflects the *in vivo* situation much better. However, fluorescently labeled virus particles need to fulfill several prerequisites to be suited for SVT. On the one hand, the fluorescent label must be bright and stable enough to trace the particle

over potentially long observation periods. On the other hand, the particle itself must not be altered in a way that its normal functionality, i.e. infectivity, is significantly altered.

There are several ways to label a virus particle, such as genetic engineering by expression of fluorescent viral fusion proteins, the attachment of chemical dyes to proteins or nucleic acids, or the incorporation of fluorescent lipid-analogs into viral envelopes. For HBV, the possibilities of particle labeling are extremely restricted. Due to its complex and small sized genome it is difficult to incorporate fluorescent proteins without interfering with particle assembly. It has been shown that an N-terminal fusion of GFP to the S-protein is tolerated when co-expressed and co-integrated together with the wild type S-protein (Lambert et al. 2004). However, infectivity of these particles has not been shown. Further attempts to label HBV with lipid analogs like DiI, or DiO resulted in the detection of fluorescence on a cellular but not a single particle level (Kerry Mills, unpublished data).

One approach that was followed here was the labeling of HBV particles by an incorporation of fluorescently labeled lipids (phosphoethanolamine-FITC). Although this method produced fluorescent particles that could be characterized as single particles, they were not suited for live-cell imaging since infectivity could not be demonstrated yet and FITC bleached rapidly.

In a second approach, we established a method to label HBV particles from HepAD38 supernatant with a stable and protein-reactive derivate of Alexa-Fluor488. A procedure that combined gel filtration, affinity chromatography and density gradient centrifugation yielded fluorescently labeled, HBV particles (HBV-Alexa488).

The concomitant detection of HBV-DNA, fluorescence and HBV-proteins in the peak fractions of sucrose-density gradients indicated the presence of fluorescent HBV particles. Significant contamination of the fractions with protein could be excluded by silver gel analysis (**Figure 21**).

The infectivity of HBV-Alexa488 preparations was confirmed for three different preparations on HepaRG cells. However, it would be necessary for future experiments to determine the multiplicity of infection by comparing HBV-Alexa488 infectivity with that of an equally produced, unlabeled HBV. In this context, it would be also important to determine the percentage of unlabeled particles within a preparation.

Confocal microscopy showed that HBV-Alexa488 could be detected as single particles. The fluorescence intensity profiles of these particles revealed that single particles could be distinguished from aggregates by their fluorescence distribution. A spherically shaped fluorescent particle emits concentric, circular fluorescence that decreases in intensity with the radius. The distribution of the fluorescence intensity of a single particle therefore shows characteristics of a Gaussian distribution. The profiles of single particles were represented a Gaussian curve and a diameter of approximately 200 - 300 nm (**Figure 22**). In contrast, aggregates imaged under equal microscopic settings, showed a broader distribution of fluorescence ( $\varnothing > 600$  nm) and sometimes two peaks. This is a result from at

least two overlapping Gaussian distribution curves that due to the optical limitations of the system could not be separated from each other.

Quantitative analysis of the distribution of particle sizes within a preparation revealed that the vast amount of particles was small-sized ( $\sim 8 \text{ nm}^2$ ). Aggregates were present but not abundant.

First attempts to visualize HBV-Alexa488 on HepaRG cells showed that particle fluorescence was bright and punctuated enough to be distinguished from autofluorescence in fixed cells. To demonstrate the comparability of HBV-Alexa488 with unlabeled HBV, we checked if established characteristics of HBV infection can also be attributed to HBV-Alexa488 (**Figure 24**). It has been shown that the addition of PEG during virus inoculation markedly increased the infection process by enhancing particle binding (presumably to GAGs) (Gripon et al. 1993b). This effect could be visualized for the first time on a single-particle level, since HBV-Alexa488 binding to HepaRG cells was significantly enhanced in presence of PEG. A second well characterized feature is the HBV infection inhibition by highly sulfated GAGs (Schulze et al. 2007). Heparin, a prototypic member of the GAGs, has been shown to interfere with HBV binding at high concentrations. We here demonstrated that also HBV-Alexa488 binding can be inhibited by heparin. Although the effects of PEG and heparin are rather unspecific, our experiments represented a first indication that HBV-Alexa488 showed high similarity to the unlabeled virus. Assays with e.g. neutralizing antibodies, or the use of entry inhibitors could provide more secure evidence of a specificity of the interaction.

When analyzed in a 3-dimensional approach, particles were found to be located almost exclusively at the plasma membrane. Only some fluorescent particles were observed within the cytoplasm, but these have to be further quantified and identified. However, massive endocytosis of the particles was not observed despite the incubation at  $37^\circ\text{C}$  for 1.5 hours. Although being consistent with the data for HBVpreS/2-48<sup>mYr</sup>-K-FITC (see **Figure 16** and **Figure 18**), it is not possible to directly compare the binding behavior of the peptide and HBV-Alexa488 since the latter involves e.g. an additional binding to proteoglycans.

Unspecific binding to proteoglycans also might be the reason why binding of HBV-Alexa488 was not restricted to differentiated cells within the HepaRG culture.

In summary, it could be shown that fluorescently labeled, infectious HBV particles can be produced with a high purity. Although aggregates were present in the preparations, the bigger part represents single particles showing a fluorescence that can be detected on HepaRG cells. Our data therefore suggest the suitability of HBV-Alexa488 for a future real-time analysis of the HBV-cell interactions.

## 5. References

- Adkins, E.M. et al., 2007. Membrane mobility and microdomain association of the dopamine transporter studied with fluorescence correlation spectroscopy and fluorescence recovery after photobleaching. *Biochemistry*, 46(37), 10484-10497.
- Araki, K. et al., 1991. Production and effect of infectious Dane particles in transgenic mice. *Japanese Journal of Cancer Research: Gann*, 82(3), 235-239.
- Barker, L.F. et al., 1975. Viral hepatitis, type B, in experimental animals. *The American Journal of the Medical Sciences*, 270(1), 189-195.
- Bchini, R. et al., 1990. In vitro infection of human hepatoma (HepG2) cells with hepatitis B virus. *Journal of Virology*, 64(6), 3025-3032.
- Berthelot, P. et al., 1984. Hepatitis B vaccine safety monitoring in the chimpanzee: interpretation of results. *Journal of Medical Primatology*, 13(3), 119-133.
- BLUMBERG, B.S., ALTER, H.J. & VISNICH, S., 1965. A "NEW" ANTIGEN IN LEUKEMIA SERA. *JAMA: The Journal of the American Medical Association*, 191, 541-546.
- Bruss, V., 2004. Envelopment of the hepatitis B virus nucleocapsid. *Virus Research*, 106(2), 199-209.
- Cable, E.E. & Isom, H.C., 1997. Exposure of primary rat hepatocytes in long-term DMSO culture to selected transition metals induces hepatocyte proliferation and formation of duct-like structures. *Hepatology (Baltimore, Md.)*, 26(6), 1444-1457.
- Cross, F.R. et al., 1984. A short sequence in the p60src N terminus is required for p60src myristylation and membrane association and for cell transformation. *Molecular and Cellular Biology*, 4(9), 1834-1842.
- Crowther, R.A. et al., 1994. Three-dimensional structure of hepatitis B virus core particles determined by electron cryomicroscopy. *Cell*, 77(6), 943-950.
- Dandri, M. et al., 2005. Chronic infection with hepatitis B viruses and antiviral drug evaluation in uPA mice after liver repopulation with tupaia hepatocytes. *Journal of Hepatology*, 42(1), 54-60.
- Dandri, M. et al., 2006. Small animal model systems for studying hepatitis B virus replication and pathogenesis. *Seminars in Liver Disease*, 26(2), 181-191.
- Dane, D.S., Cameron, C.H. & Briggs, M., 1970. Virus-like particles in serum of patients with Australia-antigen-associated hepatitis. *Lancet*, 1(7649), 695-698.
- Deres, K. et al., 2003. Inhibition of hepatitis B virus replication by drug-induced depletion of nucleocapsids. *Science (New York, N.Y.)*, 299(5608), 893-896.
- Diot, C. et al., 1992. Replication of hepatitis B virus in differentiated adult rat hepatocytes transfected with cloned viral DNA. *Journal of Medical Virology*, 36(2), 93-100.
- Dryden, K.A. et al., 2006. Native hepatitis B virions and capsids visualized by electron cryomicroscopy. *Molecular Cell*, 22(6), 843-850.

- Elaut, G. et al., 2006. Molecular mechanisms underlying the dedifferentiation process of isolated hepatocytes and their cultures. *Current Drug Metabolism*, 7(6), 629-660.
- Engelke, M. et al., 2006. Characterization of a hepatitis B and hepatitis delta virus receptor binding site. *Hepatology (Baltimore, Md.)*, 43(4), 750-760.
- Erhardt, A. et al., 2005. Response to interferon alfa is hepatitis B virus genotype dependent: genotype A is more sensitive to interferon than genotype D. *Gut*, 54(7), 1009-1013.
- Ewers, H. et al., 2005. Single-particle tracking of murine polyoma virus-like particles on live cells and artificial membranes. *Proceedings of the National Academy of Sciences of the United States of America*, 102(42), 15110-15115.
- Gerin, J.L., 2001. Animal models of hepatitis delta virus infection and disease. *ILAR Journal / National Research Council, Institute of Laboratory Animal Resources*, 42(2), 103-106.
- Gheit, T. et al., 2002. Experimental transfection of *Macaca sylvanus* with cloned human hepatitis B virus. *The Journal of General Virology*, 83(Pt 7), 1645-1649.
- Glebe, D. et al., 2003. Pre-s1 antigen-dependent infection of *Tupaia* hepatocyte cultures with human hepatitis B virus. *Journal of Virology*, 77(17), 9511-9521.
- Glebe, D. & Urban, S., 2007. Viral and cellular determinants involved in hepadnaviral entry. *World Journal of Gastroenterology: WJG*, 13(1), 22-38.
- Glebe, D. et al., 2005. Mapping of the hepatitis B virus attachment site by use of infection-inhibiting preS1 lipopeptides and *tupaia* hepatocytes. *Gastroenterology*, 129(1), 234-245.
- Goddette, D.W. & Frieden, C., 1986. Actin polymerization. The mechanism of action of cytochalasin D. *The Journal of Biological Chemistry*, 261(34), 15974-15980.
- Göttlinger, H.G., Sodroski, J.G. & Haseltine, W.A., 1989. Role of capsid precursor processing and myristoylation in morphogenesis and infectivity of human immunodeficiency virus type 1. *Proceedings of the National Academy of Sciences of the United States of America*, 86(15), 5781-5785.
- Gripon, P., Diot, C. & Guguen-Guillouzo, C., 1993a. Reproducible high level infection of cultured adult human hepatocytes by hepatitis B virus: effect of polyethylene glycol on adsorption and penetration. *Virology*, 192(2), 534-540.
- Gripon, P., Diot, C. & Guguen-Guillouzo, C., 1993b. Reproducible high level infection of cultured adult human hepatocytes by hepatitis B virus: effect of polyethylene glycol on adsorption and penetration. *Virology*, 192(2), 534-540.
- Gripon, P. et al., 1988. Hepatitis B virus infection of adult human hepatocytes cultured in the presence of dimethyl sulfoxide. *Journal of Virology*, 62(11), 4136-4143.
- Gripon, P. et al., 1995. Myristylation of the hepatitis B virus large surface protein is essential for viral infectivity. *Virology*, 213(2), 292-299.
- Gripon, P., Cannie, I. & Urban, S., 2005. Efficient inhibition of hepatitis B virus infection by acylated peptides derived from the large viral surface protein. *Journal of Virology*, 79(3), 1613-1622.
- Gripon, P. et al., 2002a. Infection of a human hepatoma cell line by hepatitis B virus. *Proceedings of the National Academy of Sciences of the United States of America*, 99(24), 15655-15660.

- Gripon, P. et al., 2002b. Infection of a human hepatoma cell line by hepatitis B virus. *Proceedings of the National Academy of Sciences of the United States of America*, 99(24), 15655-15660.
- Gudima, S. et al., 2008. Primary human hepatocytes are susceptible to infection by hepatitis delta virus assembled with envelope proteins of woodchuck hepatitis virus. *Journal of Virology*, 82(15), 7276-7283.
- Guidotti, L.G. et al., 1995. High-level hepatitis B virus replication in transgenic mice. *Journal of Virology*, 69(10), 6158-6169.
- Heermann, K.H. et al., 1984. Large surface proteins of hepatitis B virus containing the pre-s sequence. *Journal of Virology*, 52(2), 396-402.
- Huang, C. et al., 2009. Prevalence and phylogenetic analysis of hepatitis B virus among nonhuman primates in Taiwan. *Journal of Zoo and Wildlife Medicine: Official Publication of the American Association of Zoo Veterinarians*, 40(3), 519-528.
- Iwarson, S. et al., 1985. Neutralization of hepatitis B virus infectivity by a murine monoclonal antibody: an experimental study in the chimpanzee. *Journal of Medical Virology*, 16(1), 89-96.
- Jehn: Eine Ikterusepidemie in wahrscheinlichem Zusammenhang mit vorausgegangener Revaccination; Dtsch. Med. Wschr. 1885;11:354-356
- Kamps, M.P., Buss, J.E. & Sefton, B.M., 1985. Mutation of NH<sub>2</sub>-terminal glycine of p60<sub>src</sub> prevents both myristoylation and morphological transformation. *Proceedings of the National Academy of Sciences of the United States of America*, 82(14), 4625-4628.
- Kann, M. et al., 1999. Phosphorylation-dependent binding of hepatitis B virus core particles to the nuclear pore complex. *The Journal of Cell Biology*, 145(1), 45-55.
- Kim, C.M. et al., 1991. HBx gene of hepatitis B virus induces liver cancer in transgenic mice. *Nature*, 351(6324), 317-320.
- Knowles, B.B., Howe, C.C. & Aden, D.P., 1980. Human hepatocellular carcinoma cell lines secrete the major plasma proteins and hepatitis B surface antigen. *Science (New York, N.Y.)*, 209(4455), 497-499.
- Komla-Soukha, I. & Sureau, C., 2006. A tryptophan-rich motif in the carboxyl terminus of the small envelope protein of hepatitis B virus is central to the assembly of hepatitis delta virus particles. *Journal of Virology*, 80(10), 4648-4655.
- Kuntz and Kuntz, *Hepatology, Principles and Practices*, Springer-Verlag Berlin, Heidelberg, 2002
- Lakadamyali, M. et al., 2003. Visualizing infection of individual influenza viruses. *Proceedings of the National Academy of Sciences of the United States of America*, 100(16), 9280-9285.
- Lambert, C. et al., 2004. Functional incorporation of green fluorescent protein into hepatitis B virus envelope particles. *Virology*, 330(1), 158-167.
- Lange, K. & Brandt, U., 1990. Restricted localization of the adipocyte/muscle glucose transporter species to a cell surface-derived vesicle fraction of 3T3-L1 adipocytes. Inhibited lateral mobility of integral plasma membrane proteins in newly inserted membrane areas of differentiated 3T3-L1 cells. *FEBS Letters*, 276(1-2), 39-41.
- Lange, K., 2010. Fundamental role of microvilli in the main functions of differentiated cells: outline of

- a universal regulating and signaling system at the cell periphery. *Journal of Cellular Physiology*. Available at: <http://www.ncbi.nlm.nih.gov/pubmed/20607764> [Accessed August 6, 2010].
- Le Seyec, J. et al., 1999. Infection process of the hepatitis B virus depends on the presence of a defined sequence in the pre-S1 domain. *Journal of Virology*, 73(3), 2052-2057.
- Lok, A.S., Heathcote, E.J. & Hoofnagle, J.H., 2001. Management of hepatitis B: 2000--summary of a workshop. *Gastroenterology*, 120(7), 1828-1853.
- Lu, X. & Block, T., 2004. Study of the early steps of the Hepatitis B Virus life cycle. *International Journal of Medical Sciences*, 1(1), 21-33.
- Lu, X. et al., 2003. The alkylated imino sugar, n-(n-Nonyl)-deoxygalactonojirimycin, reduces the amount of hepatitis B virus nucleocapsid in tissue culture. *Journal of Virology*, 77(22), 11933-11940.
- Lürmann: Eine Ikterusepidemie. Berlin. Klin. Wschr. 1885, 22:20-30
- Lucifora, J. et al., 2010. Hepatitis B virus replication in primary macaque hepatocytes: crossing the species barrier toward a new small primate model. *Hepatology (Baltimore, Md.)*, 51(6), 1954-1960.
- MacCallum, FO. Homologous serum jaundice. 2 ed, Lancet: 1947. 691-692
- Macovei, A. et al., 2010. Hepatitis B virus requires intact caveolin-1 function for productive infection in HepaRG cells. *Journal of Virology*, 84(1), 243-253.
- Maeng, C.Y. et al., 2000. Fine mapping of virus-neutralizing epitopes on hepatitis B virus PreS1. *Virology*, 270(1), 9-16.
- Makuwa, M. et al., 2006. Hepatitis viruses in non-human primates. *Journal of Medical Primatology*, 35(6), 384-387.
- Mehta, A. et al., 2001. Inhibition of hepatitis B virus DNA replication by imino sugars without the inhibition of the DNA polymerase: therapeutic implications. *Hepatology (Baltimore, Md.)*, 33(6), 1488-1495.
- Mercer, J., Schelhaas, M. & Helenius, A., 2010. Virus entry by endocytosis. *Annual Review of Biochemistry*, 79, 803-833.
- Netter, H.J. et al., 1994. Apparent helper-independent infection of woodchucks by hepatitis delta virus and subsequent rescue with woodchuck hepatitis virus. *Journal of Virology*, 68(9), 5344-5350.
- Neurath, A.R. et al., 1986. Identification and chemical synthesis of a host cell receptor binding site on hepatitis B virus. *Cell*, 46(3), 429-436.
- Paran, N., Geiger, B. & Shaul, Y., 2001. HBV infection of cell culture: evidence for multivalent and cooperative attachment. *The EMBO Journal*, 20(16), 4443-4453.
- Peitzsch, R.M. & McLaughlin, S., 1993. Binding of acylated peptides and fatty acids to phospholipid vesicles: pertinence to myristoylated proteins. *Biochemistry*, 32(39), 10436-10443.
- Pelkmans, L., Kartenbeck, J. & Helenius, A., 2001. Caveolar endocytosis of simian virus 40 reveals a new two-step vesicular-transport pathway to the ER. *Nature Cell Biology*, 3(5), 473-483.

- Persing, D.H., Varmus, H.E. & Ganem, D., 1987. The preS1 protein of hepatitis B virus is acylated at its amino terminus with myristic acid. *Journal of Virology*, 61(5), 1672-1677.
- Petersen, J. et al., 2008. Prevention of hepatitis B virus infection in vivo by entry inhibitors derived from the large envelope protein. *Nature Biotechnology*, 26(3), 335-341.
- PRINCE, A.M., FUJI, H. & GERSHON, R.K., 1964. IMMUNOHISTOCHEMICAL STUDIES ON THE ETIOLOGY OF ANICTERIC HEPATITIS IN KOREA. *American Journal of Hygiene*, 79, 365-381.
- Prince, A.M., 1968. An antigen detected in the blood during the incubation period of serum hepatitis. *Proceedings of the National Academy of Sciences of the United States of America*, 60(3), 814-821.
- Qiao, M., Macnaughton, T.B. & Gowans, E.J., 1994. Adsorption and penetration of hepatitis B virus in a nonpermissive cell line. *Virology*, 201(2), 356-363.
- Rabe, B. et al., 2003. Nuclear import of hepatitis B virus capsids and release of the viral genome. *Proceedings of the National Academy of Sciences of the United States of America*, 100(17), 9849-9854.
- Resh, M.D., 1999. Fatty acylation of proteins: new insights into membrane targeting of myristoylated and palmitoylated proteins. *Biochimica Et Biophysica Acta*, 1451(1), 1-16.
- Resh, M.D., 1989. Specific and saturable binding of pp60v-src to plasma membranes: evidence for a myristyl-src receptor. *Cell*, 58(2), 281-286.
- Roseman, A.M. et al., 2005. A structural model for maturation of the hepatitis B virus core. *Proceedings of the National Academy of Sciences of the United States of America*, 102(44), 15821-15826.
- Schulze, A., Gripon, P. & Urban, S., 2007. Hepatitis B virus infection initiates with a large surface protein-dependent binding to heparan sulfate proteoglycans. *Hepatology (Baltimore, Md.)*, 46(6), 1759-1768.
- Schulze, A. et al., 2010. Fine mapping of pre-S sequence requirements for hepatitis B virus large envelope protein-mediated receptor interaction. *Journal of Virology*, 84(4), 1989-2000.
- Seeger, C. et al., 1991. Woodchuck hepatitis virus is a more efficient oncogenic agent than ground squirrel hepatitis virus in a common host. *Journal of Virology*, 65(4), 1673-1679.
- Seeger, C. et al., 1987. In vitro recombinants of ground squirrel and woodchuck hepatitis viral DNAs produce infectious virus in squirrels. *Journal of Virology*, 61(10), 3241-3247.
- Sells, M.A., Chen, M.L. & Acs, G., 1987. Production of hepatitis B virus particles in Hep G2 cells transfected with cloned hepatitis B virus DNA. *Proceedings of the National Academy of Sciences of the United States of America*, 84(4), 1005-1009.
- Shearer, M.H. et al., 1998. Structural characterization of viral neutralizing monoclonal antibodies to hepatitis B surface antigen. *Molecular Immunology*, 35(18), 1149-1160.
- Shih, C.H. et al., 1989. In vitro propagation of human hepatitis B virus in a rat hepatoma cell line. *Proceedings of the National Academy of Sciences of the United States of America*, 86(16), 6323-6327.
- Stray, S.J. et al., 2005. A heteroaryldihydropyrimidine activates and can misdirect hepatitis B virus

- capsid assembly. *Proceedings of the National Academy of Sciences of the United States of America*, 102(23), 8138-8143.
- Sureau, C. et al., 1986. Production of hepatitis B virus by a differentiated human hepatoma cell line after transfection with cloned circular HBV DNA. *Cell*, 47(1), 37-47.
- Thornton, S.M., Walker, S. & Zuckerman, J.N., 2001. Management of hepatitis B virus infections in two gibbons and a western lowland gorilla in a zoological collection. *The Veterinary Record*, 149(4), 113-115.
- Tsurimoto, T., Fujiyama, A. & Matsubara, K., 1987. Stable expression and replication of hepatitis B virus genome in an integrated state in a human hepatoma cell line transfected with the cloned viral DNA. *Proceedings of the National Academy of Sciences of the United States of America*, 84(2), 444-448.
- Verschuur, E.J. et al., 2001. Analysis of two genomic variants of orang-utan hepadnavirus and their relationship to other primate hepatitis B-like viruses. *The Journal of General Virology*, 82(Pt 4), 893-897.
- Walter, E. et al., 1996. Hepatitis B virus infection of tupaia hepatocytes in vitro and in vivo. *Hepatology (Baltimore, Md.)*, 24(1), 1-5.
- Weiss, T.S. et al., 2003. Cellular damage to human hepatocytes through repeated application of 5-aminolevulinic acid. *Journal of Hepatology*, 38(4), 476-482.
- Will, H. et al., 1982. Cloned HBV DNA causes hepatitis in chimpanzees. *Nature*, 299(5885), 740-742.
- Yamamura, K. et al., 1990. HBV production in transgenic mice. *Gastroenterologia Japonica*, 25 Suppl 2, 49-52.
- Yan, R.Q. et al., 1996a. Human hepatitis B virus and hepatocellular carcinoma. I. Experimental infection of tree shrews with hepatitis B virus. *Journal of Cancer Research and Clinical Oncology*, 122(5), 283-288.
- Yan, R.Q. et al., 1996b. Human hepatitis B virus and hepatocellular carcinoma. I. Experimental infection of tree shrews with hepatitis B virus. *Journal of Cancer Research and Clinical Oncology*, 122(5), 283-288.
- Zuckerman, A.J. et al., 1978. Hepatitis B outbreak among chimpanzees at the London Zoo. *Lancet*, 2(8091), 652-654.

**Publications derived from this thesis:**

First-Author publication in process.

Presentations on meetings:

2008 International Meeting on The Molecular Biology of Hepatitis B Viruses, San Diego (California)

Oral presentation: *“Analysis of cell type-specific interactions of fluorescently labeled inhibitory HBV preS-derived lip peptides.”* Anja Meier, Thomas Müller, Alexandra Müller, Walter Mier and Stephan Urban.

2009 19<sup>th</sup> Annual Meeting of the Society of Virology, Leipzig (Germany)

Oral presentation: *“Visualization of HBV envelope-derived receptor-targeting peptides as a tool to study HBV entry and species specificity.”* Anja Meier, Roland Wedlich-Söldner, Alexa Schieck, Christoph Leder, Thomas Weiss, Thomas Müller, Walter Mier and Stephan Urban.

2009 International Meeting on The Molecular Biology of Hepatitis B Viruses, Tours (France)

Oral presentation: *“Visualization of HBV L-protein-derived receptor-targeting peptides as a tool to study HBV entry and species specificity.”* Anja Meier, Alexa Schieck, Stefan Mehrle, Christoph Leder, Thomas Müller, Thomas Weiss, Roland Wedlich-Söldner, Walter Mier and Stephan Urban.

2010 EASL, The International Liver Congress, Wien (Österreich)

Poster presentation: *“Pharmacokinetic studies on a novel HBV entry inhibitor Myrcludex B demonstrate HBV-receptor expression in rodents and dogs but not in cynomolgus monkeys.”* Alexa Schieck, Anja Meier, Alexander Alexandrov, Christoph Leder, Peter Romeis, Uwe Haberkorn, Walter Mier and Stephan Urban.

## Danksagung

Bei meinem Doktorvater Stephan Urban möchte ich mich ganz herzlich bedanken für die intensive Betreuung, die vielen hilfreichen Diskussionen und natürlich für die große Unterstützung, die ich während der Durchführung dieser Arbeit in seiner Gruppe erfahren habe.

Martin Löchelt danke ich für die Übernahme des Zweitgutachtens, und auch für die konstruktive, motivierende und richtungsweisende Diskussion während meiner PhD-Komitees.

Für die Peptidsynthese danke ich Thomas Müller aus der Arbeitsgruppe von Walter Mier, und im Besonderen Alexa Schieck, die mir fachlich und menschlich jederzeit mit Rat und Tat zur Seite stand.

Alexander Alexandrov (Vision7 GmbH) ermöglichte die Studien mit primären Hepatozyten verschiedener Spezies und die massenspektrometrische Untersuchung der Proben. Seine Diskussionsbereitschaft und die russischen Witze haben mir oft geholfen. Hier möchte ich auch Christoph Leder (ehemals Vision7 GmbH) für die gemeinsame Durchführung der Durchflussszytometrie danken.

Thomas Weiss möchte ich für die Versorgung mit primären humanen Hepatozyten danken, und Roland Wedlich-Söldner sowie Mario Schelhaas für die Hilfe bei mikroskopischen Fragestellungen.

Ohne das gute Arbeitsklima in unserer Gruppe hätte ich manches Motivationstief nicht überstanden. Danke insbesondere an Caro, nicht nur für die gemeinsame Etablierung der Hepatozytenpräparation.

Nicht zuletzt geht ein besonderer Dank an Stefan Seitz, dessen Nebelscheinwerfer maßgeblich zum Erfolg dieser Arbeit beigetragen haben.



